Montanuniversität Leoben

Diamond Materials for Construction Applications

The present work was made at the Institut für Struktur-und Funktionskeramik at the Montanuniversitaet in Leoben in cooperation with HILTI AG headquartered in Liechtenstein.

Leoben, 07.03.2017

AFFIDAVIT

I declare in lieu of oath, that I wrote this thesis and performed the associated research myself, using only literature cited in this volume.

EIDESSTATTLICHE ERKLÄRUNG

Ich erkläre an Eides statt, dass ich die vorliegende Diplomarbeit selbständig und ohne fremde Hilfe verfasst, andere als die angegebenen Quellen und Hilfsmittel nicht benutzt und die den benutzten Quellen wörtlich und inhaltlich entnommenen Stellen als solche erkenntlich gemacht habe.

_____ _____

Datum Unterschrift

ACKNOWLEDGMENTS

First of all, I would like to thank the team of the “Institut für Struktur- und Funktionskermamik Leoben” and the Team of the BU-Diamond at Hilti Headquarter in Schaan for their cooperatives and heartiness.

I also thank my supervisors, o. Univ. Prof. Dr. Robert Danzer and Dr. Walter Harrer, from the ISFK at the Montanuniversity Leoben, for their help and support in any case, making this thesis possible. Also, I would like to express my gratitude to Dr. Stuart Nailer in Hilti Headquarter for his personal and professional guidance and generous supervision throughout the last 12 months.

A special thanks to my friends and colleagues at the Montanuniversity in Leoben, I could not imagine to have better friends. I thank them for their relentless positive harassment, without which I would never have got this far, in particular my friends Thomas Zauchner, Wolfgang Rübenbauer, Stefan Ebenbauer, Christin Aumayr, Florian Zielbauer and Fabian Niklas, which were not only a help when I had to deal with university challenges but they were also a huge help for me to get the balance between exams, sport and recreation.

A huge thanks to my girlfriend Johanna Andrea Gill, her patience and support in the last 3 years and especially the last 6 months have been immeasurable.

And finally, I would like to thank my parents, Christine and Dietmar Fabbro, my sister and my brother in law, Nicole Fabbro and Markus Struggl, and of course my nieces, Alessia and Chiara Fabbro, for their love and support in the past. You gave me the emotional and financial support to make this possible. Alessia and Chiara in particular show me the real important things in life, family.

DANKSAGUNG

Als Erstes möchte ich mich beim Team vom Institut für Struktur- und Funktionskeramik in Leoben und dem Team der BU-Diamant der Firma Hilti in Schaan für ihre Zusammenarbeit und ihre Herzlichkeit bedanken.

Großen Dank gilt auch meinen Betreuern, o. Univ. Prof. Dr. Robert Danzer und Dr. Walter Harrer vom ISFK Leoben, für ihre Unterstützung ohne die diese Diplomarbeit nicht möglich gewesen wäre. Für seine persönliche und professionelle Betreuung aber auch für die zeitintensive Unterstützung der letzten 12 Monate möchte ich mich bei Dr. Stuart Nailer von der Firma Hilti in Liechtenstein herzlichst bedanken.

Ein spezieller Dank gilt auch meinen Freunden und Kollegen der Montanuniversität Leoben. Ich könnte mir keine besseren Weggefährten vorstellen und ich möchte ihnen vor allem für deren unermüdlichen Bemühungen, ohne die ich nicht so weit gekommen wäre, danken. Im Speziellen gilt dies Thomas Zauchner, Wolfgang Rübenbauer, Stefan Ebenbauer, Christin Aumayr, Florian Zielbauer und Fabian Niklas, die mich nicht nur bei universitären Herausforderungen unterstütz haben, sondern auch eine große Hilfe waren um die Balance zwischen Prüfungen, Sport und Freizeit zu finden.

Ein großes Dankeschön gilt auch meiner Freundin Johanna Andrea Gill. Ihre Geduld und Rückhalt in den letzten 3 Jahren und speziell in den letzten 6 Monaten sind unermesslich.

Letztlich möchte ich mich bei meinen Eltern, Christine und Dietmar Fabbro, meiner Schwester und meinem Schwager, Nicole Fabbro und Markus Struggl, und bei meinen Nichten, Alessia und Chiara Fabbro, für ihre Liebe und Rückhalt auf das herzlichste bedanken. Sie waren mir eine emotionale und finanzielle Unterstützung und speziell Alessia und Chiara zeigen mir die wirklich wichtigen Dinge im Leben, Familie.

Abstract

Diamond Materials for Construction Applications

This work is engaged in research and development on diamond materials for use in insert tools for construction applications. ‘Diamond insert tools’ may be used for demolition processes such as sawing, coring or grinding on masonry materials (brick, limestone) and concretes. A diamond insert tool comprises a steel blank (such as a saw blade centre, core bit barrel or cup wheel) and cutting elements. These cutting elements are in most cases either metal-matrix segments with embedded diamond particles or carriers supporting large diamond cutters. The two principal performance characteristics of a diamond insert tool are cutting speed and lifetime. In this project, different diamond materials will be assessed for their potential suitability for use in insert tools. Laboratory techniques such as optical and electron microscopy and x-ray methods will be used to study the material structure and composition of the diamond materials. The mechanical properties and behaviour of these diamond materials will also be studied, together with their thermal dependence, as these materials may experience elevated temperatures during the manufacturing and/or use of the diamond insert tool. The experiments performed and the results obtained will be described in detail.

Kurzfassung

Diamantmaterialien für Anwendungen in der Bauindustrie

Diese Arbeit beschäftigt sich mit der Untersuchung und Entwicklung von Diamantmaterialien die in der Bauindustrie zur Anwendung kommen. Die Diamantwerkzeuge werden vorwiegend bei Abbrucharbeiten verwendet. Dabei werden Werkstoffe wie z.B. Ziegel, Kalkstein und Beton geschliffen, gebohrt oder gesägt. Ein Diamantwerkzeug besteht aus einem Stahlteil (wie z.B. das Zentrum eines Sägeblattes oder einer Schleifscheibe) und den Schneidelementen. Die Schneidelemente bestehen meistens aus einer Metallmatrix in der Diamantpartikel eingebettet sind oder aus Trägerplatten mit großen Schneidwerkzeugen aus Diamant. Die zwei wichtigsten Leistungsmerkmale von Diamantwerkzeugen sind die Bohrgeschwindigkeit und die Lebensdauer. In diesem Projekt werden verschiedene Diamantmaterialien hinsichtlich ihrer möglichen Eignung für die Anwendung in Werkzeugen bewertet. Zur Bestimmung des Gefüges und der Zusammensetzung werden licht- und elektronenmikroskopische Methoden sowie röntgenographische Verfahren eingesetzt. Bei der Herstellung und im Einsatz können sehr hohe Temperaturen entstehen. Daher wird neben den mechanischen auch das thermische Verhalten untersucht. Die Laborstudien werden durch Feldversuche ergänzt. Die Diamantwerkzeuge werden dabei in die dafür vorgesehenen Geräte eingebaut und nach dem Einsatz untersucht. In dieser Arbeit werden die durchgeführten Experimente und die erhaltenen Resultate im Detail beschrieben.

Contents

Page

Acronyms and Abbreviations

Al_2O_3	Aluminium Oxide
B3B	Ball on Three Balls
cBN	Cubic Boron Nitride
DMA	Dynamic Mechanical Analysis
DSC	Differential Scanning Calorimetry
EDM	Electro Discharge Machining
EDX	Energy Dispersive X-Ray Analysis
hBN	Hexagonal Boron Nitride
HTHP	High Temperature High Pressure
PcBN	Polycrystalline Cubic Boron Nitride
PCD	Polycrystalline Diamond
SEM	Scanning Electron Microscope
SEVNB	Single Edge V-Notch Beam
Si	Silicon
SiC	Silicon Carbide
TEM	Transmission Electron Microscope
TSDC	Thermally Stable Diamond Composite
XRD	X-Ray Diffraction
4PB	Four-Point-Bending

1 Introduction

1.1 Project Objectives and Thesis Outline

In order to improve the behaviour during construction applications, it is necessary to get a fundamental understanding of the material and its mechanical properties.

There are a lot of different hard material classes and each class splits into different production processes and structures. However, the challenge in investigating very brittle materials is to find a right and well-known test procedure to get information like strength, edge chip resistance or thermal behaviour. The investigations of mechanical properties at room temperature and after heat-treatment to simulate attachment of the diamond material to the insert are followed by microstructural analysis under a light microscope and a scanning electron microscope. There is a big influence of the binder material, either cobalt in PCD, SiC in TSDC, or the complex binder material in PcBN, which has an effect on the cost and mechanical or thermal properties.

The main objective of the project is to get a ranking of hard material classes, a better understanding of the material properties and the effect of microstructural changes.

- The introduction gives an overview of hard material classes with the focus on thermally stable diamond composites, polycrystalline diamond composites and polycrystalline cubic boron nitride. Additional to the manufacturing processes, examples of commercial grades and applications are given.

- Furthermore PCD, TSDC and PcBN materials were pre-selected and heat treated in special conditions followed by mechanical testing. Additional to the heat treatment a technique called differential scanning calorimetry was used to investigate the chemical behaviour of polycrystalline diamond and the thermally stable diamond composites at high temperatures.

- The mechanical testing of the materials starts with a short introduction and explains the motivation behind the tests. The introduction is followed by the theoretical and experimental procedure to investigate the mechanical properties of the hard material classes also as a function of temperature. The focus was on the so called “Ball on Three Balls Test” and the “Edge Chip Resistance Test”. However, both testing methods are described for technical ceramics followed by a discussion of experimental procedure and results. A short overview of the fracture toughness is given with the focus on the difficulty of this method in testing hard materials.

1.2 Natural Diamonds

The first written tradition about diamonds is a Sanskrit-text from India, which was created in the period about 320-296 B.C. These raw diamonds were sold to Europe where professional workshops began to grind and polish this valuable material in the 14th century [1]. So far, people did not exactly know how diamonds were formed in nature. The diamonds from India were predominantly from secondary deposits and could be used for the jewellery industry as a result of their purity [2]. Diamonds from secondary deposits, known as alluvial diamonds, are mostly eroded from diamond-containing rocks, washed into rivers where they are transported over long distances and finally they get deposited in so-called placers [1]. The increased demand for pure diamonds was easily satisfied for a long time only with these secondary deposits [3].

At the beginning of the 18th century, new secondary deposits were found in Brazil [2]. 150 years later, the deposits in South America were exhausted and new ones were found in South Africa, particularly in Kimberley. This town was also the name-giver of the diamond containing mineral, Kimberlite. In 1872, the mineralogist Cohan described a theory that Kimberlite comes from the inner core and solidified on its way to the earth`s mantle [1]. These diamonds found in the original volcanic pipe are called pipe diamonds. This was the main breakthrough in finding new deposits and after that, China and Russia became amongst the biggest countries which were mining Kimberlite deposits. The last big deposit was found in Australia in 1979. Many scientists were surprised because the diamond containing mineral was not Kimberlite but Lamproite. Lamproite is very similar to Kimberlite but with a slightly higher Magnesia content of 20 mass % [3]. Scientists then were able to perform a laboratory experiment were they detected the crystallisation of diamonds in Kimberlite in a high temperature / high pressure process. The pressure had to be higher than 7 GPa and temperatures should not be below under 1830 °C [4]. This successful experiment was the start of a lot of controversial debates, but nevertheless the geological society agreed with the theory that diamonds grew under high pressure and temperature, operated by chemical reactions (contact metamorphoses) in ultra-alkaline magmas geologically older carbonaceous rocks or gases [1].

However, a very small proportion of diamonds that occur in nature were the results of iron-carbon-meteor impacts. People assumed that the pressures and temperatures which are needed to form diamonds arise during the impact. New investigations revealed that one of the iron-carbon meteors did contain grown diamonds during its entering in the earth`s atmosphere starting a discussion about diamond growth during a supernova [1]. Either diamonds came from meteors or from the earth`s mantle. Natural diamonds are one of the most valuable raw materials for jewellery industries and companies are constantly in search for new deposits and new ways to improve their mining processes.

1.3 Synthetic Diamonds and hard phase BN Composites

It is perhaps comprehensible that people invest a huge amount of money to get diamonds worked into rings, necklaces, ornamental objects or other jewellery pieces. However, the extreme hardness of diamond makes it a very interesting material for a lot of other industries, as will be described later in this section.

Many people see diamonds as the typical covalent solid with carbon atoms with saturated directional bonds [5]. It was not as easy as people might think and needed a lot of technical experience to produce the first synthetic diamonds. In the 1950s, a development team of General Electric first reported the major breakthrough in producing synthetic diamonds [6]. The most common form of diamond synthesis is the transformation from graphite into diamond, supported by transition metal-solvent catalysts, for example in a belt press or a cubic press, together with high temperatures and high pressures (Figure 1). The typical temperature and pressure are 1530 °C and 6 GPa, where the natural diamond growth is simulated [7] (Figure 2).

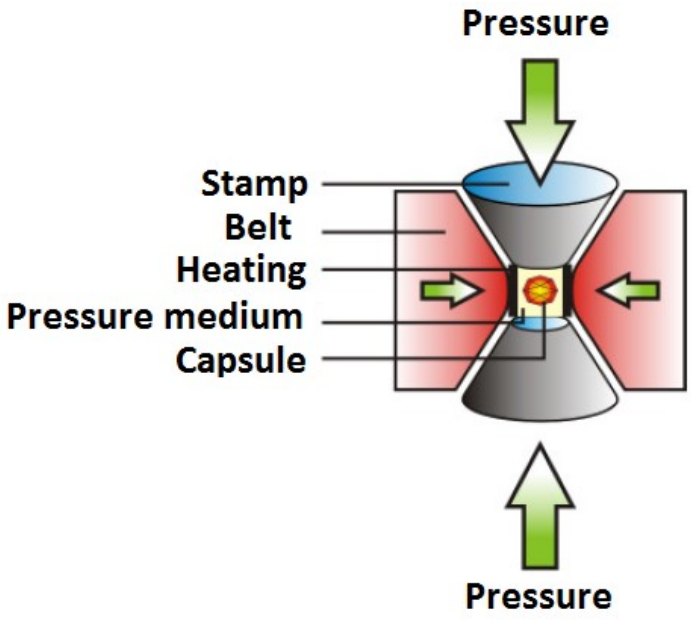

Figure 1: Diamond synthesis press [8]

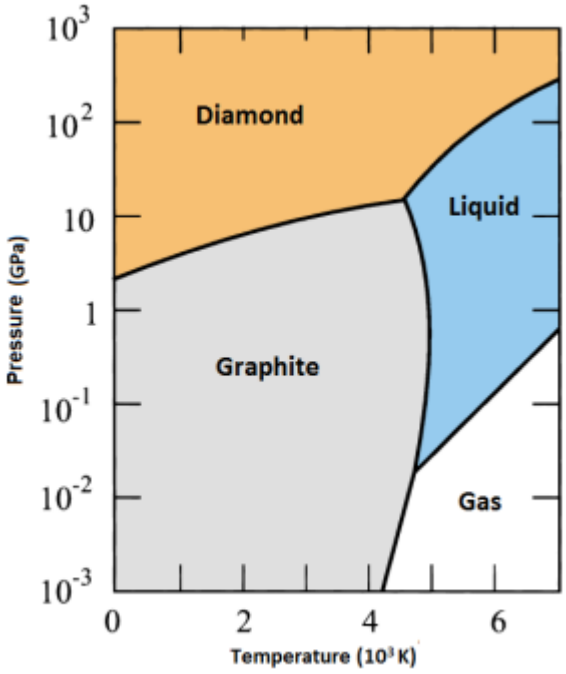

Figure 2: p,T-phase diagram of carbon with linear temperature scale and logarithmic pressure scale [9]

Diamonds from a synthesis process have yellow discolouration (Figure 3a) which comes from single substitutional nitrogen and show an optical absorption in visible light as a result of the different form compared to natural diamonds (Figure 3b) [7]. Natural diamonds tend to have a higher nitrogen content than synthetics, but here the nitrogen atoms are aggregated as pairs or 4 atoms surrounding a vacancy – neither of these aggregation states create colouration.

Traces of the solvent catalyst metals can be found in all but the highest grade synthetic diamonds, having a negative influence of the thermal stability of the material.

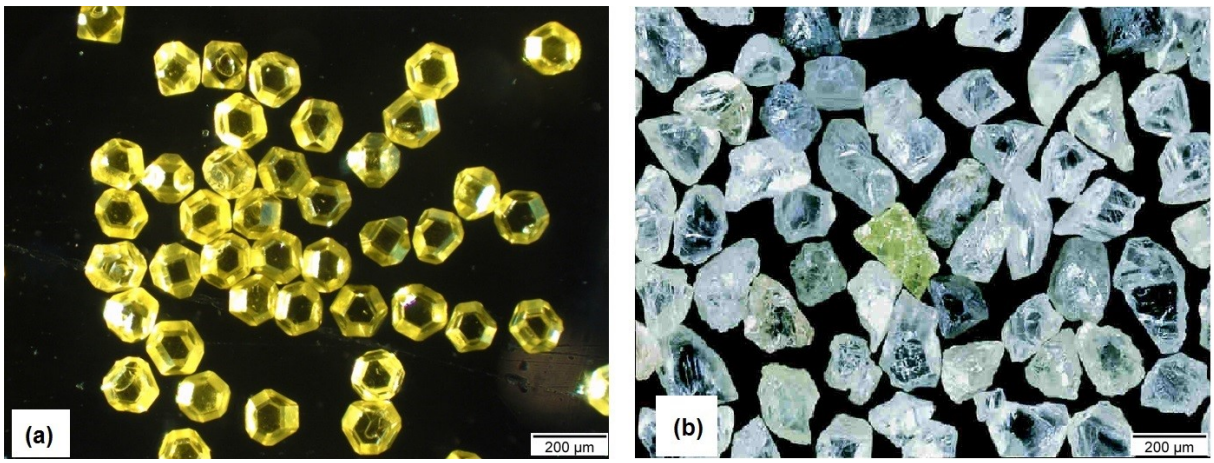

Figure 3: Left, Synthetic diamond with its typical yellow discoloration [10]. Right, natural diamonds for sawing application without the yellow discoloration but with impurities [11]

In the 1970s, Stromberg, Stephens and Hall have reported the synthesis of a polycrystalline diamond compact at high pressure/high temperature [9]. This process was not useful for commercial application, as a consequence of the extreme thermodynamic requirements during the synthesis. One year later, Katzman and Libby discovered a process of sintering diamond powder in combination with cobalt as a binder material and as a catalyst during the sintering process [9]. Since this technical achievement it was possible to produce PCD at much lower temperature and pressure and therefore reduce the costs of the process. As a consequence of this work, polycrystalline diamond composites moved into the focus of drilling companies in the oil, gas and rock industries. Either as an abrasive particulate material or as diamond composites, it is nearly impossible to find a production process in modern industry in which diamond does not play an important role. It is used for most machining processes like the turning, milling and grinding of nonferrous metals but also for sawing and drilling concrete and natural stones [5].

However, PCD material shows a thermally unstable behaviour in applications that reach a temperature of approximately 680 °C. Reasons include the different thermal expansion coefficient of cobalt and diamond and the ability of the cobalt to catalyse the transformation of diamond back to graphite at high temperatures but low pressures. The solution for this problem is a change in the binder material and replacing the metallic cobalt with ceramic silicon carbide, whether SiC is produced by reactive bonding during sintering or as an original component to the sintering operation. This material is named as thermally stable diamond composite [10]. TSDCs are produced with high or low pressure and high temperature. In either case, the diamond grains are cemented together, rather than sintered together (intergrown) as in PCD.

The last hard material class which is investigated in this thesis is polycrystalline cubic boron nitride, so called PcBN. Polycrystalline cubic boron nitride is a material containing fine grains of cBN cemented together with a binder material, which can be either ceramic or metallic. Similar to PCD, PcBN was developed by General Electrics in the 1950s to find a material with nearly the same mechanical properties but without the problems at high temperatures [11]. It is known that diamond and cubic boron nitride are the two hardest materials. Diamond and cBN both have the same cubic crystallographic structure and exhibit a high thermal conductivity [12]. But there are also differences in the application behaviour and mechanical properties which makes it interesting for e.g. the milling industry. Diamond is susceptible to graphitisation, will oxidise at higher temperatures in air and, which is the most problematic factor in grinding and milling, reacts with ferrous metals at high temperatures, whereas cubic boron nitride is both stable in higher temperatures in air and when machining ferrous work pieces [12]. Figure 4 shows the transformation of graphite into diamond (a), and the transformation of hexagonal boron nitride into its cubic structure.

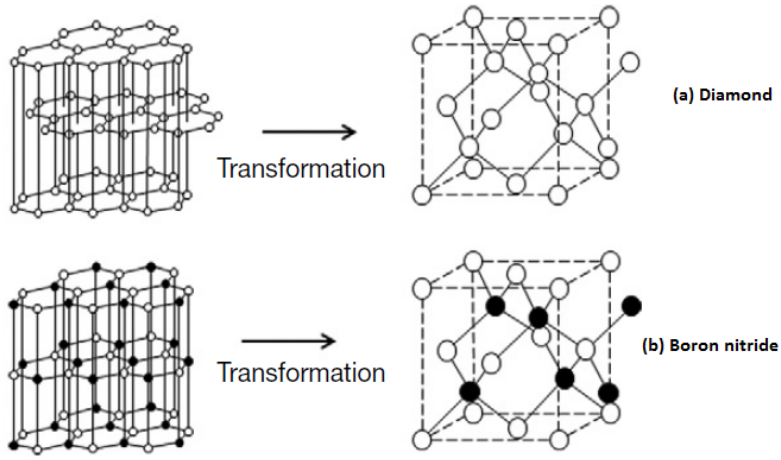

Figure 4: The transformation of graphite into diamond (a) and hexagonal boron nitride to cubic boron nitride (b) showing the arrangement of the boron (black) and the nitrogen (white) [13]

2 Materials

2.1 Polycrystalline Diamond

2.1.1 PCD Manufacture

PCD is a class member of super hard material like polycrystalline cubic boron nitride (PcBN) and thermally stable diamond composites. This broad range of materials allows the industry to optimize their tools and develop application specific solutions. PCD is a diamond composite material which is manufactured with high temperature under high pressure. The carbon diamond phase diagram is shown in Figure 5. According to the phase diagram the conditions with catalytic synthesis are approximately 1430 °C and 5-10 GPa, much lower than they are in a process without the help of catalytic elements [14].

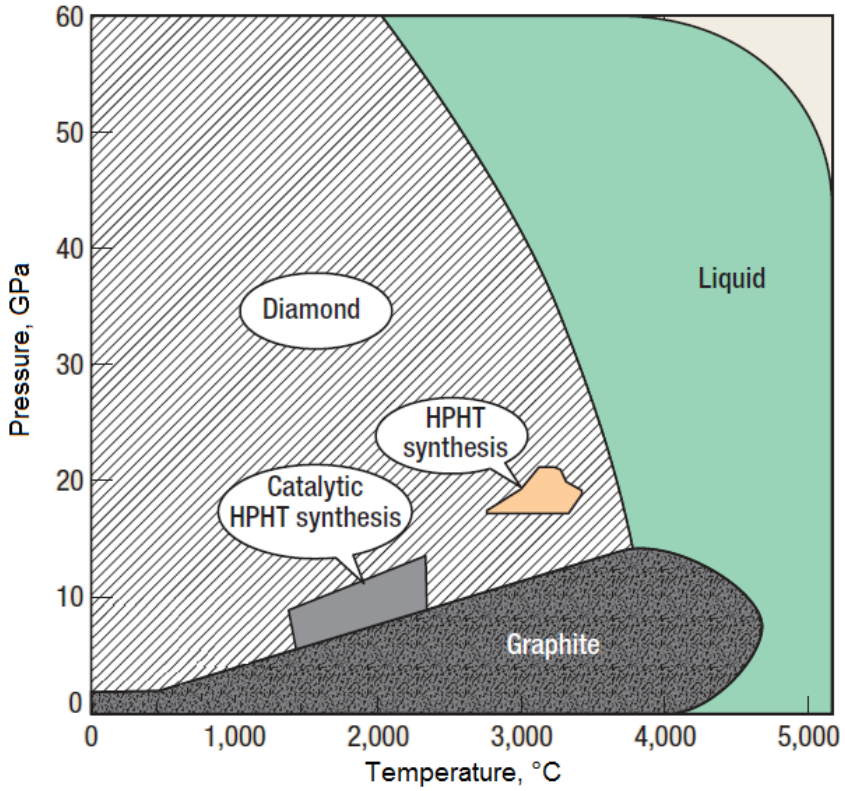

Figure 5: Carbon diamond phase diagram showing higher temperatures and pressures required for diamond synthesis without catalysts [14]

The conditions, especially the pressure and the temperature, in which the PCD is manufactured, are critical to the properties of the sintered polycrystalline diamond [14]. Only a cubic press (Figure 6a) or a belt press (Figure 6b) are able to deliver these extreme conditions to ensure the thermodynamic stable region of diamond and the diamond-diamond direct bonding.

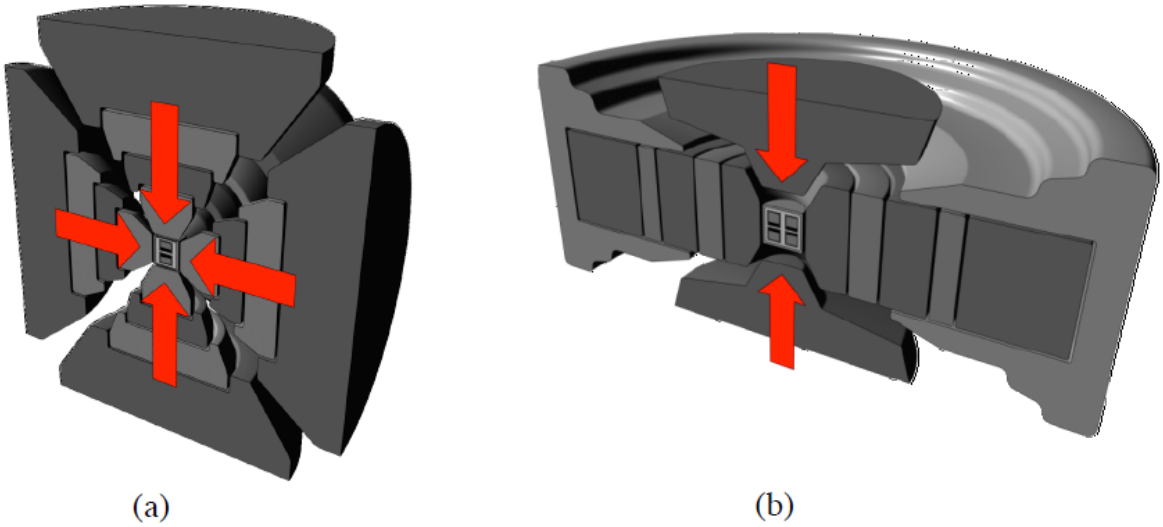

Figure 6: Schematic drawing of a cubic press (a) and a belt press (b) used in a HPHT synthesis process for a diamond capsule [15]

Commercially manufactured polycrystalline diamonds are synthesised in a capsule by sintering diamond powder as a laminate on WC/Co substrate. The cobalt in the substrate is necessary because it infiltrates through the diamond particles and serves as an agent to form diamond-diamond direct bonding [16]. The absolute reaction rate is controlled by the temperature and restricted to the maximum achievable pressure of the belt press or cubic press. It takes a few steps to get the diamond-diamond direct bonding and therefore this multistate manufacturing process is sectioned in cold compaction, hot compaction, cobalt infiltration and liquid phase sintering (Figure 7). In the cold compaction state the diamonds undergo a lot of pressure where the packing density increases and the diamonds are in punctual contact to each other.

As a function of the high strength on a small contact area the diamond particles fracture and the powder density increases. The following stage is the hot compaction stage. The temperatures and therefore the powder density increase. If the required temperature and pressure are reached, the cobalt infiltration phase starts. After reaching the sintering temperature the cobalt from WC/Co substrate starts to melt and flows under pressure into the pores between the diamond-diamond bonds. The remaining impurities are removed by the flowing cobalt front. At a stage where all pores are filled with liquid cobalt and any impurities are removed, the material undergoes the final stage in the HTHP process, so called liquid phase sintering. The cobalt acts as a catalyst and after the liquid cobalt forms a carbon-cobalt eutectic, the carbon from the diamond dissolves into this eutectic and can re-deposit as diamond, which forms very strong intergranular bonds and enlarge the diamond matrix structure with diamond-diamond direct bonds filled with cobalt [15].

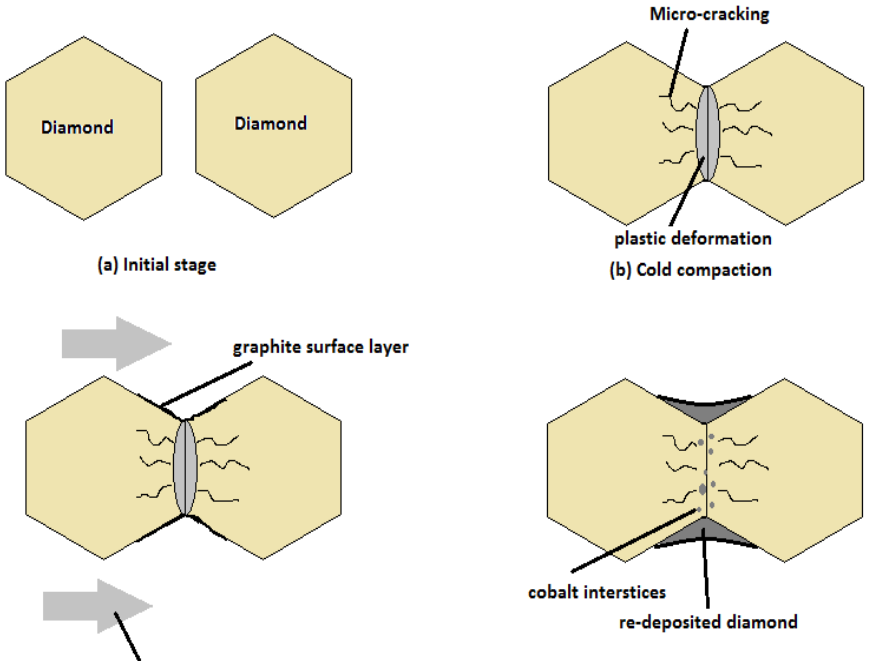

Figure 7: The four principal mechanism of diamond deposition during the HPHT manufacturing process (based on [15])

There is also the possibility in choosing two or even three different diamond sizes, where the small one sits in between the gaps of the bigger one, so-called multimodal (Figure 8). A multimodal sintered diamond composite has a higher packing density which decreases the distance between the diamonds during the manufacturing process and enhances the chip resistance of the material.

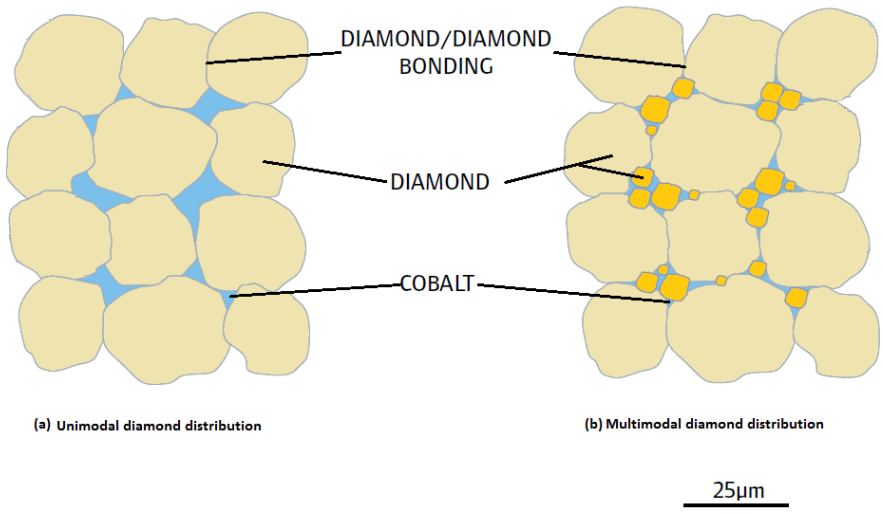

Figure 8: (a) a unimodal diamond distribution with one grain size and (b) multimodal diamond distribution with two different grain sizes for PCD material (based on [17])

2.2 Thermally Stable Diamond Composites

2.2.1 TSDC Manufacture

The use of polycrystalline diamond material is limited by either the high cost and size restrictions as a result of the high pressure manufacturing process needed to produce them [17] or by the limited maximum application temperatures, which should not be higher than 700 °C. The cobalt content in commercial PCDs is between 6 - 10 mass percent, which causes a significant reduction of the thermal stability of the PCD material. Especially in the machining or drilling industry, tools equipped with polycrystalline diamond materials and used at high cutting speed are exposed to high temperatures (above 700 °C). This leads to a thermochemical wear of the PCD material [18]. The cobalt which is present in PCD materials from the liquid phase sintering acts as a catalyst for the graphitisation of the diamond and gives its temperature limit. Therefore it is necessary to develop a new thermally stable diamond composite material. The solution is replacing the cobalt with silicon carbide which works well as a binder material. A strong bond between the diamond and the SiC gets formed as a consequence of the structural similarities, with the result in getting a material with a very strong adhesion between the diamond grains and the SiC matrix. This material can be used at temperatures above 1000 °C because the SiC does not catalyse the re-graphitisation of diamond, unlike cobalt [19].

The limiting factor with this material is the toughness of the interface between the SiC and the diamond coating. For such applications where the wear during application is higher than the stability of the interface, bulk super hard materials are preferred. The manufacturing process is very similar to the PCD manufacturing route and is a diffusion-controlled mass transport in a sintering process with a belt or cubic press (see Figure 6, chapter 2.1.1). Nevertheless, to avoid the transformation to graphite from diamond, high temperatures but also high pressures have to be used during the sintering process as a consequence of the metastability. High pressure manufacturing processes are the cost-pushing factors and producing a thermally stable diamond composite with a reasonable price is a challenging task. To avoid the transformation into the stable phase (graphite) without applying high pressure, a composite with a high content of the hard phase that is strongly bonded to the matrix is used. To generate a nearly as dense material, the volume content of the hard phase (about 30 vol% diamond) can be increased if the inclusions are partially solved in the matrix. It is required that the dissolved carbon reacts with the matrix to avoid the precipitation to the thermodynamically metastable modification. This newly-formed SiC grows into the pores of the diamond, increasing the density and closing the infiltration channels without changing the outer dimensions [17]. The typical manufacturing stages of the low pressure Si infliction are shown in Figure 9.

Another method to manufacture SiC diamond composites is the HPHT process. Commercially available thermally stable diamond composites are made of micron sized diamond powders. It was not possible to use a powder with smaller diamonds because the liquid phase infiltration would immediately stop if the pores get closed and hinder the

sintering process. In the 2000s the first nanocrystalline diamond composites were synthesized at 7.7 GPa and 1400 - 2000 °C. Silicon is used as binder material in a HPHT process because it shows a lot of advantages. The decreasing melting point by increasing pressure allows reducing the costs, the structural similarity of SiC and diamond gives a strong bond and the high melting point of Si makes it suitable for high temperature applications [20].

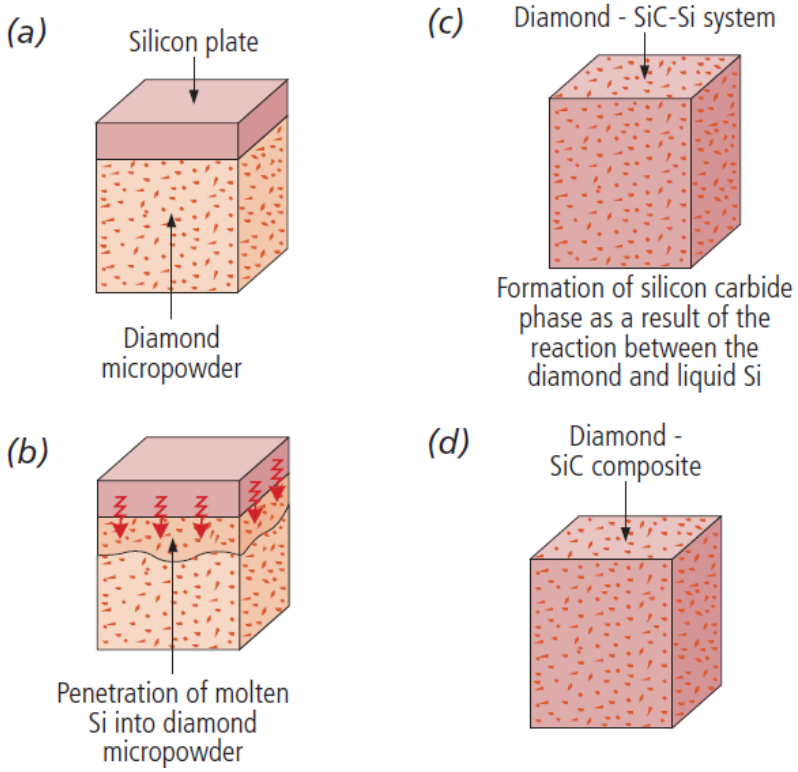

Figure 9: The different stages during the manufacturing process of thermally stable diamond composites with molten silicon: (a) start of the process, (b) melting and infiltration stage, (c) phase formations, (d) end of the process [18] at 40 MPa and temperatures above 1450 °C

There is a big difference in operating mechanical properties between PCD, low pressure TSDC, high pressure TSDC, monocrystalline diamond and tungsten carbide, such as hardness and wear resistance. PCD materials show slightly better values for strength, fracture toughness and hardness but this advantage is undermined when temperatures of 700 °C are exceeded and the thermally stable material keeps the mechanical properties and shows the advantage of its compound.

Table 1: Basic properties of standard PCD, TSDC, synthetic monocrystalline diamond and cemented tungsten carbide [21]

Property	Standard PCD	Thermally stable PCD (low pressure)	Synthetic monocrystalline diamond	Cemented tungsten carbide (WC/15 mass% Co)
Density [g/cm^3]	3.90 – 4.10	3.42 - 3.46	3.51 - 3.52	13.80 - 14.10
Knoop micro hardness [GPa]	50 - 60	50 - 55	70 - 105	15 - 18
Compressive strength [GPa]	7.5 - 8.5	2 - 3.5	7.0 - 9.0	12.0 - 14.0
Fracture toughness [MPa m$^{1/2}$]	9.0 - 10.0	7.0 - 8.0	3.0 - 4.0	11.0 - 12.0
Young`s Modulus [GPa]	810 - 850	920 - 960	1000 - 1150	400 - 650
Thermal conductivity [W m^{-1} K^{-1}]	550 - 750	120 - 250	700 - 1500	70 - 100
Thermal stability [°C]	700	1200	900	1400

2.3 Polycrystalline cubic Boron Nitride

Boron nitride does not exist in nature, neither in hexagonal nor in cubic form. It is a man-made material, synthesised from boron (B) and nitrogen (N). The first stage is to synthesise a hexagonal structured boron nitride according to the following reaction [21]:

$$BCl_3 + NH_3 \rightarrow \text{hex-}BN + 3HCl$$

hBN has a white, slippery solid structure similar to graphite but with alternating nitrogen and boron atoms. It is a good thermal conductor and a good electric insulator. The main difference to graphite is that hBN can be used in an oxidising atmosphere up to 900 °C [22]. Cubic boron nitride was synthesized for the first time in 1957 by a team of General Electrics with the lead of Wentorf [23]. Wentorf used a metal capsule heated by resistance to about 1800°C, while increasing the pressure to about 8.6 GPa. The cubic structure is thermodynamically unstable and the transformation from cubic to hexagonal is very slow. cBN is the second hardest material known next to diamond and is stable in contact with ferrous metals at high temperatures which makes it useful for application where diamond starts to react with the work piece.

Table 2: Comparison of properties of cubic boron nitride and a synthetic diamond monocrystal [25]

Property	cBN	Synthetic monocrystalline diamond
Density [g/cm^3]	3.48	3.51-3.52
Knoop microhardness [GPa]	45	70-105
Fracture toughness [Mpa m$^{1/2}$]	2.8	3.0-4.0
Young`s Modulus [GPa]	890	1000-1150
Thermal conductivity [W m^{-1} K^{-1}]	740	700-1500
Expansion coefficient [10^{-6}/°C]	4.8	1.5-4.8
Stability against oxidation [°C]	1200	600
Graphitisation [°C]	>1500	1400

In 1969, General Electric started to sell the first grade of cBN, so called Borazon^{TM}, and in 1975 they introduced the first grade of PcBN, BZN^{TM}, to the market. A composite material consisting of cubic boron nitride, a ceramic or metallic binder and additional substrates, is called polycrystalline cubic boron nitride. The different grades of PcBN are characterised by their binder material, grain size and cBN content. A cBN content between 40-70 % is called low content PcBN and above 70 % high content PcBN [22].

2.3.1 PcBN Manufacture

PcBN is a two-phase polycrystalline material consisting of cBN in a ceramic or metallic matrix. PcBN materials are usually sintered in a high pressure/high temperature manufacturing process. The challenge is to avoid the transformation from the cubic into its stable hexagonal form. Therefore, the process has to be carried out in the region where cubic BN is thermodynamically stable (Figure 10).

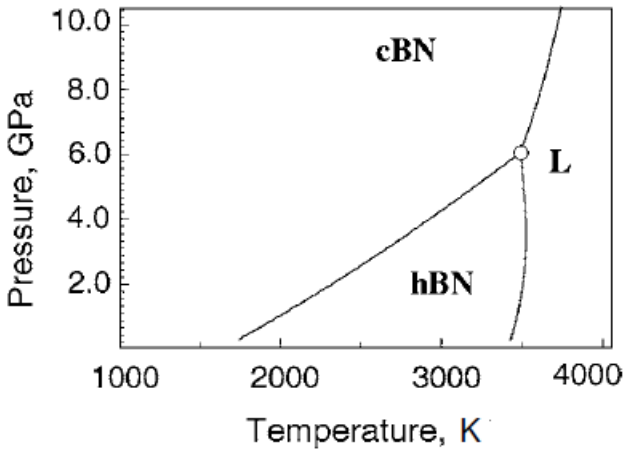

Figure 10: Phase diagram of boron nitride and the stable region of its cubic and hexagonal structure [22]

The PcBN is assembled in cylindrical discs (similar to PCD or TSDC) and then sintered for 3 - 120 minutes at about 1100 °C under a pressure of 2 GPa [24]. Like the cold compaction stage during PCD manufacture, the high pressure increases the densification by causing a significant plastic deformation of the cBN grains. To generate the required high pressure, a belt press is used which limits the size of the PcBN compact [22]. Additional to ceramic binder materials, metals of groups IV, V and VI from the periodic table and/or other elements like aluminium, nickel and cobalt [25] are used. The binder material in high content PcBN is usually an aluminium-based binder like aluminium, aluminium nitride or aluminium diboride. The grain sizes of high content PcBN are between 5 - 20 µm. Low content PcBN generally have a titanium-based binder material, such as titanium nitride, titanium carbide or titanium carbonitride and the grain sizes vary from sub-micron up to 2 µm [22]. The most frequently-used binder material in high content PcBNs is aluminium which reacts with BN in a wide temperature and pressure region forming a AlB_{12} or a two two-component phase made of AlB_2 – AlN and AlB_{12} – AlN.

It strongly depends on the pressure whether a one phase or a two phase is formed [25]. Another advantage is the low melting point of aluminium which makes it possible to reduce the pressure without any risk of a cBN to hBN transformation and therefore lowering the costs of the manufacturing process. Besides aluminium, titanium is a very popular binder material. TiN is well known and widely used in the industry because of its corrosion resistance, good wear behaviour and high hardness [26]. TiN and TiC is very affinitive to BN. As a binder material TiN has a positive influence on the thermal stability of the cBN cutting tools. New investigations in adding small amounts of aluminium to the cBN-Ti(C,N) system show that it is possible to enhance the sintering rates but once the Al content reaches a level of 20 wt% of the binder material, the hardness gets reduced [22]. Similar to other super hard composite materials, the strength of a cBN composite, whether it has a metallic or ceramic binder, strongly depends on the strength between the cBN and the matrix. PcBN is a very useful material in machining ferrous and non-ferrous metals compared to PCD materials where graphitisation of the diamond during the application at high temperatures is a permanent risk. A comparison of the mechanical properties is shown in Figure 11.

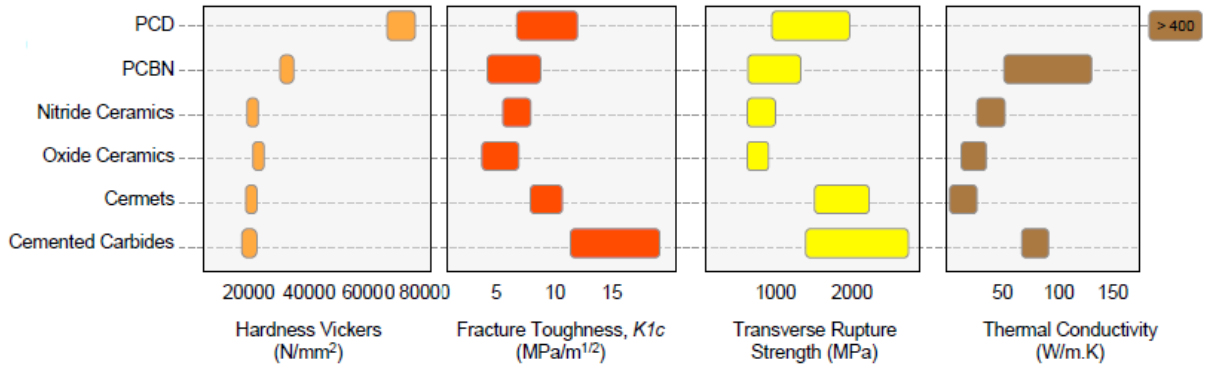

Figure 11: Hardness, Fracture toughness, transverse rupture strength and thermal conductivity of commercially used cutting tool materials [22]

3 Used Testing Methods

A huge range of mechanical testing methods for brittle materials like diamond composites exists. But it is difficult to produce the right shape and geometry for all the different tests. Therefore this work focuses on available and well-known tests at the ISFK Montanuniversity Leoben. Both, the B3B and the edge chip resistance test have been tested in the past and a database for diamond composites exists.

3.1 Differential Scanning Calorimetry (DSC)

DSC is the determination of the heat quantity which occurs during a chemical or physical conversion. It changes the inner energy of the material at constant pressure. This means in practice, a measurement of enthalpy changes between two points. The measured parameter is the changed heat quantity depending on time and/or temperature. A furnace in which the specimen and a reference sample are fixed is heated and cooled under controlled conditions while two conductive metal discs continuously measure the temperature of the crucible. A changing of the heat quantity occurs if there is a thermodynamic change (e.g. graphitisation) in the specimen either during the heating process or during the cooling process. In this thesis, diamond grit with different grades, a thermally stable (T-B) and two non-thermally stable materials (S-D and S-E) are investigated to prove if graphitisation at high temperature occurs. The non-thermally stable PCD samples were cut to their final shapes using electro discharge machining (EDM), which uses a copper wire. To exclude any phase changes at high temperatures of any copper residues left on the PCD one additional run with a PCD which got sandblasted at the cutting surfaces to remove the remaining copper and a PCD with copper powder were made. The heating rate is 25 °C per minute up to a temperature of 1100 °C and cooled down to room temperature with 10 °C per minute. To avoid any oxidation of the diamond, argon is used as a protective atmosphere. A schematic drawing of a DSC furnace is shown in (Figure 12).

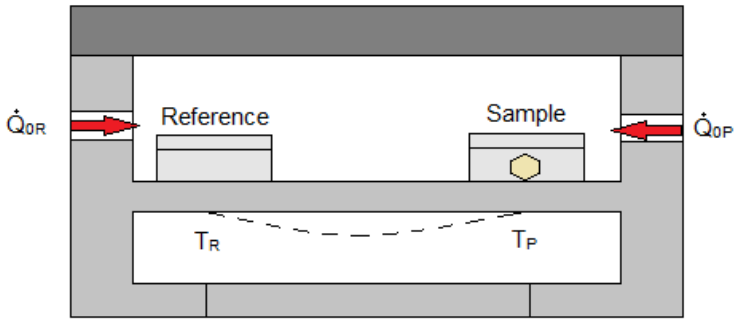

Figure 12: A schematic drawing of a DSC furnace where TR is the temperature of the reference, TP is the temperature of the specimen and $\dot{Q}_{0R}$ and $\dot{Q}_{0P}$ are the two different heat flows (based on [27])

3.2 Strength Tests - Ball on 3 Balls Test

The ball on three balls test is a useful tool for direct strength testing of disc shaped specimen. Solid PCD and TSDC, being single-layer materials, are easily tested using the B3B test. There are nearly no problems with aligning of the samples and it is possible to reduce the mistakes made from the operator to a minimum [28]. Different approaches have been made for the analytical calculation of the stress distribution in centrally-loaded biaxial disc tests. They are all based on the linear-elastic axisymmetric thin-plate theory where the basic work was done by Bassali [29] and later in more specific way by Kirstein and Woolley [30].

The highest tensile stress of the sample occurs on the opposite site of the loading ball in the centre of the disc and is therefore far from the edges of the specimen. B3B test is not sensitive to concave or convex sample geometry, the flatness or roughness of the samples, or to surface damages at the edge of the discs (e.g. notches), in comparison to uniaxial or biaxial bending tests. The test set up with the pre-load and after applying the pre-load is shown in Figure 13. Where the specimen is centrally positioned over the loading ball and the guide positions the three supporting ball and the specimen [28]. After applying a pre-load the positioning aid is pulled down and the supporting balls can freely move. The loading ball is fixed. The friction between the balls and the specimens held the specimens in place and the force increases until fracture occurs. This fracture load can be used for the calculation of the tensile stress at the moment of fracture [28].

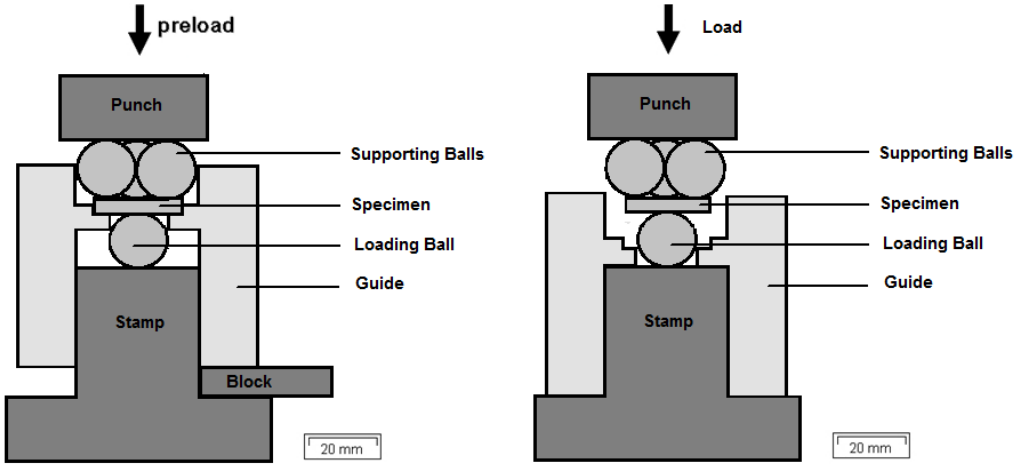

Figure 13: Test set up, pre-load left with the block and after applying a pre-load right, without the block (based on [31] and [32])

The stress field is influenced of the mechanical properties of the tested materials and the geometries of the specimens. To reduce the number of parameters which will complicate the analysis, the loading ball and the support balls have the same size [33]. The loading ball touches the sample on the compressive side at its centre. The three supporting balls touch the specimen on the opposite side of the disc at the surface where the tensile strength occurs.

The maximum tensile stress σ_{max} in the specimen is a function of the fracture load and can be calculated for an elastically isotropic material with the following equation [33]:

$$\sigma_{max}=f\,\frac{F}{t^2} \tag{1}$$

where *f* is a dimensionless factor which depends on the geometry of the balls and the specimen, the Poisson`s ratio of the tested material and the load transfer from the jig into the specimen, *t* is the thickness of the disc and *F* is the applied force [33].

3.3 Fracture Statistics (Weibull)

The origin of fracture of brittle materials like ceramics and diamond composites is usually based on defects in the inner part of the material. Hence the stability is based on the most precarious flaw within the material. In this thesis, all calculations rest on the fact that the size of a defect is the main factor of possible failure [34]. In general, the size of a critical defect is tied to the amplitude of the applied stress, meaning the larger the defect, the smaller is the amplitude of stress [35]. Since the size of defects varies from sample to sample, the stability also varies, resulting in the need to describe this in the form of a distribution function instead of a simple number. For calculations of static fracture behavior, the distribution of strength within the material has to be determined with the help of mechanical testing of the specimens. The problem with this method is the fact that for sufficient assertions a very large number of specimens need to be tested. This fact nullifies when the mathematical structure of strength distribution is known, therefore reducing both the number of tests and cost for determination of strength. These results can subsequently be reduced to standard parameters, e.g. median strength. The Swedish engineer W. Weibull was the first scientists to contribute to this topic in the 50s [34].

For brittle materials such as diamond composites or many other brittle ceramics, a solution can be assumed to the well-known Weibull statistics [36]:

$$F\,(\sigma, V)=1-\exp\left[-\frac{V}{V_0}\left(\frac{\sigma}{\sigma_0}\right)^m\right] \tag{2}$$

The scatter of the strength is described by the Weibull modulus, *m*, and the characteristic strength, σ_0, is the stress where the probability of failure, *F*, is 63 % with a standardized volume V_0.

The size effect is a well understood problem and describes that large specimens of brittle materials have higher probability of failure than small specimens of the same material under the same applied load. This is a consequence of the smaller flaws of smaller samples, or that the possibility to find larger flaws is much higher in bigger specimens than it is in smaller ones.

Therefore, an effective surface, S_{eff}, or effective volume, V_{eff}, have to be calculated with following equations [36]:

$$S_{eff} = \int_{\sigma>0} \left(\frac{\sigma(\vec{r})}{\sigma_r}\right)^m dS \quad (3)$$

$$V_{eff} = \int_{\sigma>0} \left(\frac{\sigma(\vec{r})}{\sigma_r}\right)^m dV \quad (4)$$

where σ_r is in general the maximum of the stress field and the integration is done over the volume or surface elements where the stress $\sigma(\vec{r})$ is positive.

3.3.1 Comparison of B3B-test strength values to bending test strength values

It is possible to compare B3B test results with bending strength test values. The challenge is to find a way to compare the relatively small volume tested in the biaxial B3B-Test with the much bigger tested volume of the uniaxial four point bending test. Therefore, the relation between uniaxial and biaxial failure and secondly a procedure for the volume-extrapolation has to be known.

To find a relationship between biaxial and uniaxial failure, an equivalent stress has to be defined. This equivalent stress is explained with the principle of independent action, PIA, and can be defined by:

$$\sigma_{eq,\,PIA} = (\sigma_I^m + \sigma_{II}^m + \sigma_{III}^m)^{1/m} \quad (5)$$

where σ_I, σ_{II} and σ_{III} are the stress components and m is the Weibull-modulus [37]. The influence of the specimen size is described in the previous chapter. However, if the flaws are volume flaws or surface flaws, the influence of the volume can be written by:

$$\sigma_{2eq} = \sigma_{1eq} * \left(\frac{V_1}{V_2}\right)^{1/m} \quad (6)$$

$$\sigma_{2eq} = \sigma_{1eq} * \left(\frac{S_1}{S_2}\right)^{1/m} \quad (7)$$

V_1 and V_2 respectively S_1 and S_2, are the effective volumes and surfaces of the specimens and σ_1, σ_2 the related strength values. The equations for the effective surfaces and volumes are described in equation 6 and 7. The effective volumes and surfaces of the specimens coincide to the volume and surface where the highest stress occurs and depend on the Weibull modulus [33].

3.4 Edge Toughness Test

A lot of investigations in understanding the edge chipping behaviour of brittle materials have been done in the past and the data were analysed following CEN/TS 843-9 [38]. The chipping behaviour of these material classes is related to the fracture energy. Of relevance to superhard composites such as PCD, TSDC and PcBN, whose main applications are rock drilling and machining of ferrous or non-ferrous metals, the lifetime of the material is related to the chipping behaviour and/or edge chip resistance [39]. In the late 1980s Almond and McCormick investigated the behaviour of edges under mechanical loading [40]. A Rockwell-C indenter is used to apply the load near to the edge of the tested material until edge flaking occurs. This method can be used to rank different material classes, characterize brittle materials and calculate the so-called edge toughness [39]. The test set up is shown in Figure 14.

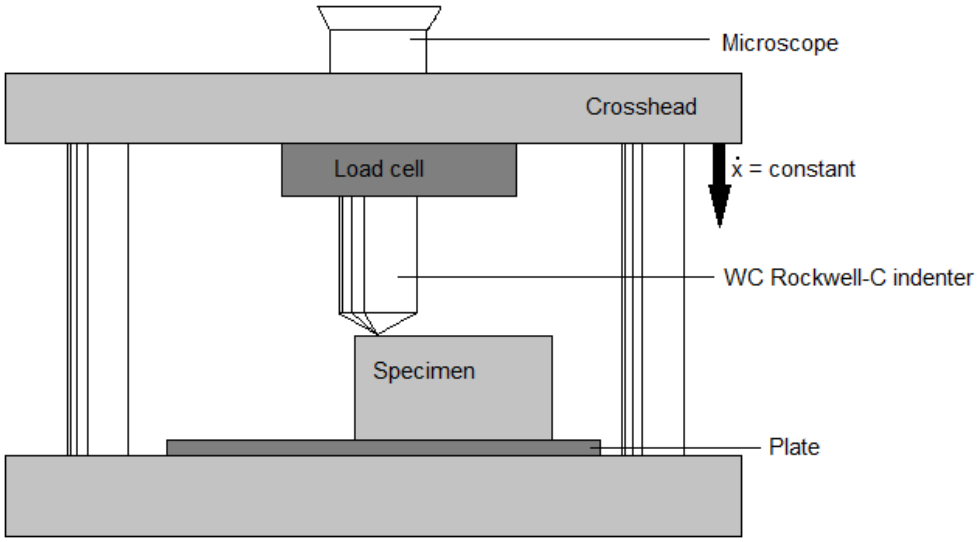

Figure 14: Test set up for rectangular specimens with a constant test speed and a tungsten carbide indenter (based on [41])

In fact, there are two ways in testing with this set up. The first one is to test with a constant distance from the edge and calculate the average edge toughness. The second one is to increase or decrease the distance and plot the different values, where the slope of the regression line gives the edge toughness. The definition of the loading point and the distance from the edge is shown in Figure 15 [38].

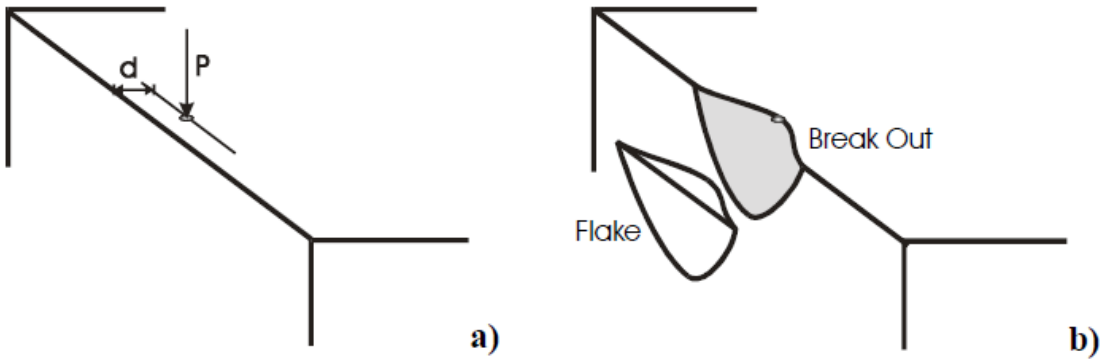

Figure 15: Schematic drawing which shows the loading point and the distance from the edge before (a) and after (b) the test [41]

The peak load required to create a chip must be recorded after each indentation and when plotting the distance of the edge versus the peak load a linear relationship exhibits. The slope, M, of the regression line is characteristic for each material if the testing conditions (indenter material, indenter shape, indentation speed, edge geometry, etc.) are the same and is calculated as followed [41]:

$$P = P_0 + M*d \tag{8}$$

(8) explains the linear behaviour of the edge toughness and it is shown that the slope of the regressions line does not go through the origin. P_0 is a finite force and it describes the force which is necessary to create a chip at d = 0. Explanations could be that P_0 is a consequence of the measurement inaccuracies [40], internal stresses of the material or the increasing contact zone due the deformation process of the indenter and the material [42], or a combination of these. For tests performed near the edge the deviations are very small and the formula (8) can be simplified [41]:

$$P \approx M*d \tag{9}$$

3.5 Fracture Toughness

The lower plasticity of brittle materials at room temperature allows the use of LEFM (linear elastic fracture mechanics) for quantification and characterization of defects. One prerequisite for the use of LEFM is the fact that the 2D defect is initialized atomically sharp. For that reason a razor blade is used to create a sharp crack initiation for the measurement of fracture toughness [43].

A major problem of fracture toughness testing of brittle materials is the difficulty in reliably introducing reproducible and easily measurable sharp cracks into the samples. In the SEVNB method, most of these problems are avoided, since an accurate notch is relatively to machine, the exact depth of which is easily discernible in an optical microscope [44].

To generate fracture toughness results for different diamond composites, a sharp V-shaped notch has to be created with razor blades.

The fracture toughness of PCD-type materials is a potentially very important property but it is time consuming to generate a sharp notch into the beam. The notch diameter is critical to obtain good results. A 2 µm notch diameter is suitable for the most ceramics, but in diamond 5 - 10 µm is acceptable. Therefore, at least 5 specimens for a good reproducibility of the test are needed [45].

The “stress at failure” is used to calculate the critical stress intensity factor from a relationship based on the standard linear elastic fracture mechanics relationship:

$$K_{IC}=Y\sigma\sqrt{\pi a_c} \tag{10}$$

where *Y* is a correction factor allowing the influence of sample geometry and crack configuration [44]. It is possible to calculate the critical defect size (a_c) [45], either on the surface or in the volume, from the Griffith/Irwin criterion as follows ([46] and [47]):

$$a_c=\frac{1}{\pi}\left(\frac{K_{IC}}{Y\sigma}\right)^2 \tag{11}$$

4 Tested Material

It is very important to investigate different material classes after a controlled heat treatment concerning to their mechanical properties. PCDs, TSDCs and PcBNs react completely differently to high temperatures. Properties, such as strength or edge toughness, could get dramatically reduced. Especially PCD, with cobalt as binder material, is sensitive to high temperatures due to the different thermal expansion coefficients of cobalt and diamond and the fact that cobalt acts as a catalyst for re-graphitisation. The thermal investigations include the testing of mechanical properties before and after heat treatment as well as investigating PCD and TSDC with differential scanning calorimetry to detect any graphitisation during the heating process.

4.1 Sample Preparation

PcBN, TSDC and PCD all contain different binder materials which are described in previous chapters and have therefore different requirements in sample preparation. However, these materials are manufactured in a sintering process and are disc shaped after removing them from the sintering cylinder. The next step is to cut them into the shape which is needed for the tests. All PCDs are electrically conductive which makes them suitable for EDM. Therefore, a thin copper wire cuts the material in shape whereby one electrode is the wire and the other one is the work piece. The reason why PCD materials are cut in an EDM process and for example TSDCs are not, is that PCD materials are based on their cobalt binder electrically conductive. Even if TSDCs are not electrically conductive, somehow they have to be cut. Therefore TSDCs and PcBNs are laser cut. This laser cut process could damage the cutting surface and gives the material individual burning marks, compared to EDM cut surfaces. Polycrystalline diamonds with a cobalt binder are therefore the only material in this thesis which could be cut in an EDM process. To get a deeper understanding of the influence on mechanical properties of these completely different cutting methods, a comparison of the same PCD material cut by both methods is investigated and analysed with the edge chip resistance test. Table 3 shows the test matrix of all the tested material.

Table 3: Test matrix before (RT) and after heat treatment (HT)

Type	Designation	Test Method without Heat Treatment		Test Method with Heat Treatment	
		B3B	Edge Chip Resistance	B3B	Edge Chip Resistance
TSDC	T-A	x	x	x	x
TSDC	T-B		x		x
TSDC	T-C		x		x
TSDC	T-D		x		x
TSDC	T-E		x		x
TSDC	T-F		x		x
TSDC	T-G		x		x
PCD	H-A		x		x
PCD	H-B		x		x
PCD	H-C		x		x
PCD	S-A	x	x	x	x
PCD	S-B	x	x	x	x
PCD	S-C		x		x
PCD	S-D	x	x	x	x
PcBN	P-A		x		x
PcBN	P-B		x		x
PcBN	P-C		x		x
PcBN	P-D		x		x
PcBN	P-E		x		x

4.2 Heat Treatment

To investigate any changes in the mechanical properties, all materials have to be heat treated under controlled and reproducible conditions. A program controlled laboratory furnace (Rohode^{TM} ME) is heated up to a final temperature of 850 °C with a heating rate of 85 °C per minute and held at that temperature for 3 minutes before the specimens get cooled down in protective atmosphere to room temperature. The whole experiment is done in a protected atmosphere (N_2) to avoid any oxidation of the diamond. The first run is done with the thermally stable material (Figure 16a). As expected, there is no visible damage on the surface of the material. Secondly the PcBN is heat treated and after an investigation under the light microscope the surface looks like it did before (Figure 16b). The high cBN content and the low cBN content PcBN show the same behaviour under high temperatures. A possible reason could be a nearly same strong bonding between the matrix and cBN. The

transformation from the cubic in its thermochemical more stable form, the hexagonal boron nitride, occurs at normal pressure only at high temperatures and therefore not relevant for this test. However, the polycrystalline diamond composite with the cobalt binder shows a less desirable behaviour. All carbide backed PCDs (Figure 16c) and all solid PCDs (Figure 16d) show visible cracks either at the edges or through the entire surface of the material. Even if the edges of the carbide backed PCDs get damaged, the interface between the tungsten carbide and the PCD is not affected. As a consequence of the thermal stability of solid and carbide backed PCD, this is an expected result.

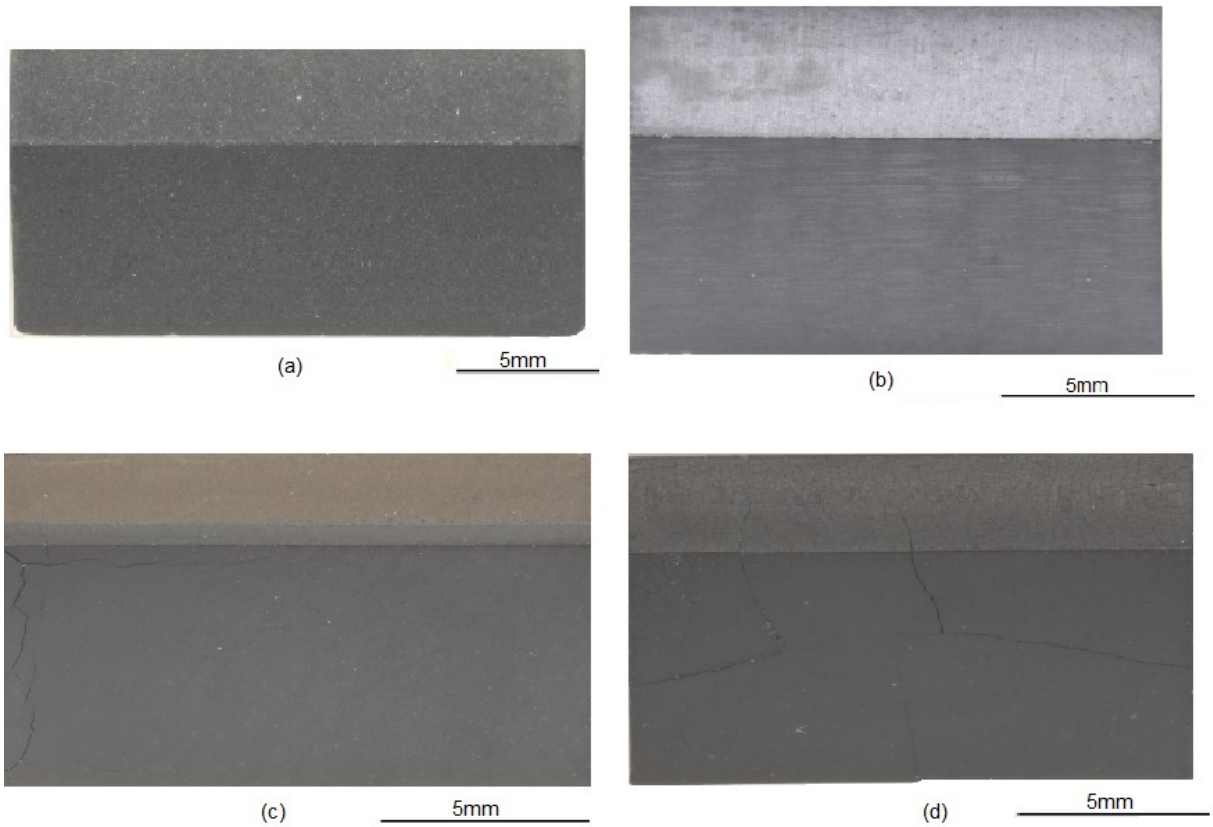

Figure 16: Examples for heat treated edge chip specimens. The surfaces of the T-B, (a), and P-C, (b), show, like all the materials in these classes, no visible damage. Carbide backed H-A, (c), and S-A, (d), cracks through the whole surface were found

5 Results and Discussion

5.1 DSC and X-Ray Phase Analysis

To determine the exothermic and endothermic reactions during the heating and cooling process a DSC404C calorimeter from Netzsch™ is used (Figure 17). The reference crucible is made out of Al_2O_3 and it is very important to do the first run without any specimens only with the Al_2O_3 crucible to get the so-called blind curve. With the blind curve it is possible to exclude any thermochemical or thermophysical changes from the Al_2O_3 during the analysis to focus and interpret the changes only from the investigated specimen.

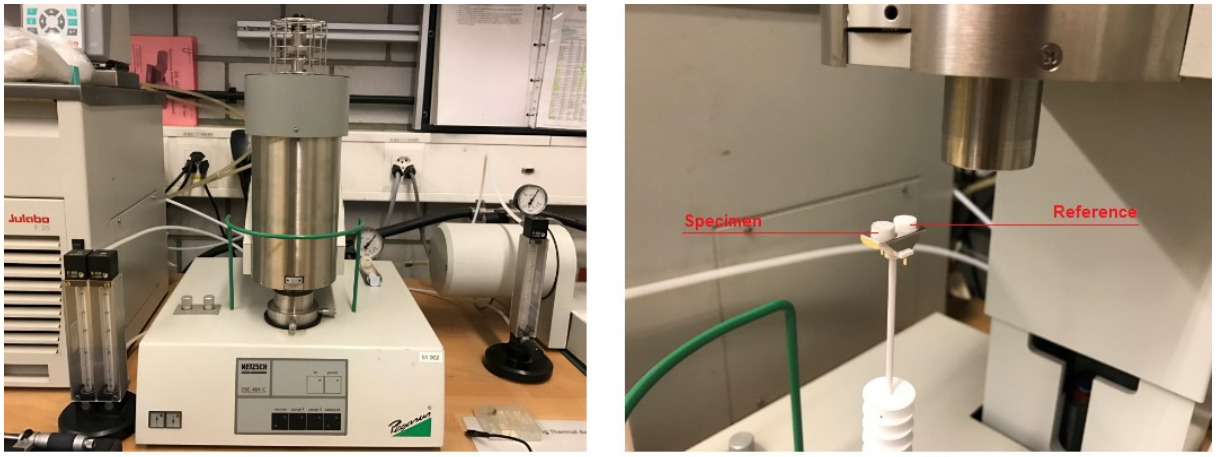

(a) (b)

Figure 17: Used equipment to determine the exothermic and endothermic reactions during the heating and cooling operation (a). The heating chamber with the conductive metal plates, the reference and the specimen crucible made out of Al_2O_3 (b)

5.1.1 DSC Results

As a first experiment with the DSC system, different grades of particulate diamond grit were tested. These grades had inclusions of two different catalyst alloys (iron-nickel and cobalt-iron) present in different levels.

As it is shown in Figure 18, there is no significant reaction even with the grade with the highest inclusion content, Grit-F. If there is catalytic graphitisation, a significant exothermic peak would occur at approximately 900 °C. The reason is that the metal content of even the lowest grade (Grit-F) is so low that catalytic graphitisation is not detected. The amount of catalytic material is certainly less than 1 %. This is at least a factor of 10 less than that in the PCD materials tested.

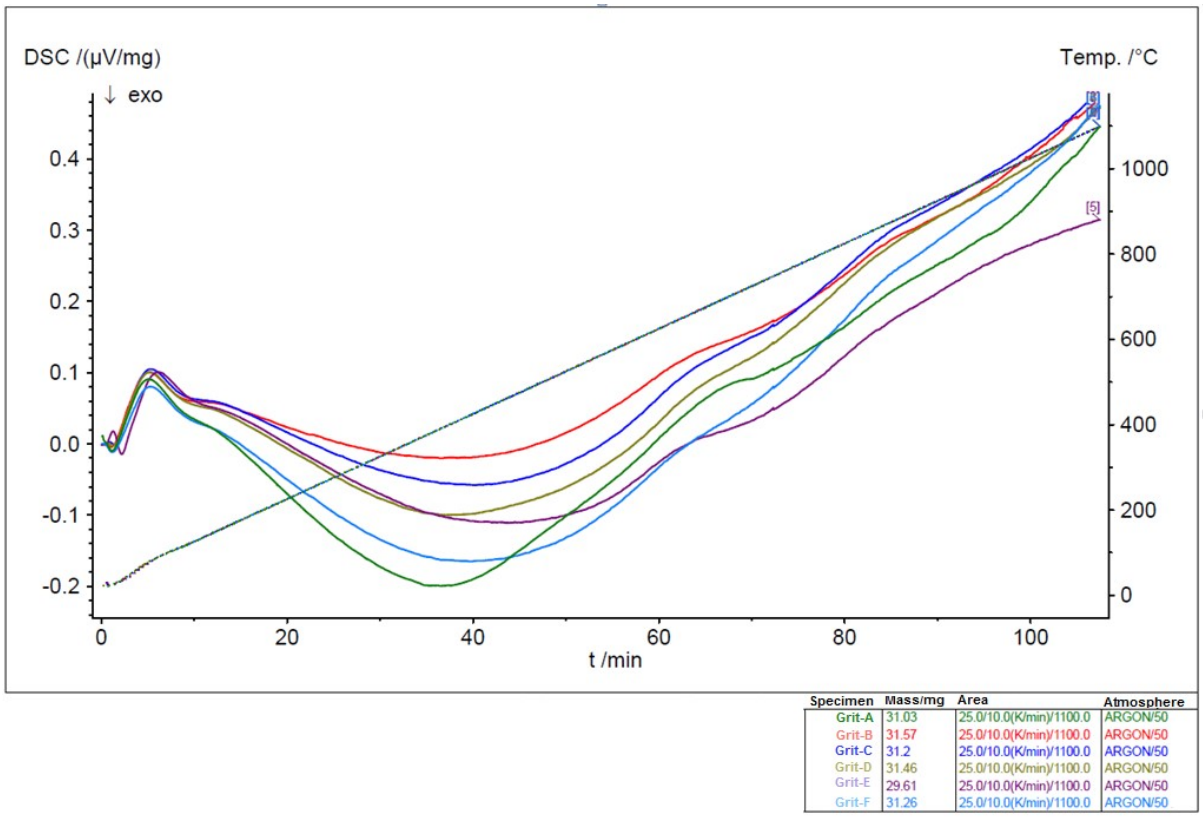

Figure 18: Different DSC curves of different diamond qualities: Green: Grit-A, Red: Grit-B, Blue: Grit-C, Gold: Grit-D, Violet: Grit-E, light blue: Grit-F

Secondly, one Co-bonded solid PCD (S-D) and a TSDC (T-B) are tested. The amount of cobalt in solid PCD is much higher than the amount of an equal catalyst in diamond grit. Figure 19 shows the comparison of S-D with a cobalt content of 10 % and T-B. There is a significant peak at about 900 °C on the S-D, which could be catalytic graphitisation, and no corresponding peak on the thermally stable material. A repeat run (“second run”) with the Co-bonded PCD showed no significant peak at 900 °C. This fits to the assumption the peak corresponds to graphitisation, as further graphitisation would not be expected on the second run.

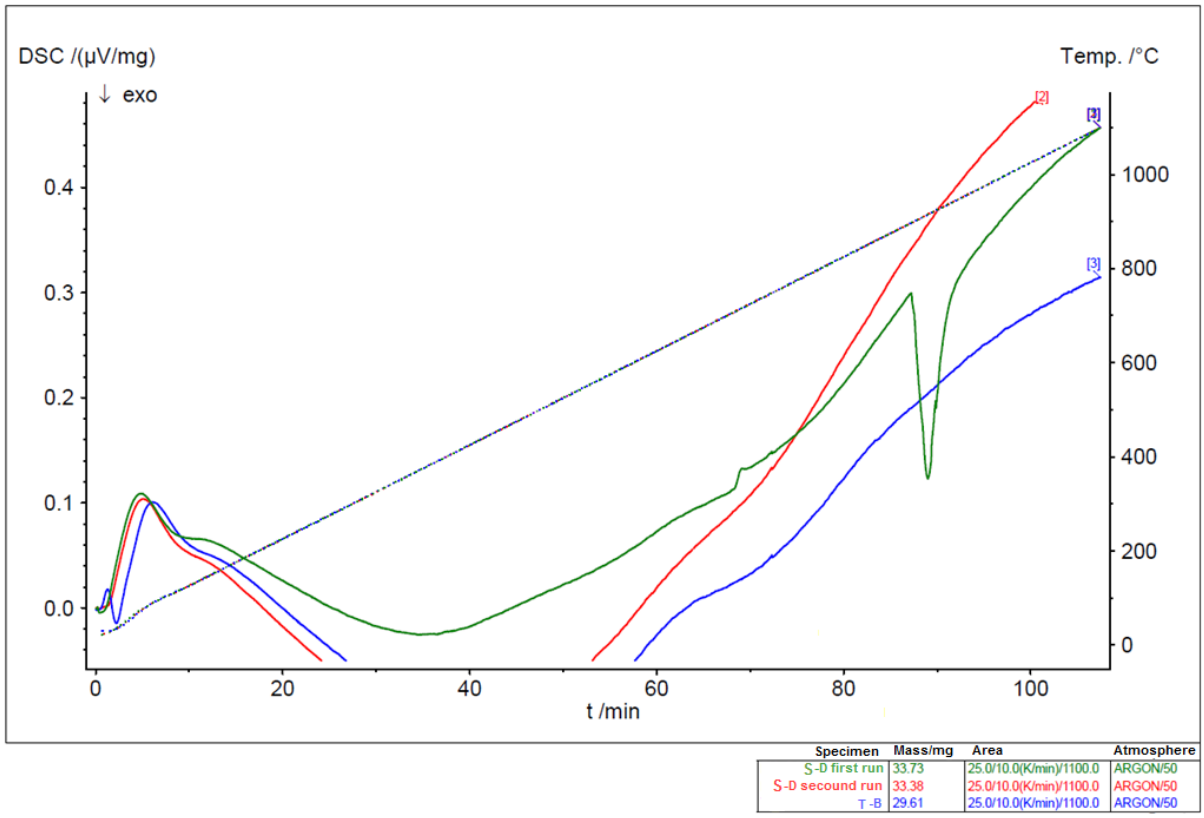

Figure 19: Comparison of a Co-bonded PCD and T-B. The S-D shows a significant peak at 900 °C. After the second run with the same specimen in the same conditions, the peak disappeared. Green: First run S-D, Red: Second run S-D, Blue: T-B

The cutting process of PCD material works with EDM. The EDM wire is made of copper and there could be some residuals on the PCD surface from the EDMing process. Figure 20 shows two DSC curves, one with copper and one without copper from S-D. The material without copper was cleaned with sandblasting; the material with copper was then tested with a small amount of additional pure copper powder. The results show an expected behaviour. There is a significant endothermic peak at 1084 °C, the melting point of copper. That is why any phase changes in copper can be excluded and all peaks that occur in the DSC curves are therefore from diamond-cobalt or diamond-SiC interactions.

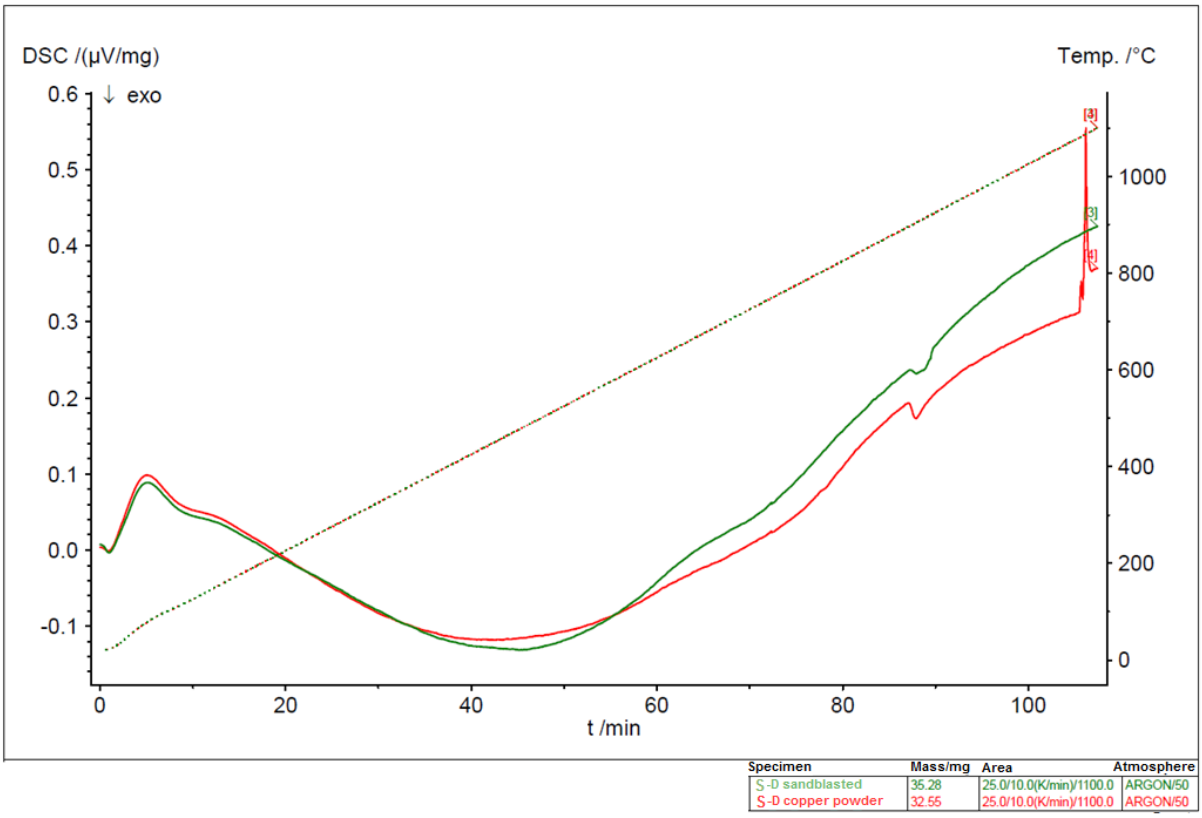

Figure 20: DSC curves of S-D material with and without copper with a significant peak at 1084 °C. Red: with copper, Green: without copper

The tests with diamond grit did not show peaks at 900 °C, as a result of the low metal content in the material. The thermally stable diamond composites show not exothermic or endothermic peak as a consequence of the absence of catalytic metal. There is a reaction of PCD at 900 °C which could be graphitisation. It is excluded that this is a phase change in copper, because this behaviour does not appear in a second run. However, to prove that the peak at 900 °C is catalytic graphitisation, further investigations with S-D are made.

5.1.2 X-Ray Phase Analysis

For the last step x-ray phase analysis is done in Leoben at the Materials Center Leoben. The measuring system is a Bruker^{TM} D8 Discover with a copper beam on the primary side. An energy dispersive detector is placed on the secondary side and the 2-theta range is from 9° to 21.5°. The specimens are shown in Figure 21.

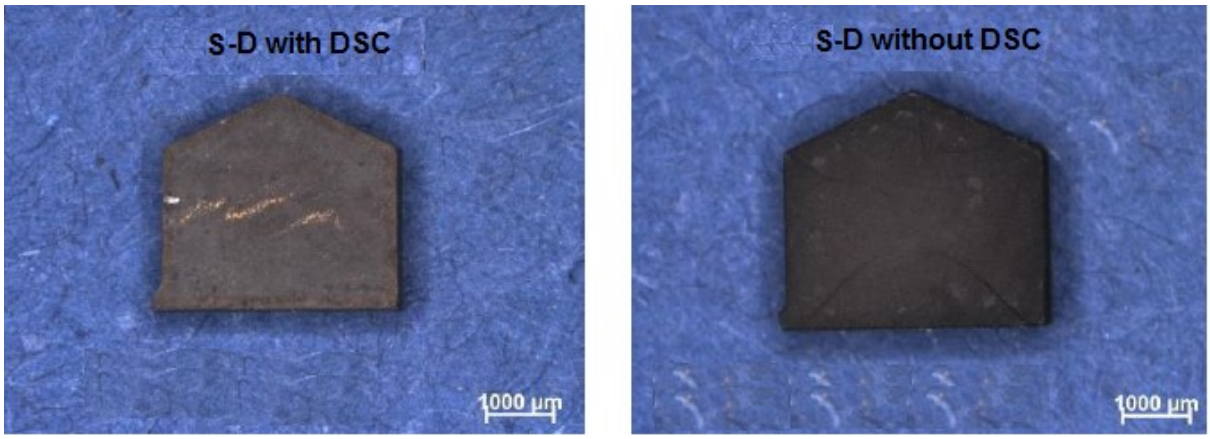

Figure 21: The S-D samples before (left) and after (right) one DSC cycle for x-ray phase analysis

Figure 22 shows an x-ray phase analysis of a Co-bonded PCD material. The red line is a specimen after one DSC cycle with a significant peak on the 2-theta scale at approximately 12° which proves the existence of graphite. This peak was not found on the sample without a DSC run and therefore it is clear that catalytic graphitisation happens as a result of the Co-diamond reaction at approximately 900 °C.

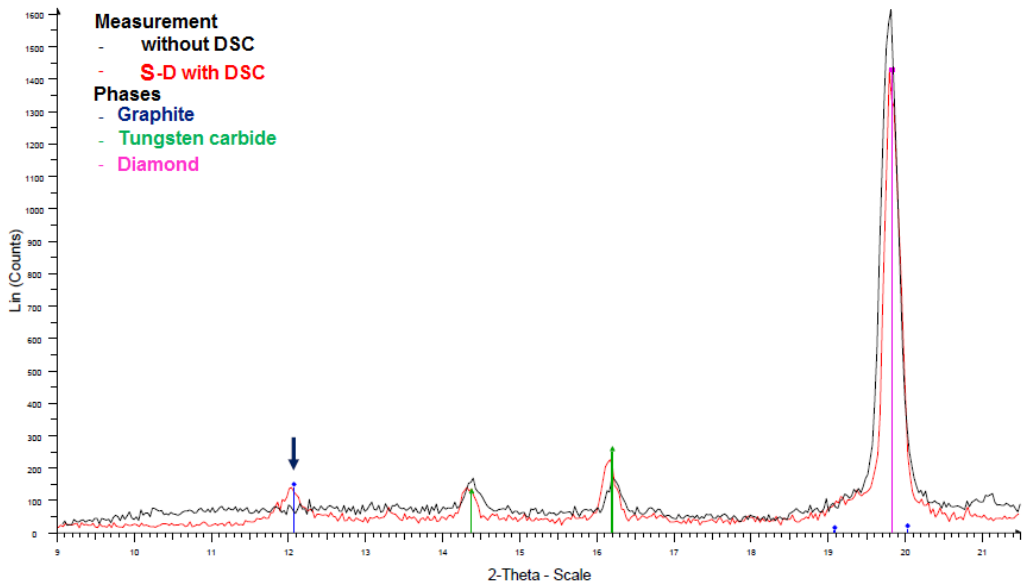

Figure 22: X-ray phase analysis of S-D with and without a DSC run

5.2 Strength Tests (B3B)

Strength tests were performed with the biaxial Ball-on-Three-Balls Test. The first step of the test is to apply a pre-force (10 N) to hold the specimen and the balls in position. Afterwards, the force is increased until fracture occurs. The test is invalid if the fracture of the samples does not start in the centre. The analysing process in this thesis was done with the help of “Interactive Web Mathematica” at the ISFK homepage [31]. The disc and the supporting balls are modelled with brick elements and surface-to-surface contact elements are used to simulate contacts between the balls and the disc [32]. The main difference in testing such

brittle materials like diamond composites compared to metals is the number of non-metallic inclusions, binderless agglomerates and microstructural inhomogeneities which come from a different diamond allocation in the workpiece.

In this thesis three different grades of Co-bonded solid PCDs and one grade of TSDC are investigated for strength. The test matrix is shown in Table 4. The reason for the different amount of tested specimens, especially after a heat treatment, is that it is very difficult and expensive to cut and prepare disc-shaped samples with a thickness to diameter ratio of 1:10 to 1:20 as a result of residual stresses which occurs during the sintering process.

Table 4: Test matrix for B3B tests and the number of specimens with and without heat treatment

Material	Number of specimens without heat treatment	Number of specimens with heat treatment	Diameter	Thickness
[/]	[/]	[/]	[mm]	[mm]
T-A	20	15	14,04 ± 0.02	1,0 ± 0.009
S-A	20	9	10,2 ± 0.02	0,6 ± 0.042
S-B	20	14	10,1 ± 0.06	0,6 ± 0.013
S-D	22	22	10,0 ± 0.03	0,9 ± 0.101

The heat treatment is described in a previous chapter. For determining the strength a universal testing machine from Zwick/Roel^{TM} (Zwick Z010 with a 10 KN load cell) is used. The test set up is shown in Figure 23. The T-A disks (14 mm diameter) are tested with a ball diameter of 9.525 mm and for the SPCD disks (10 mm diameter), balls with a diameter of 6.35 mm are used. All specimens are tested under laboratory conditions. The first step is to investigate all specimens for cracks and damages on the surface with an Olympus^{TM} SZH10 stereo microscope and the image analysis system analySIS^{TM} before the thickness and the diameter of the discs are recorded. The pictures from the specimens tested without any heat treatment show no visible damage on the surface from the production process (Figure 24).

Figure 23: The jig with the three supporting balls as used in the B3B test

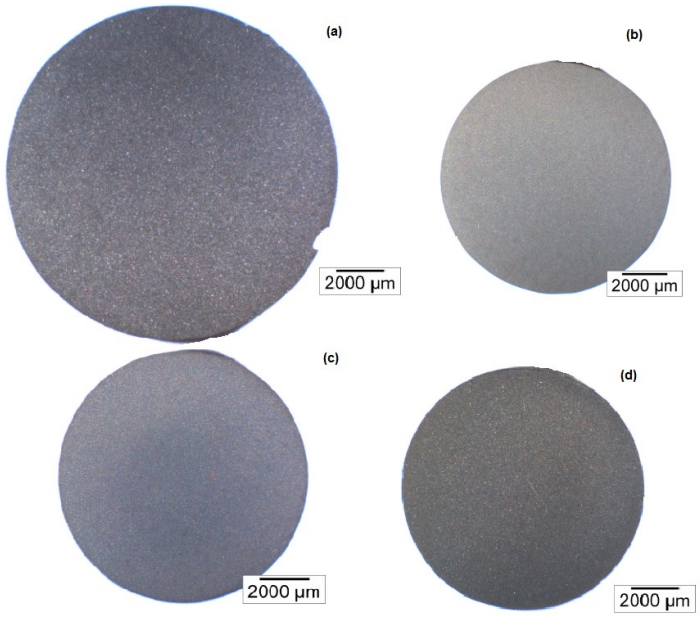

Figure 24: Microscope imaging before the strength tests without any heat treatment. No damage was found on the surface and no cracks are visible. (a) T-A, (b) S-A, (c) S-C, (d) S-D

After the heat treatment two of the Co-bonded diamond composites (S-B, S-C) show a network of cracks at the surface. The reason therefore could be the influence of the different thermal expansion coefficients, residual stresses from the sintering or a combination of these two effects. However, the grade S-D and the thermally stable T-A remain unaffected (Figure 25).

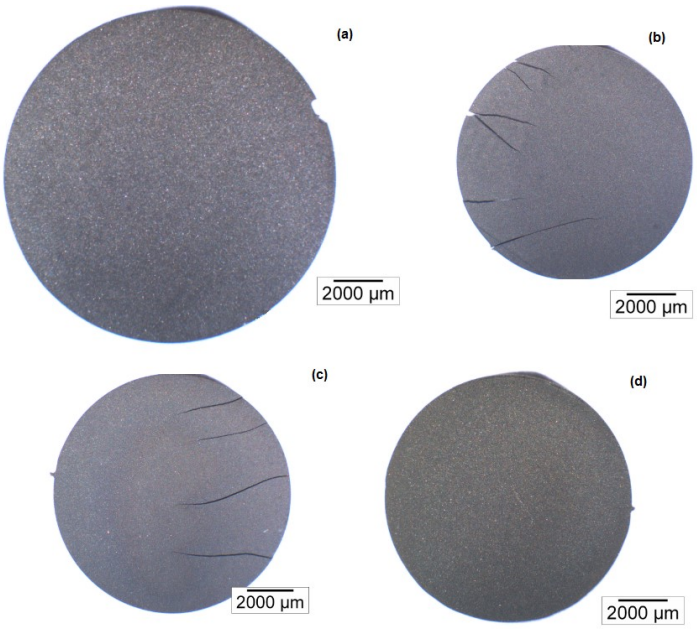

Figure 25: Microscope imaging after heat treatment before the B3B test. A network of cracks and huge damage on the surface of the low grade SPCDs are visible. (a) T-A, (b) S-A, (c) S-C, (d) S-D.

After this procedure each disc gets a number and the tension side is marked with a pen to localise it for further investigation. Next, each disc is put into the correct jig and after applying a pre-load of 10 N to hold the specimen in place between the three supporting balls and the loading ball, the tests are conducted with a constant loading rate of 0.5 - 0.8 mm/min. The load is increased until the specimens fail under the fracture load. The fracture force and the time from the start until the discs failed are recorded and the fracture strength is calculated using the applet at the ISFK homepage [31] for each disc.

5.2.1 Results

This section analyses the Ball on Three Balls strength test results using Weibull analysis and is done according to the standard EN843-5 [48]. All materials are tested with and without heat treatment and a comparison between them is made. Finally, a ranking between all materials with and without heat treatment is drawn to allow a comparison of the different classes but as mentioned above fewer specimens were tested.

The full number of specimens required for a reliable statistic interpretation is 30 specimens. For this investigation less than 30 specimens were investigated, therefore a possibility of an inaccuracy in the Weibull-parameters can become sufficient. The results are listed in Table 5.

Table 5: Results from the biaxial bending test with the confidence intervals

Material without Heat Treatment	m	σ_0
[/]	[/]	[MPa]
T-A	29,1 [20,1-36,8]	896 [883-910]
S-A	6,7 [4,6-8,4]	1617 [1518-1724]
S-C	11,6 [8,0-14,7]	1435 [1383-1489]
S-D	10,1 [7,1-12,6]	1572 [1510-1637]
Material with Heat Treatment		
T-A	22,1 [14,2-28,8]	993 [971-1016]
S-A	2,0 [1,1-2,7]	408 [290-582]
S-C	2,1 [1,3-2,7]	1041 [812-1341]
S-D	5,5 [3,9-6,9]	1167 [1085-1258]

A comparison between all the materials tested without heat treatment is shown in Figure 26. There is a cluster of Co-bonded material (S-A, S-C, S-D) which have a higher strength compared to the thermally stable T-A. The reason is that the stronger diamond-to-diamond bond is absent in in T-A. The 5 µm diamond PCD is the material with the highest strength but also with the highest scatter and therefore lowest Weibull modulus, in this PCD cluster. The multimodal S-D and the 25 µm S-C are very similar in strength and Weibull modulus.

The Weibull distributions of all tested materials after heat treatment are shown in Figure 27. The thermally stable material, T-A, shows nearly the same strength as it does without heat treatment. There is a loss in strength and Weibull modulus of the multimodal S-D but it is still the most consistent Co-bonded material. S-C is the best unimodal solid PCD and S-A is the worst Co-bonded diamond composite. The loss of strength of the solid PCDs could be a result of catalytic graphitisation and the huge damage during the heat treatment shown in Figure 25, where S-A and S-C exhibit networks of cracks all over the sample surfaces. There is no visible damage of the multimodal Co-bonded and the SiC bonded materials, which explains the lower scatter and higher strength after heat treatment.

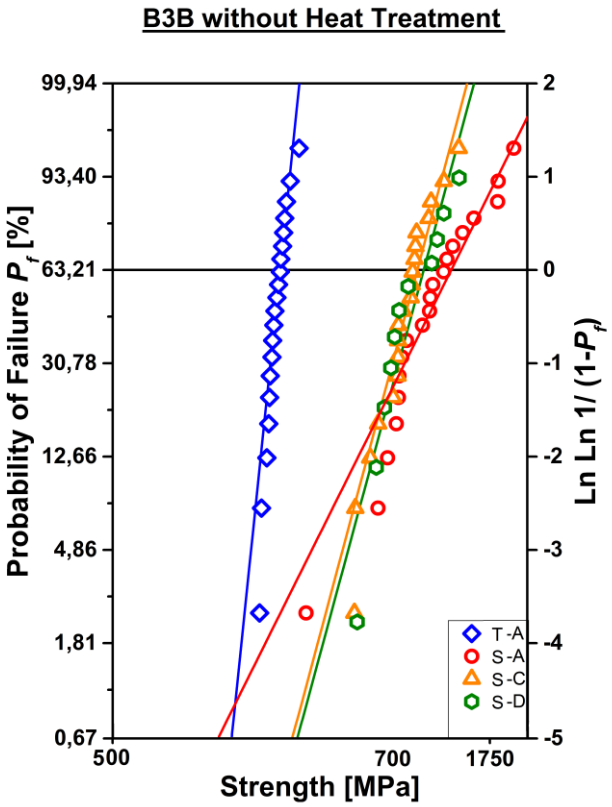

Figure 26: Weibull distributions for all tested material without heat treatment

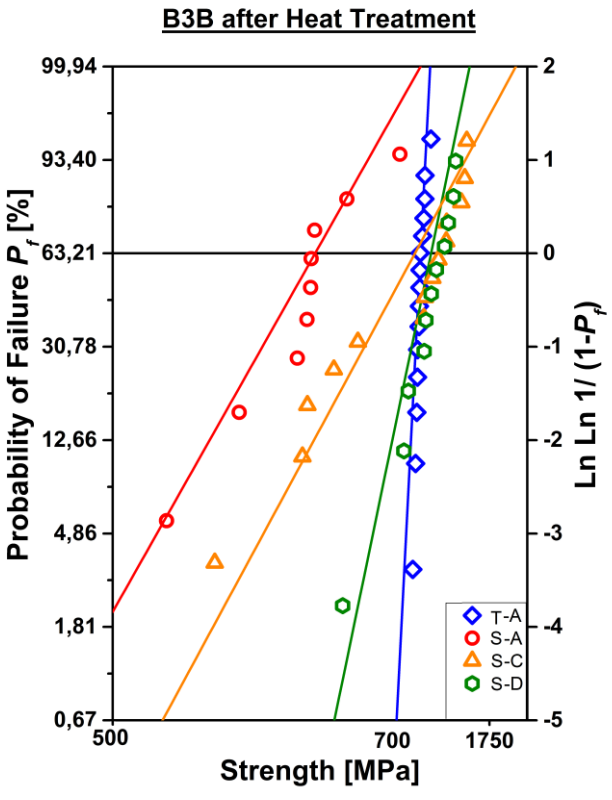

Figure 27: Weibull distributions for all tested material with heat treatment

The fact that the strength after the heat treatment is slightly higher compared to the strength without any heat treatment could have statistical reasons (experimental error) and in general it is possible to say that the material would not be influenced from the heat treatment under 850 °C. There is also an overlap of the confidence intervals from strength and Weibull modulus which shows a good reproducibility of the manufacture process and the thermally stable behaviour of the material.

The material with the highest strength is S-A (see Figure 28). However, this material consisting of about 10 mass% cobalt and a 5 µm diamond grain size has the biggest loss in strength and as material with the biggest scatter, also the worst Weibull modulus. Figure 25b shows the influence of the heat treatment and how high temperatures affect the surface quality. The effect of catalytic graphitisation is a likely explanation for the decreasing strength. S-A is the material with the smallest diamond grain size and therefore the material with the highest concentration of diamond-to-diamond bonds. The more diamond-to-diamond bonds the higher the strength which matches with the results from the non-heat treated material. The loss in reliability might be the consequence of the low number of discs which were tested. It is very difficult to cut the material and a lot of specimens broke during the EDMing as a result of the residual stress from the manufacturing process. Figure 26 and Figure 27 show the dramatic decrease of the strength after the furnace treatment and the Weibull modulus decreased from 6.7 to 2.0 which is depicted with the slope of the line.

S-C is a polycrystalline diamond composite with nearly the same amount of cobalt but with a 25 µm diamond grain size. The grain size has an influence on the diamond-to-diamond bond concentration. There is a loss in strength if the diamond-to-diamond concentration decreases which is why S-C has a lower strength compared to S-A. Catalytic graphitisation is always a problem with PCD at high temperatures and this explains the decreasing strength after heat treatment. Figure 27 highlights the temperature sensitivity of the material. It was slightly easier to cut the test specimens and therefore the number of discs available was higher compared to the 5 µm S-A.

S-D is a multimodal sintered diamond composite in contrast to the two unimodal S-A and S-C. S-D has a higher packing density which decreases the distance between the diamonds and enhances the strength as a result of the diamond-to-diamond bonding. S-D shows the highest strength after the heat treatment and is the second strongest material tested without a temperature influence. The cutting process of this solid PCD is better-known than for the other two grades, and therefore the largest number of discs was available for testing. The decrease in strength and of the Weibull modulus is a result of the catalytic graphitisation even if it is a multimodal material. The bond material is cobalt which makes it not as suitable as TSDCs for higher temperatures. S-D is the most promising solid PCD and the Weibull distribution is shown in Figure 26 and Figure 27.

Figure 28 shows strengths versus Weibull modulus diagrams of heat treated and not heat treated specimens. If the strength values and the Weibull-modulus do not overlap, a statistically significant difference between the samples exists. The results show an expected

behaviour. There is a cluster of the solid PCDs with the heat treated and not heat treated specimens, the thermally stable material, T-A, shows a different behaviour.

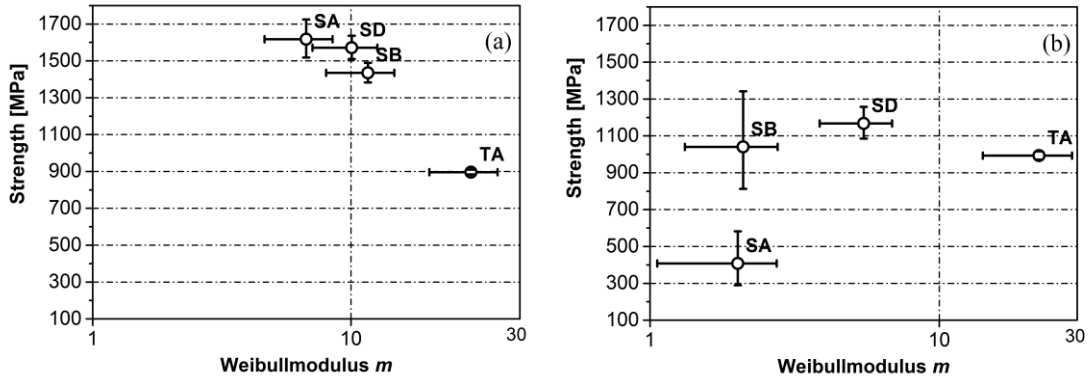

Figure 28: Comparison of the strength test results for the not heat treated (a) and heat treated (b) samples

Conversion to Standard Bending Specimens

Table 6 and Table 7 represent the results for the conversion to standard bending tests. The calculation is based on the formulas explained and listed in chapter 3.3.1.

There is a big difference between the results of the B3B-Test and the calculated results for Four-Point-Bending test. This could be explained according to the size effect of strength in brittle materials, as mentioned in previous chapters. Very interesting is the small difference between 4PB and B3B strength of grade T-A. This is a result from the high Weibull modulus and the homogeneous defect distribution of the material. By increasing the Weibull modulus the approach of the B3B strength to the 4PB strength gets much better. This explains the big difference between the strength conversion after the heat treatment, where the Weibull modulus dramatically decreases.

Table 6: Conversion to standard Four-Point-Bending test for not heat treated material

Material without HT	Weibull Parameters		
	B3B		4PB calculated with the effective surface
	σ_0	m	σ_0
	[MPa]	[/]	[MPa]
T-A	896 [883-910]	29,1 [20,1-36,8]	761
S-A	1617 [1518-1724]	6,7 [4,6-8,4]	834
S-C	1435 [1383-1489]	11,6 [8,0-14,7]	915
S-D	1572 [1510-1637]	10,1 [7,1-12,6]	1073

Table 7: Conversion to standard Four-Point-Bending test for heat treated material

Material HT	Weibull Parameters		
	B3B		4PB calculated with the effective surface
	σ_0	m	σ_0
	[MPa]	[/]	[MPa]
T-A	993 [971-1016]	22,1 [14,2-28,8]	813
S-A	408 [290-582]	2,0 [1,1-2,7]	218
S-C	1041 [812-1341]	2,1 [1,3-2,7]	554
S-D	1167 [1085-1258]	5,5 [3,9-6,9]	685

5.2.2 Fractography

The practical application of fractography is divided into three main endeavors:

- To analyze unexpected in-service failure,
- To improve a material, and
- To control the quality of a production.

It is crucial to analyze the material behavior at or during fracture. The identification of the origin of a defect shows possible weak points within the microstructure and can lead to improvements during manufacturing. Fractography is generally an effective way to determine the load situation and quality of the material or compound [49].

During development, fractography is essential for continuous controlling of the material and is a major part of product improvement. Through fractography the mechanically weakest area, found through the origin of fracture, can be determined. When the type of fracture is defined, it is possible to prevent further defects based on this knowledge, e.g. in improvements of the production chain to augment the stability of compounds [49]. Microfractography is a type of fractography that investigates the interaction of crack and microstructure at microscopic levels that has been used especially during the last years [50].

All mentioned methods of fractography of materials and structural compounds can also be applied for use in quality control [49].

The fractographic analysis is performed on selected surfaces of specimens without heat treatment from T-A, S-A and S-C (see Figure 24 chapter 5.2). The tensile strength side of the specimens is orientated on the top side of the picture. All critical defect sizes are calculated with the well-known Griffith criterion (equation 4), which connects the critical load, σ, with the flaw size, a.

This criterion implies that crack-like flaws become critical, if their stress intensity factor

$$K=\sigma Y\sqrt{\pi a} \tag{12}$$

exceeds the fracture toughness K_{IC} [51]

$$K \gg K_{IC} \tag{13}$$

where σ is the applied stress and Y is a geometric factor. This geometric factor is 1.12 for critical defect size for semi ellipsoid cracks and 0.63 for critical defect size for penny shaped cracks. It is possible to calculate the critical defect size (a_c), either on the surface or in the volume, from the Griffith/Irwin criterion as follows:

$$a_c= \frac{1}{\pi}\left(\frac{K_{IC}}{Y\sigma}\right)^2 \tag{14}$$

Table 8 shows the critical defect sizes for all investigated materials. All defect sizes are calculated with a fracture toughness of 10 $MPam^{1/2}$.

Table 8: Critical defect sizes for surface and volume defects

Material	Without heat treatment		Without heat treatment	
	a_{cV}	a_{cV}	a_{cV}	a_{cS}
[/]	[µm]	[µm]	[µm]	[µm]
T-A	95	95	101	33
S-A	2082	2082	37	12
S-C	543	543	42	14
S-D	97	97	41	13

The critical defect sizes are much bigger in the heat treated specimens compared to the specimens tested without heat treatment. This is an effect of the lower strength, where the lower the strength the higher the critical defect size is. Figure 29 shows a SEM picture of the surface of the thermally stable diamond composite, T-A. The surface shows a lot of defects and pores, which are much bigger compared to the cobalt bonded PCDs. SEM pictures from the not thermally stable diamond composite S-A and S-C are shown in Figure 30 and Figure 31. The surface structures are completely different to T-A, which is a result of the different binder material. All measured surface defects are lower than the calculated critical defect sizes and therefore, volume defects could be the main influence on the strength of this material.

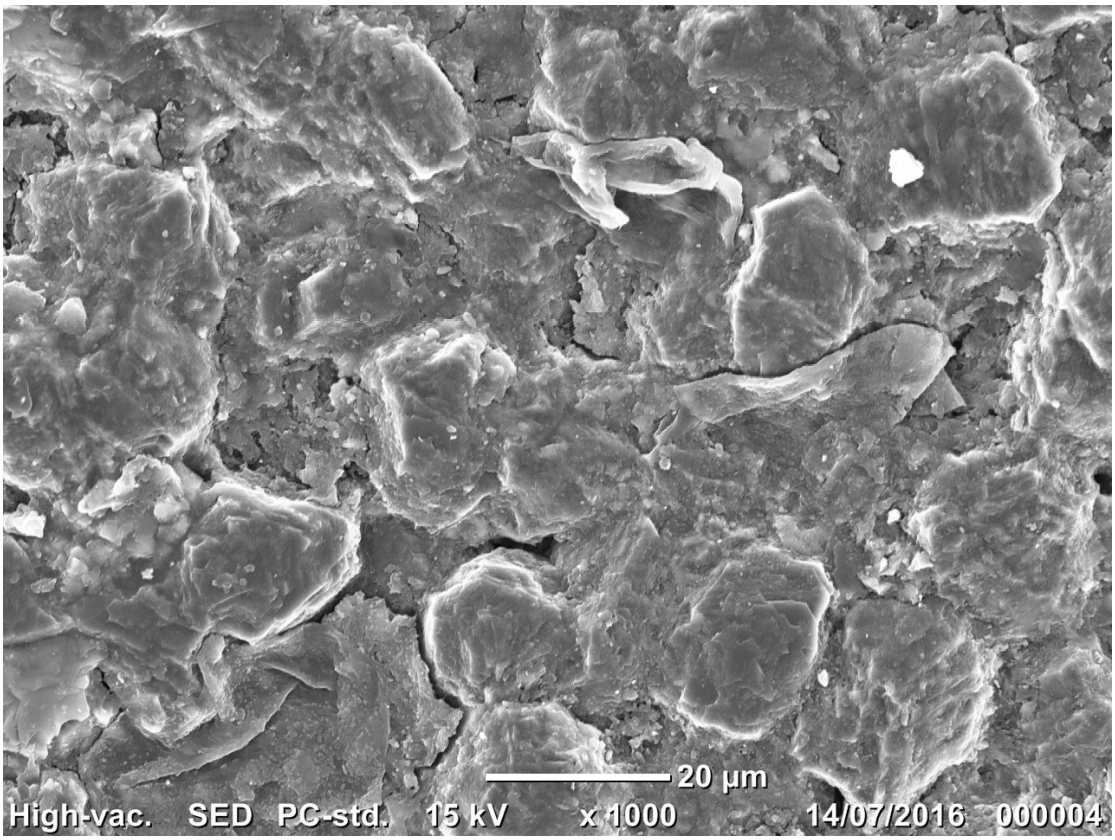

Figure 29: SEM picture of the surface of T-A without heat treatment

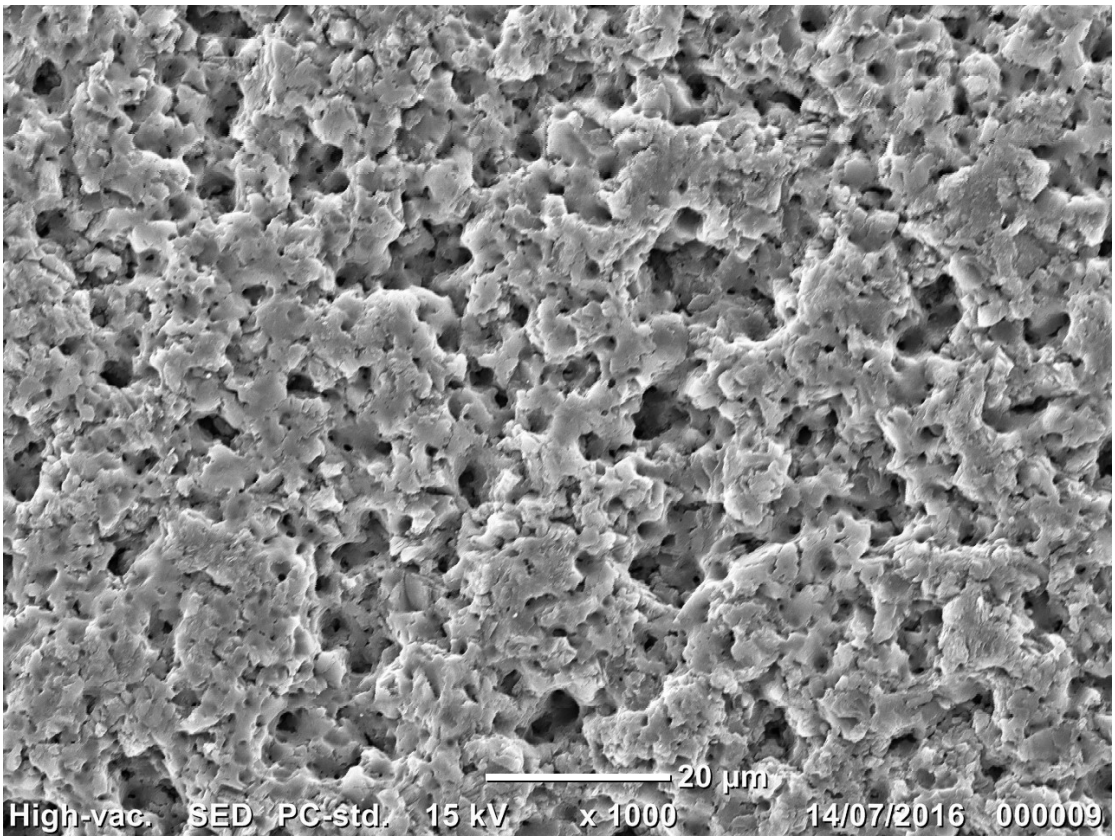

Figure 30: SEM picture of the surface of S-A without heat treatment

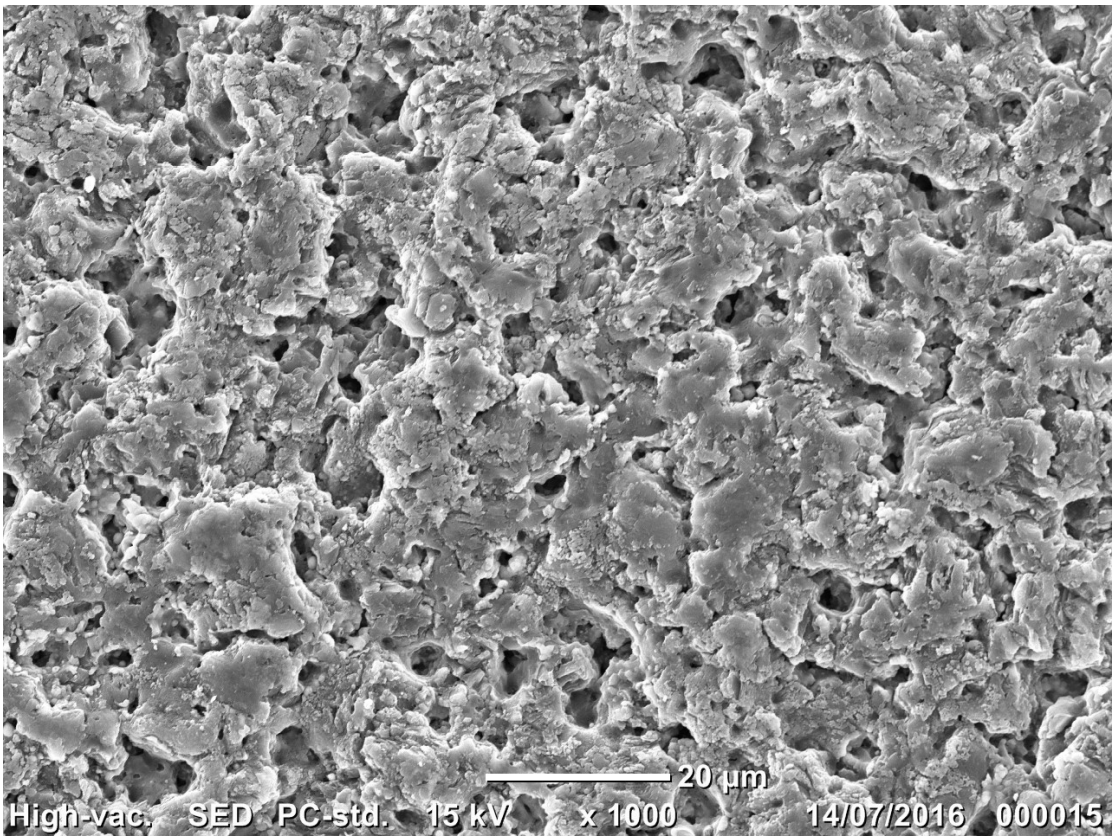

Figure 31: SEM picture of the surface of S-C without heat treatment

However, additional SEM investigations to investigate the fracture surface on selected specimens are done. The selection is based on the strength results and specimens with the lowest strengths and therefore with the biggest critical defect sizes are investigated. Figure 32 and Figure 33 show the fractographic investigations of the T-A. Figure 34 and Figure 35 show the fracture surface of S-A and Figure 36 respectively Figure 37 show the fracture surface of S-C. It is not possible to identify an exact fracture starting point even with the SEM and higher magnifications. As a result of the high pressure manufacturing process, it is possible to say that volume defects, like pores, could be excluded and the critical defect and therefore the laminating factor for the strength depends on the surface quality.

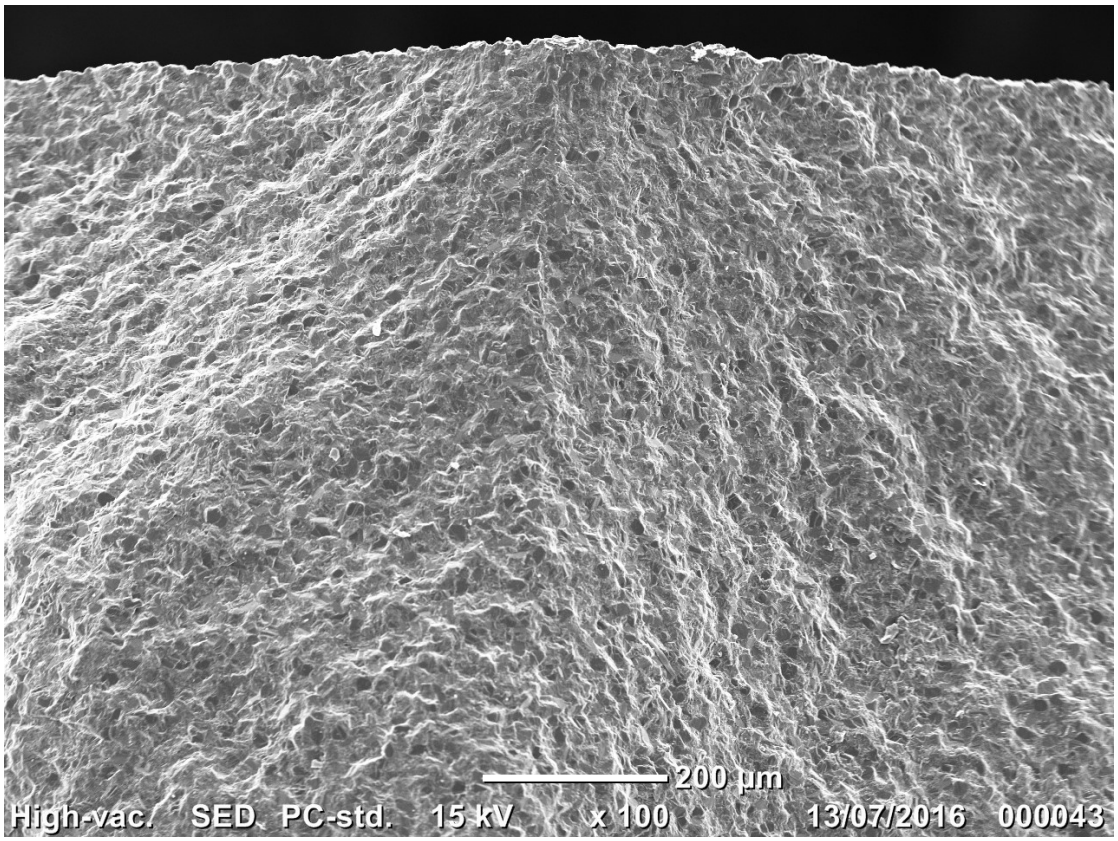

Figure 32: SEM picture of the fracture surface of T-A without heat treatment. The tensile strength side is orientated on the top side of the picture

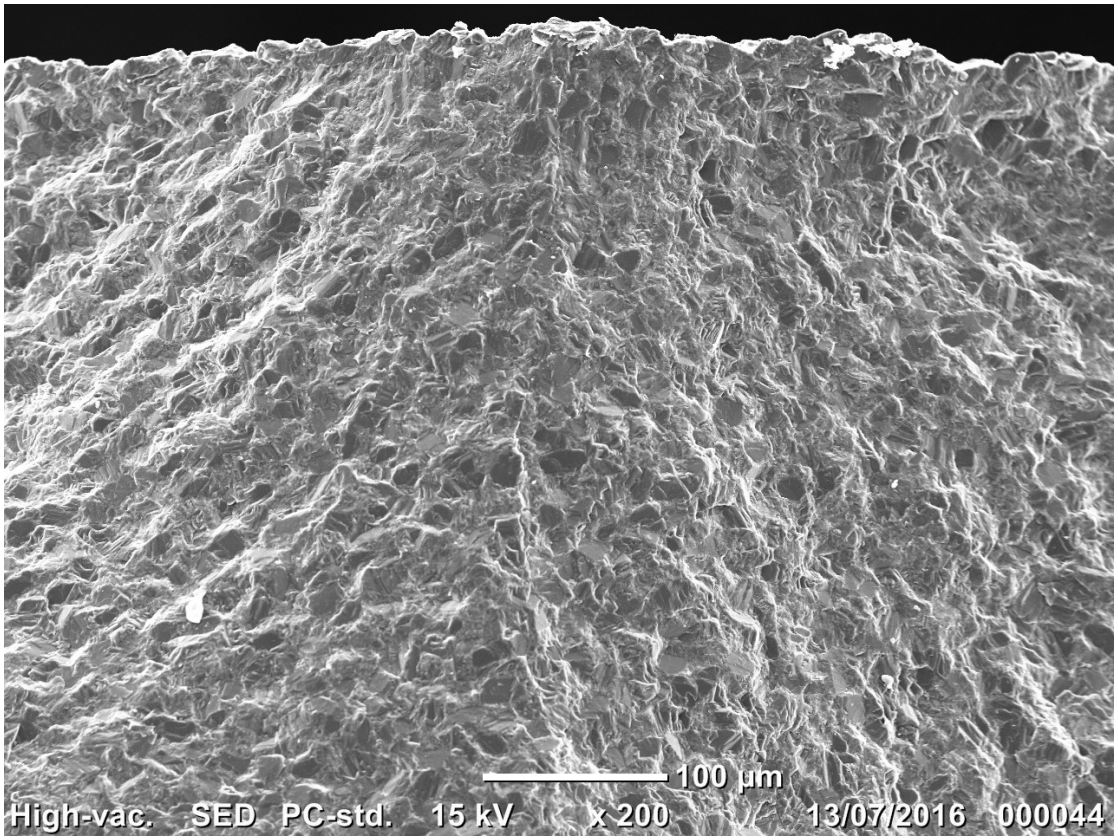

Figure 33: SEM picture with a higher magnification of the fracture surface of T-A without heat treatment. The tensile strength side is orientated on the top side of the picture

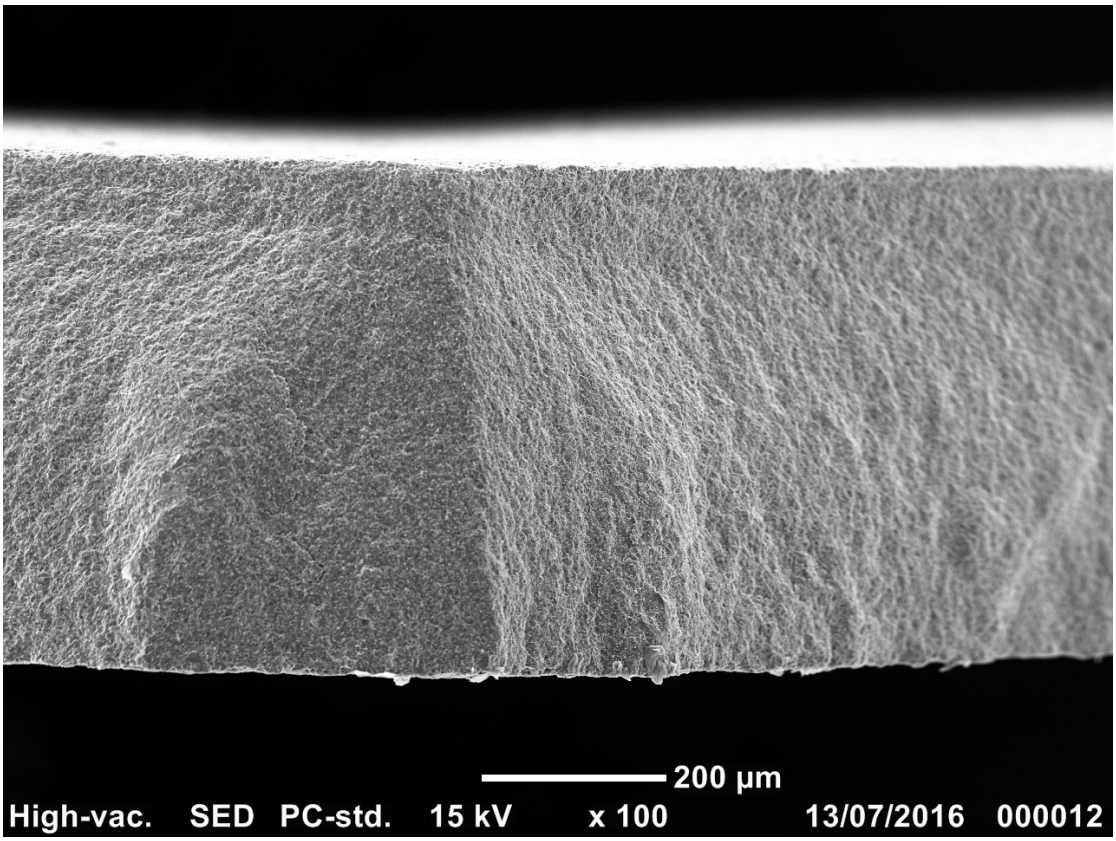

Figure 34: SEM picture of the fracture surface of S-A without heat treatment. The tensile strength side is orientated on the top side of the picture

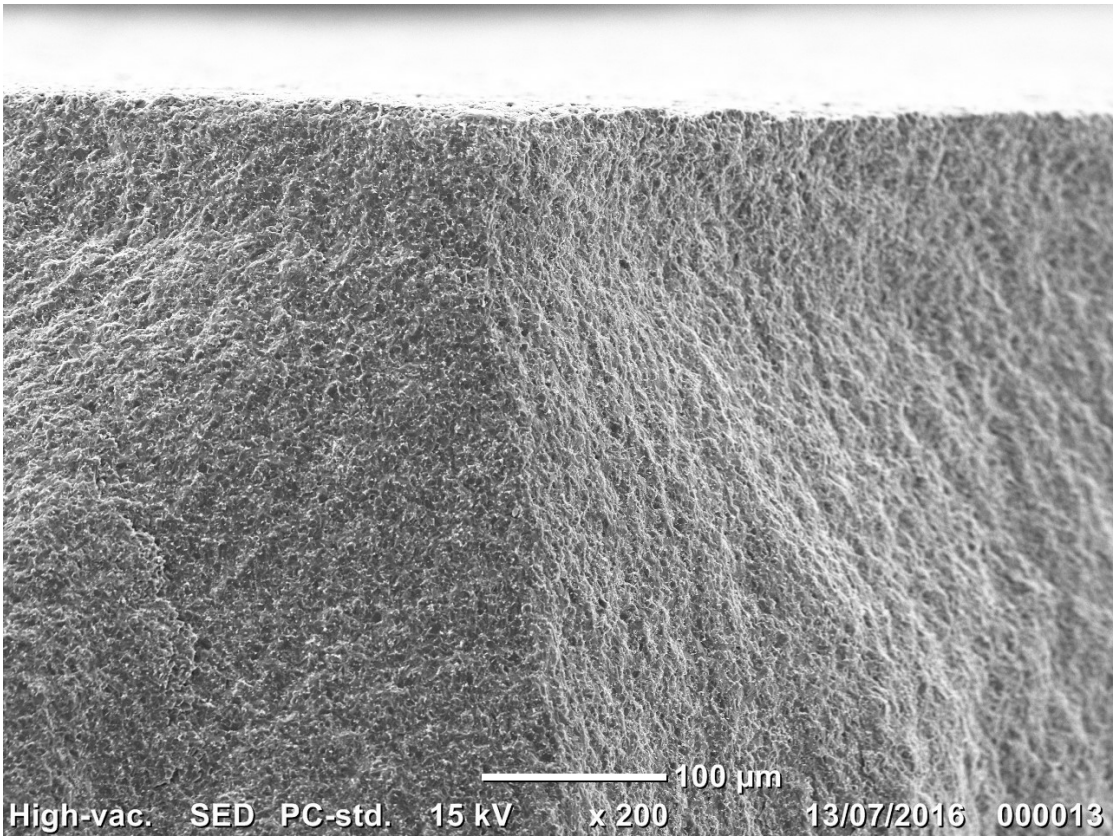

Figure 35: SEM picture with a higher magnification of the fracture surface of S-A without heat treatment. The tensile strength side is orientated on the top side of the picture

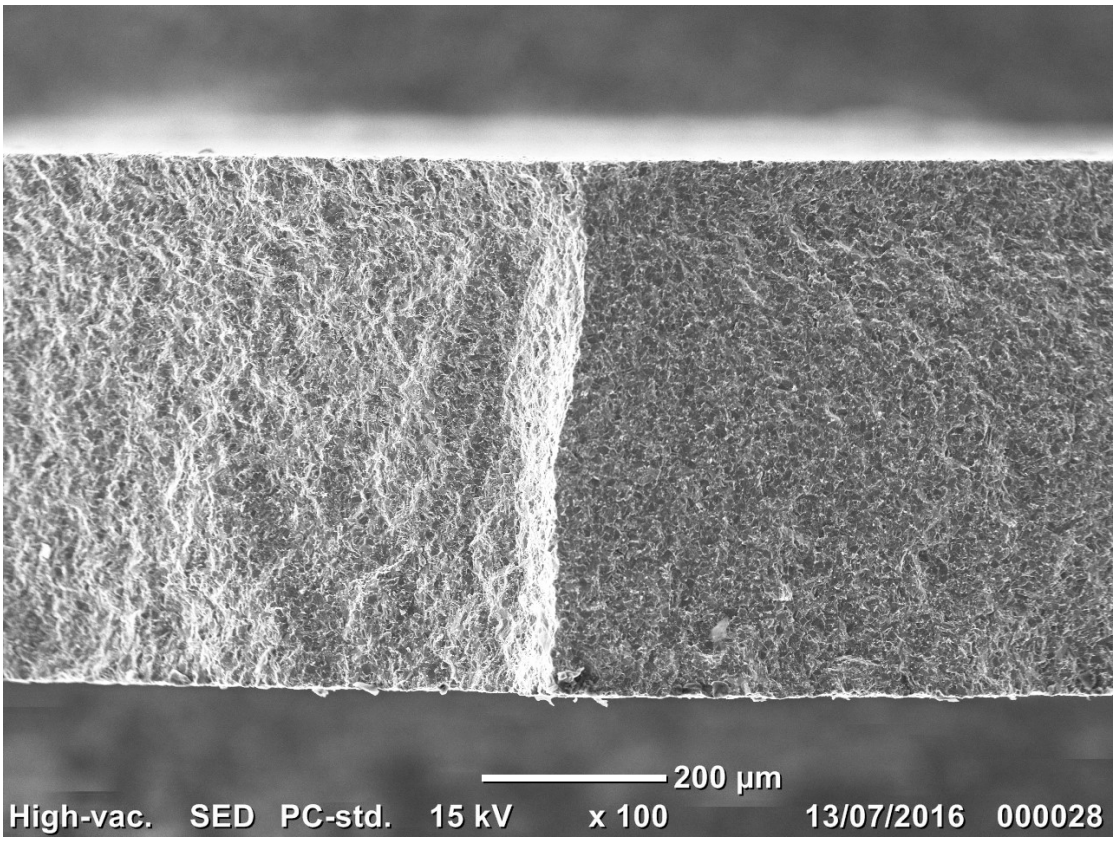

Figure 36: SEM picture of the fracture surface of S-C without heat treatment. The tensile strength side is orientated on the top side of the picture

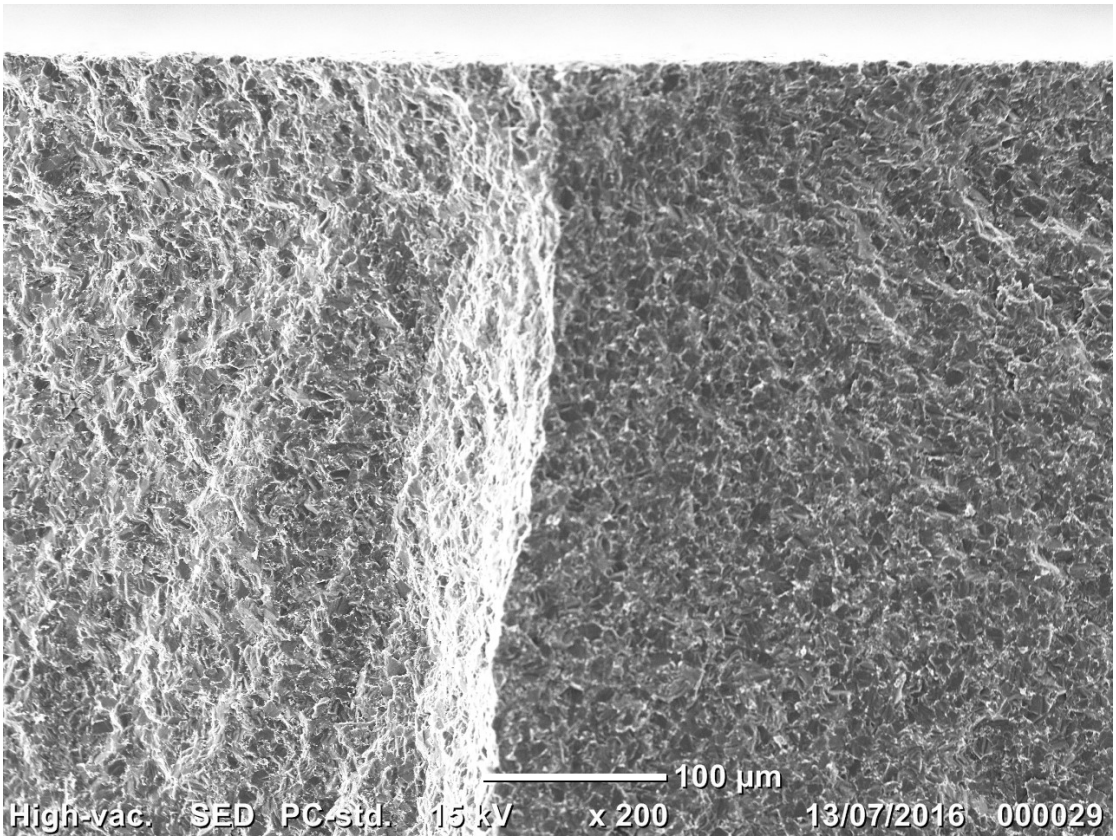

Figure 37: SEM picture with a higher magnification of the fracture surface of S-C without heat treatment. The tensile strength side is orientated on the top side of the picture

5.3 Edge Toughness Test

For determining the edge toughness of different polycrystalline diamond composites, thermally stable diamond composites and polycrystalline cubic boron nitride, a 500 kg testing machine (ET500) from Engineering Systems (NOTTM, UKK) is used (Figure 38).

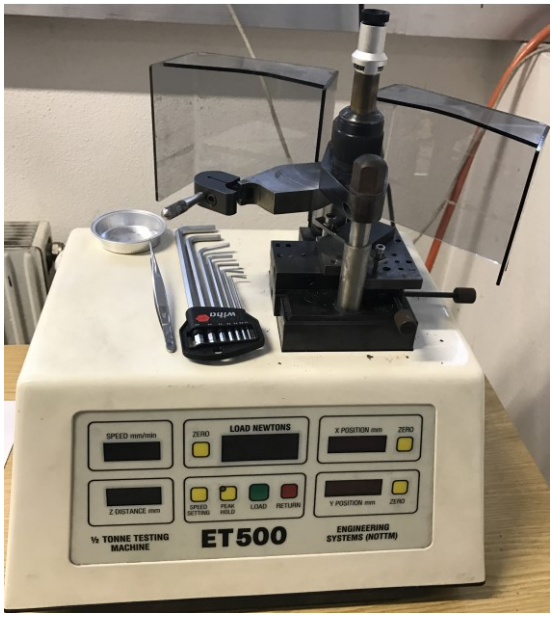

Figure 38: ET500 testing machine for edge toughness tests

In this thesis, the edge of the specimen is loaded by a tungsten carbide Rockwell indenter with 10 % cobalt content (CTS20 from Ceratizit^{TM}). The specimen is loaded with an increasing load and different distances from the edge until edge flaking occurs. The testing speed is 0.5 mm/min and the chipping load, *F*, is recorded each time. All tests are performed in standard laboratory conditions at room temperature and according to CEN/TS 843-9 [38] a 90° angle between the plane surfaces is 90° is obtained. An example for a new indenter and an indenter after one indentation is shown in Figure 39.

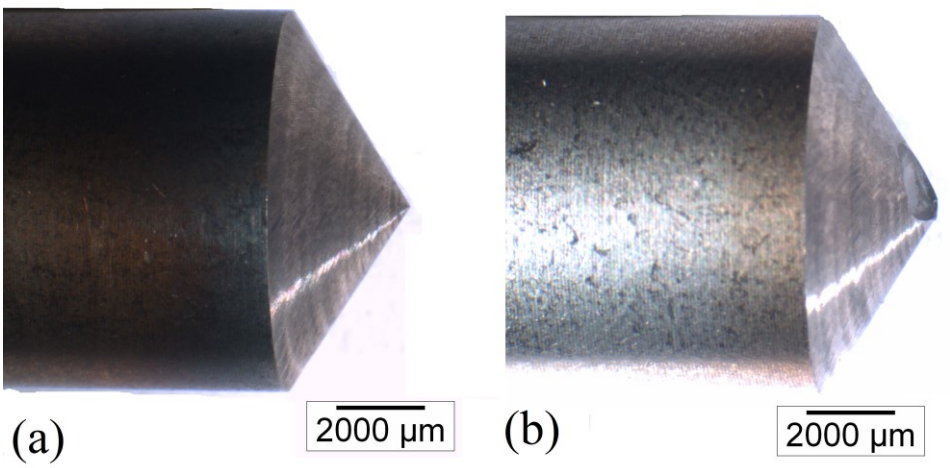

Figure 39: Indenter before (a) and after the test with the typical damage on the tip (b)

To verify the 90° angle, all specimens are investigated with an Alicona^{TM} measuring instrument (Figure 40).

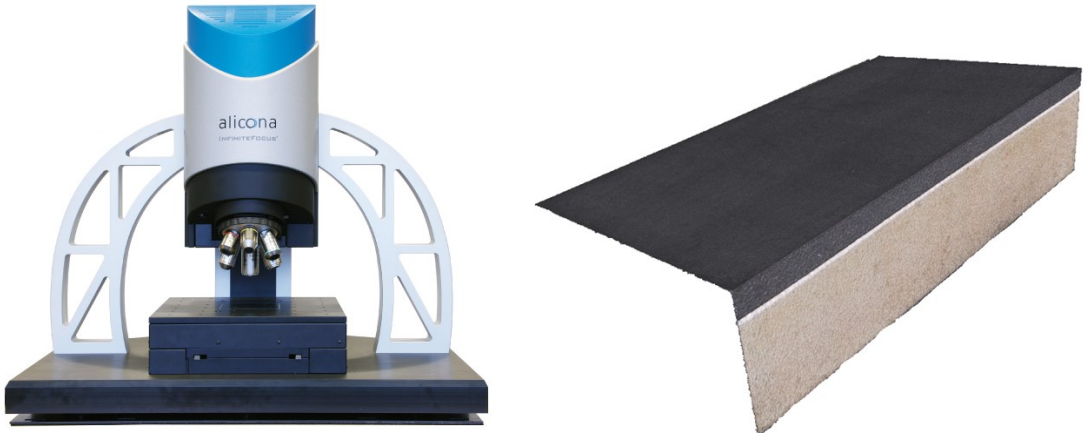

Figure 40: AliconaTM measurement equipment (left) and a visualisation of a carbide backed PCD to verify the 90° angle left

The indenter is positioned using a microscope which is assembled on the ET500. It is not possible to determine the distance from the edge by using this microscope in accuracy which is needed. Therefore, an Olympus^{TM} SZH10 stereo microscope and the image analysis system analySIS^{TM} are used to measure the exact distance of the loading point from the edge after the test.

It is critical that the tip of the indenter is re-sharpened after each indentation. Nevertheless, sometimes the damage to the indenter is so great that the indenter breaks into two pieces and cannot be used anymore. However, testing very brittle materials like PCD could be very difficult and often show invalid results. It is not allowed to use a result if a chip overlaps with another chip or if a chip breaks through the whole plane and reaches the bottom edge (Figure 41). An example of a valid test is given in Figure 42

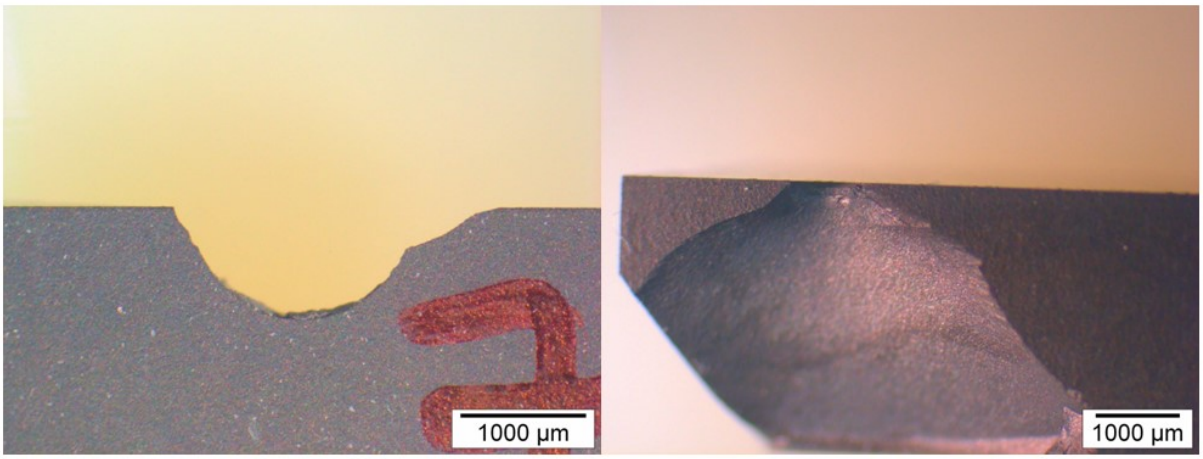

Figure 41: An invalid edge flake test on PCD material. The chip broke through the entire specimen. It is important to investigate all planes of the sample.

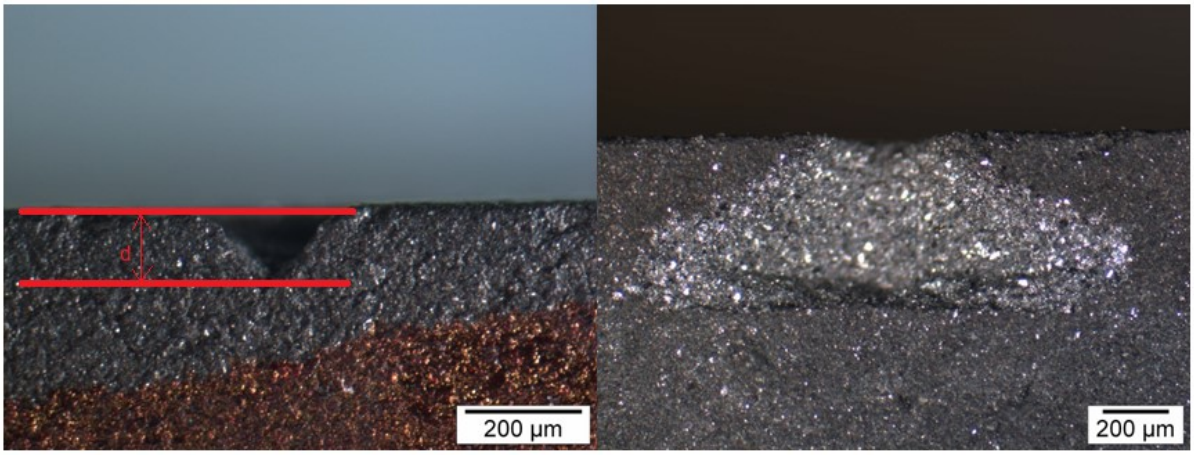

Figure 42: A valid result of an edge flake test on TSDC. The chip does not interact with another chip and the break out is not at the bottom edge

5.3.1 Results of Edge Toughness Tests

This section considers the results of the edge toughness test and allows a comparison between the different materials in one class, for example T-A and T-B. Table 9 gives an overview of all tested materials. 5 indentations were done for each material except on T-C which was also used for setting up the test. Nevertheless, a total of 7 grades of SiC-bonded diamond composite, 3 different Co-bonded PCDs with and without a tungsten carbide backing and 5 different grades of cubic boron nitride were tested with a total number of 200 indentations.

Table 9: Results of edge chipping test and tested material

Material	Results not Heat Treated	Results Heat Treated
[/]	[N/mm]	[N/m]
T-A	2527 ± 197	2402 ± 1333
T-B	1872 ± 649	1791 ± 479
T-C	1384 ± 468	1723 ± 548
T-D	2946 ± 443	1735 ± 223
T-E	1240 ± 166	1572 ± 397
T-F	2748 ± 275	2808 ± 527
T-G	2251 ± 222	2283 ± 151
H-A	2823 ± 661	3575 ± 2420
H-B	3359 ± 599	3224 ± 316
H-C	2987 ± 821	2418 ± 917
S-A	2832 ± 420	858 ±681
S-C	3029 ± 588	3028 ±1690
S-D	3508 ± 379	3172 ± 1388
P-A	2558 ± 1110	3882 ± 2565
P-B	2261 ± 438	2463 ± 698
P-C	3919 ± 705	2554 ± 749
P-D	2209 ± 206	2002 ± 703
P-E	2504 ± 452	2219 ± 311

The first part of this section focuses on the comparison between the different grades in the different material classes.

5.3.1.1 Solid PCD

The heights of the solid PCD specimens are all the same with 3.2 mm except the S-D with 2 mm. As outlined in the previous chapter, testing of brittle materials is very difficult. Therefore the distance from the edge has to be chosen very carefully to avoid invalid measurements like an overlapping of the breakouts or damage to the indenter before damaging the specimen. It was not possible to test S-B because the material was completely damaged during the heat treatment. Nevertheless, three different grades of solid PCD (two unimodal and one multimodal) were investigated. Figure 43 shows the edge toughness for the different grades of tested solid PCD. S-A is a 5 µm diamond grain size material. The behaviour is very similar to the biaxial strength testing in the previous chapter. The decrease in edge toughness is likely to be the result of catalytic graphitisation. The standard deviations of the S-C and S-D increases significantly after the heat treatment and the mean edge toughness is slightly higher compared to the S-A. The best result for the Co-bonded solid diamond composite comes from S-D. The multimodal material is very consistent without heat treatment and losses a little bit of its edge toughness after the heat treatment. However, the edge toughness of S-D after heat treatment is still higher than the edge toughness of the other samples without the temperature treatment which makes it suitable for applications in higher temperatures. Nevertheless, it is not possible to say that S-C and S-D show a big significant difference in the edge toughness.

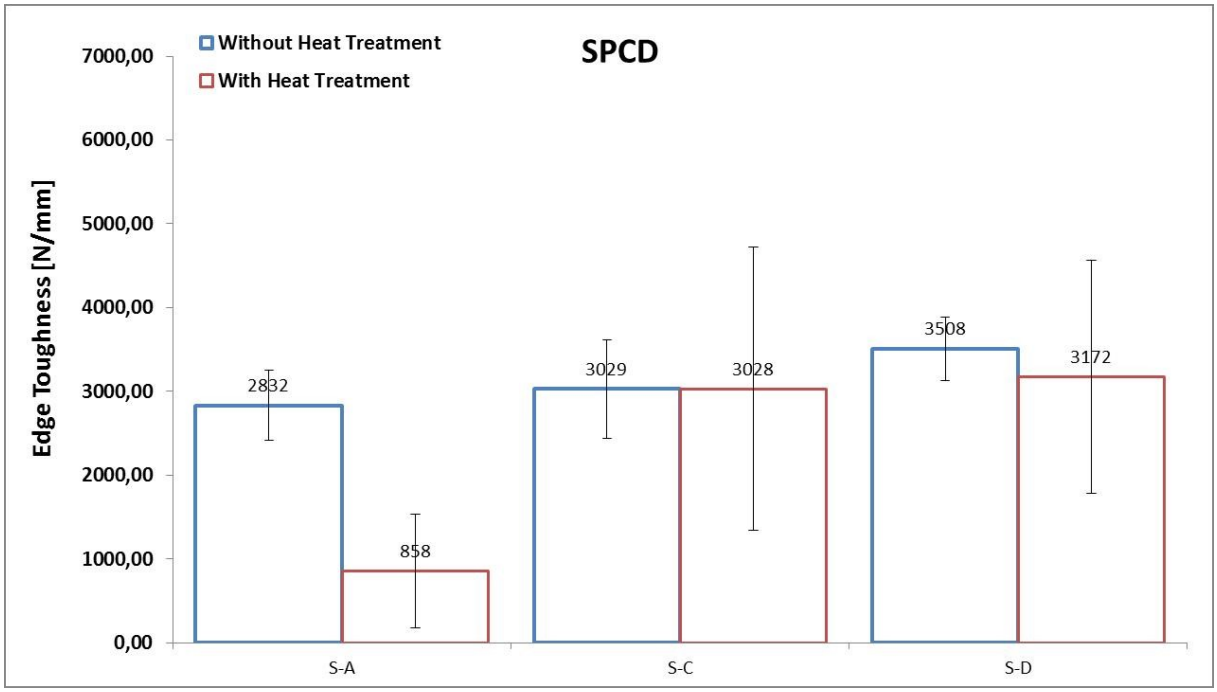

Figure 43: Edge toughness of three different grades of solid PCD. S-A and S-C are a unimodal and S-D a multimodal diamond composite

5.3.1.2 Carbide Backed PCD

There are two main differences in the chipping behaviour. Either the chip stops at the interface between the PCD and the tungsten carbide or the chip breaks through the entire surface. The general tendency is that carbide backed PCDs lose their edge toughness after the heat treatment. This could be the result of the catalytic graphitisation of the diamond, the interface between the tungsten carbide, the strength loss of the PCD or a combination of these. The different edge toughness and the changes after the heat treatment are shown in Figure 44. All three materials are unimodal with increasing diamond grain size. H-A with a diamond grain size of 5 µm shows an increasing edge toughness which, considering the standard deviation, may have statistical reasons. H-B, with 10 µm diamond particles has slightly lower edge toughness after the heat treatment and the loss of both with and without heat treatment is the biggest with the 25 µm diamond particle. It seems that the carbide backing influences the thermal behaviour in a positive way but has no influence on the edge toughness. As a result of the big scatter of all three carbide backed PCDs, it is not possible to distinguish the grades by their edge toughness.

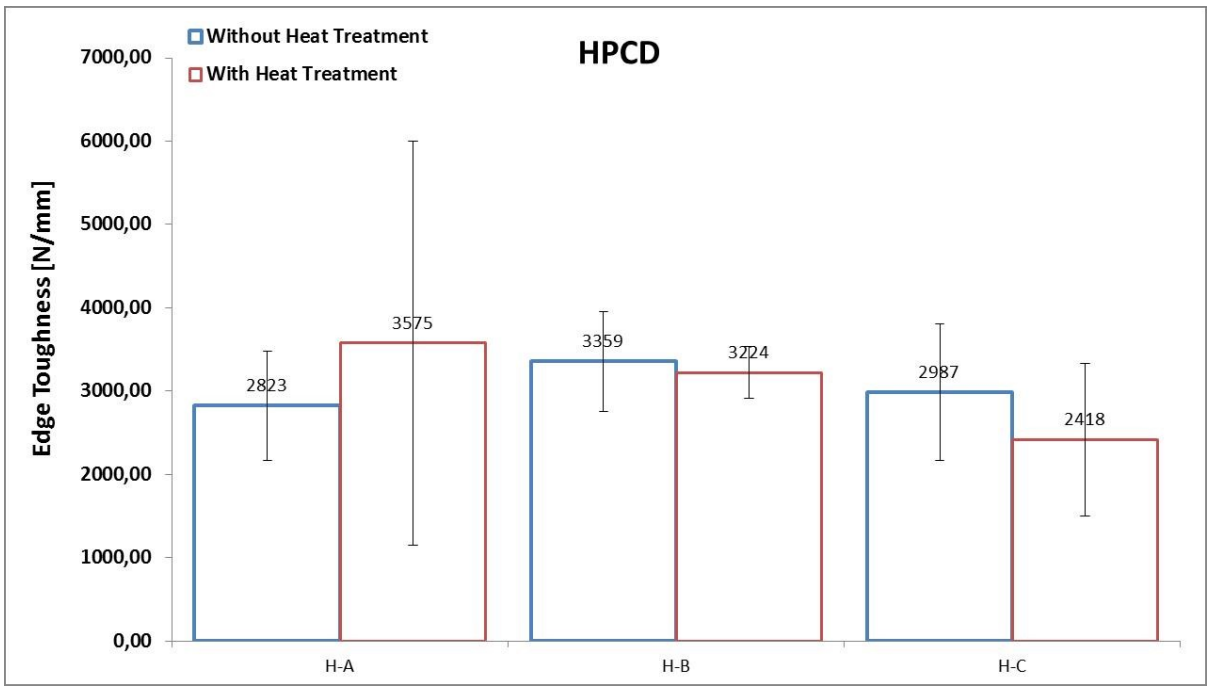

Figure 44: Edge toughness of three different grades of tungsten carbide backed PCD. H-A, H-B and H-C are all unimodal diamond composites

5.3.1.3 Thermally Stable Diamond Composite

The last diamond composite materials which are tested are the thermally stable SiC diamond composites. These specimens are not as dense as the Co-bonded ones but the challenge is to find the right distance from the edge without damaging the whole specimen. That means, if the distance reaches a critical number the whole specimen breaks in two pieces and cannot be used anymore. This is the result of the SiC matrix and the non-existing diamond-to-diamond bond which would avoid such fracture behaviour. However, the main difference between T-A and T-B to T-G is the manufacturing process. T-A is produced in a high

pressure/high temperature synthesis which causes a high densification, no graphitisation, no porosity and therefore higher strength. All materials, except T-D, show the expected behaviour and nearly no decrease in the edge toughness after the heat treatment (Figure 45). An explanation for the edge toughness of T-D could be the piece-to-piece variation of the sintering process. However, T-F is also a low-pressure TSDC and this material is even better than the high pressure grade T-A. Generally it is possible to say that T-B, T-C and T-E have nearly the same edge toughness, where T-D, T-F and T-G show a slightly higher edge toughness compared to the other SiC bonded materials in this group.

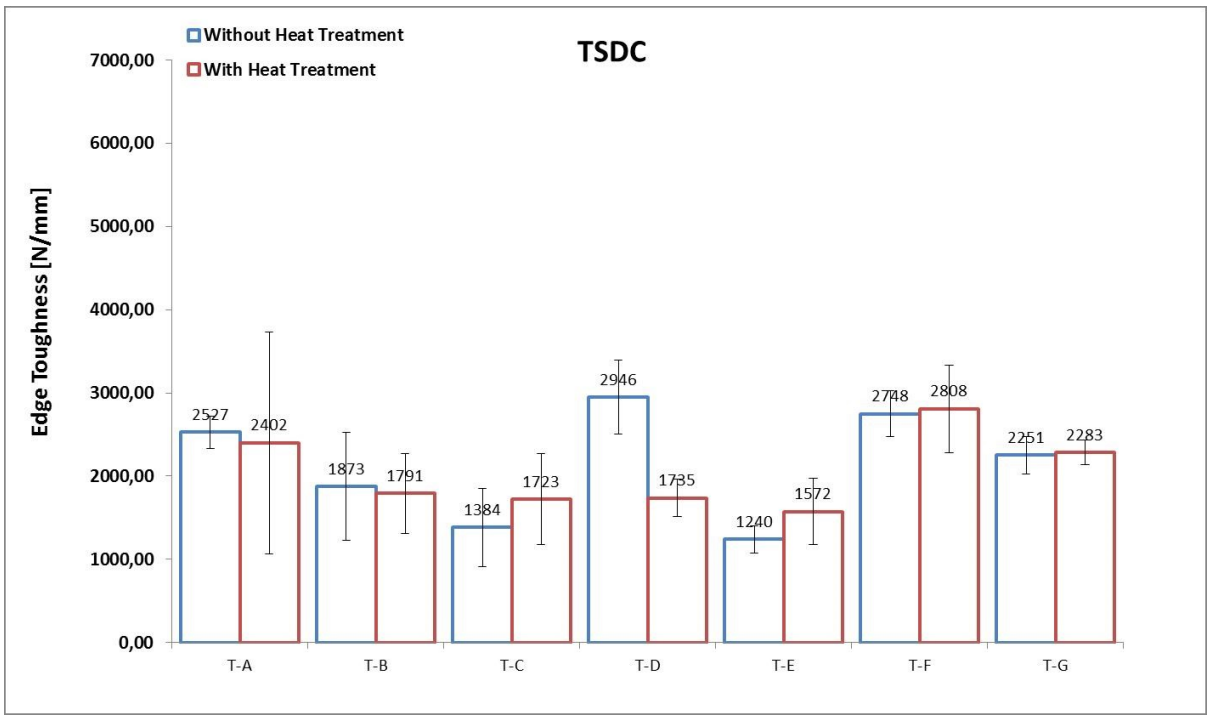

Figure 45: Edge toughness of one grade of high pressure TSDC (T-A) and 6 different grades of low pressure TSDCs

5.3.1.4 Polycrystalline Cubic Boron Nitride

The edge toughness tests are carried out on 5 different PcBN materials with a high cBN content and different binder materials. As mentioned in previous chapters, the most frequently used binder material in high content PcBNs is aluminium which reacts with BN in a wide temperature and pressure region forming a AlB_{12} or a two two-component phase made of AlB_2 – AlN and AlB_{12} – AlN. This binder material creates a good chipping behaviour and these PcBN grades have the most easy-to-manage test behaviour during the edge toughness tests of all tested material in this thesis. The exact binder material composition is internal knowledge confidential to the manufacturing company and it is not possible to get detailed information. However, most PcBNs are thermally stable and, except P-A and P-C, the decrease or increase of the edge toughness from the specimens tested with or without heat treatment is very low. The high scatter of the heat treated P-A can be explained as a result of aluminium based diffusion processes where the aluminium diffuses in the pores between the cBN. Generally all PcBNs have high edge toughness and a very good chipping behaviour which makes it interesting for high temperature applications and dynamic loads.

The results of all PcBNs tested for their edge toughness are shown in Figure 46. PcBN-C is the best material tested in this class. It is not possible to distinguish the other PcBNs as a result of the high scatter.

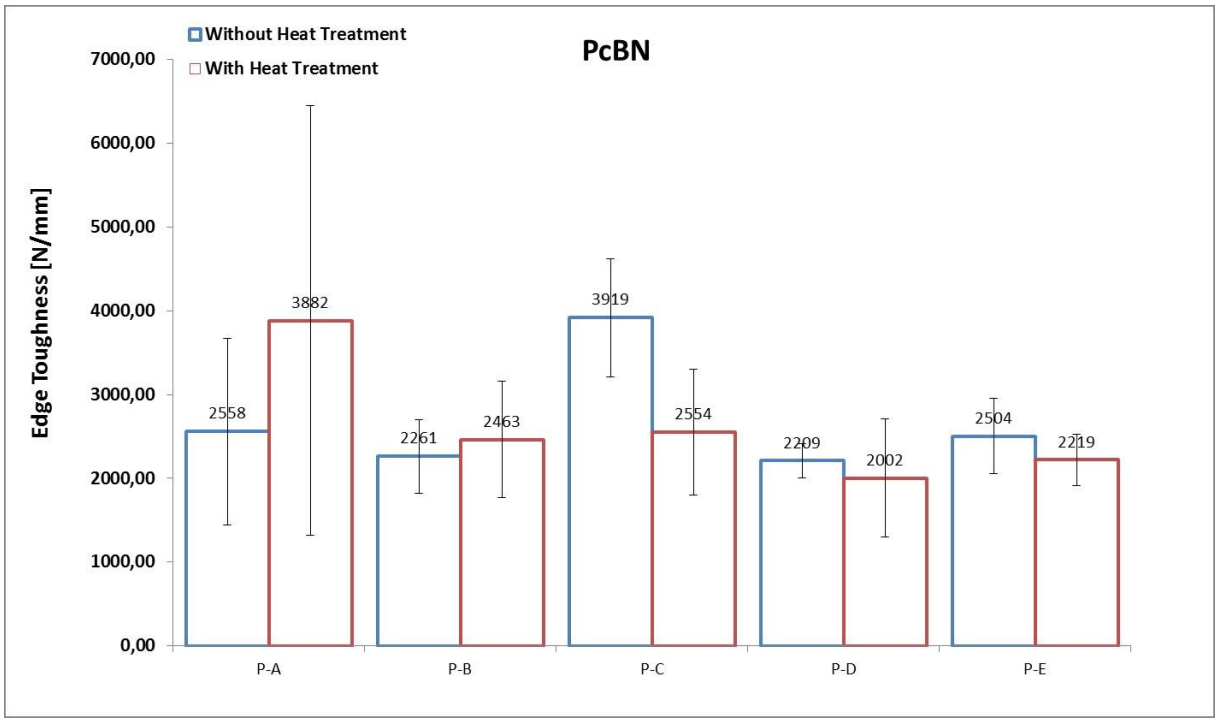

Figure 46: Edge toughness of 5 different grades of PcBN

5.3.1.5 Comparison of Different Indenter Materials

To investigate the influence of the different indenter material, a low pressure thermally stable SiC bonded diamond composite, T-B, is tested with one indenter used at the ISFK Montanuniversity Leoben (Indenter 1) and one ordered from Ceratizit^{TM} (Indenter 2). Firstly the indenter materials are investigated for its hardness (Table 10). Indenter 2, a fine grained cobalt bonded hard metal material, has a significantly lower hardness compared to the indenter material number 1. Therefore, it is proved that the two indenter materials are different and the influence results of the edge toughness test can be investigated.

Table 10: Results Vickers hardness test for different indenter materials

Material	HV5	HV5 [GPa]	H5 [GPa]
Indenter 1	1769	17.4	18.7
Indenter 2	1288	12.6	13.6

Table 11 and Figure 47 show the results of the edge toughness tests. The results from indenter 1 are slightly higher than the results from indenter 2. The lowest result obtained with indenter 1 is 2330 N/mm and the highest with indenter 2 is 2323 N/mm. There is no overlap of the standard deviations and therefore it is not possible to say that the indenter material has not a significant influence on the results as a consequence of the different edge toughnesses.

Table 11: Results for T-B for different indenter material

Material	Edge Toughness Results for not Heat Treated
[/]	[N/m]
T-B Indenter 1	2527 ± 197
T-B Indenter 2	2032 ± 291

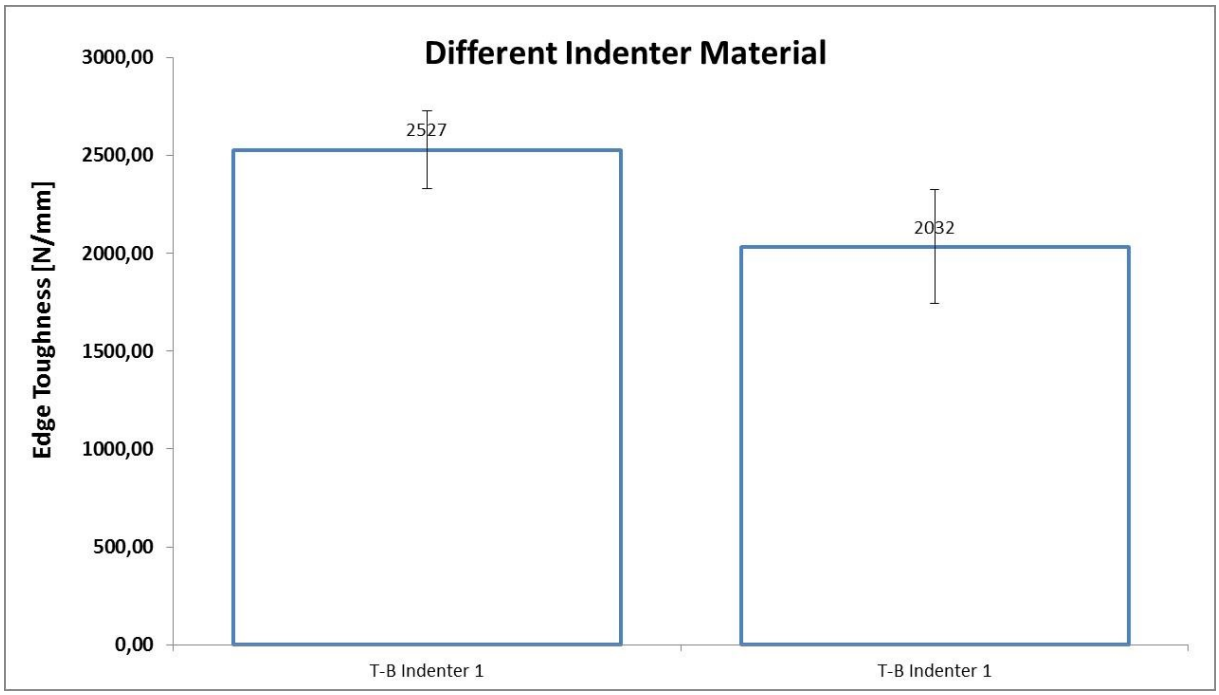

Figure 47: Comparison of the different indenter materials. The tested specimen was T-B

5.4 Study: Possibility of Notching of Specimens

The used material was a 1.6 mm H-B bar with a 1.6 mm hard metal support. To increase the speed in creating the notch a 6 µm, diamond paste is used in the first step. The depth of the notch is measured with an Olympus^{TM} SZH10 stereo microscope and the image analysis system analySIS^{TM}.

To create an accurate notch, special equipment is used (Figure 48). It is possible to notch 4 samples at the same time, but the razor blades have to be changed every half an hour.

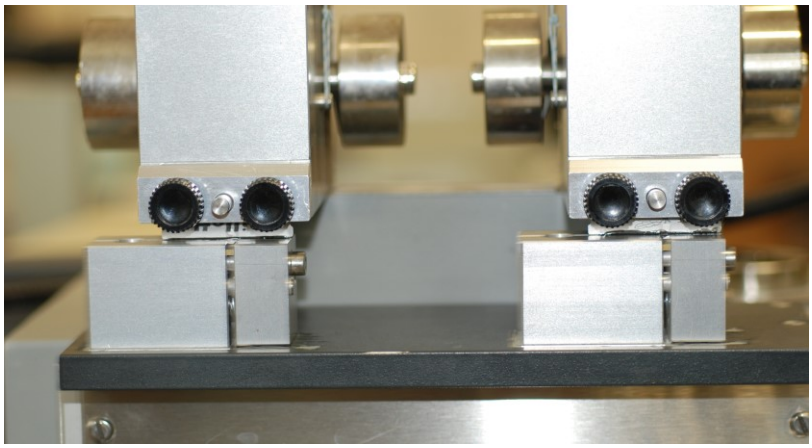

Figure 48: Fixed samples with a 6 micron diamond paste

5.4.1 Results

The results from the notch preparation process are listed in Table 12. Different weights were used. By increasing the weight, the wear of the razor blade gets much bigger without reducing the material in the notch. Nevertheless, 200 g at maximum speed and a changing rate of the razor blades every 30 minutes shows the best results. A comparison of two different razor blades is given in Figure 49.

Table 12: Results of creating the depth with the razor blades in PCD bars

	Weight	Speed	Changing the Razor Blades	Duration	Depth	Razor Blades
	[g]	[/]	[per hour]	[hours]	[µm]	[/]
Day 1	300	10	1	6	40	Blade-B
Day 2	400	10	1	6	60	Blade-B
Day 3	200	10	2	7	70	Blade-B

There is a difference between the cheaper razor blade, Blade-A, and the more expensive one, Blade-B. This could be a result of the wear of the razor blades.

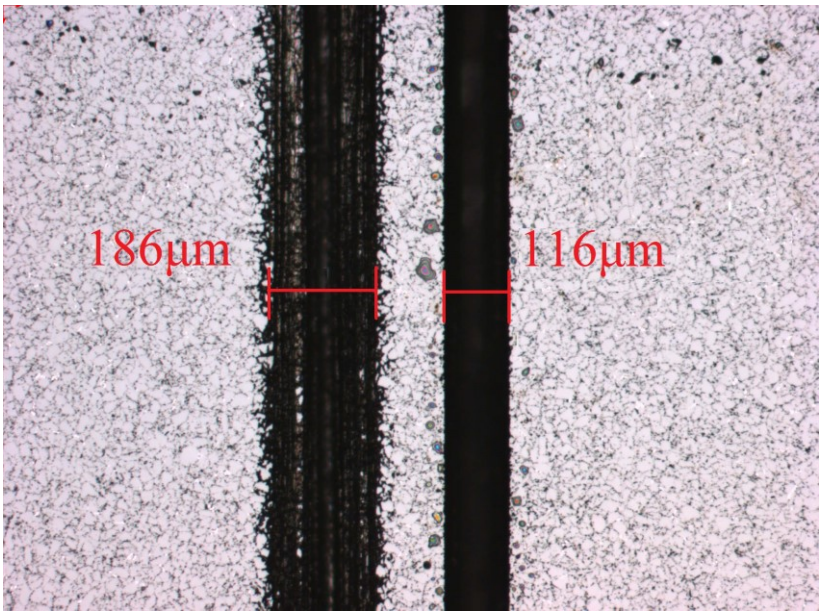

Figure 49: Comparison of different razor blades. Left Blade-A; Right Blade-B

After 6 hours of scratching, with a weight of 300 g and diamond paste with a grain size of 6 µm, it was possible to get to a depth of 43 µm. The razor blades were changed every 60 min.

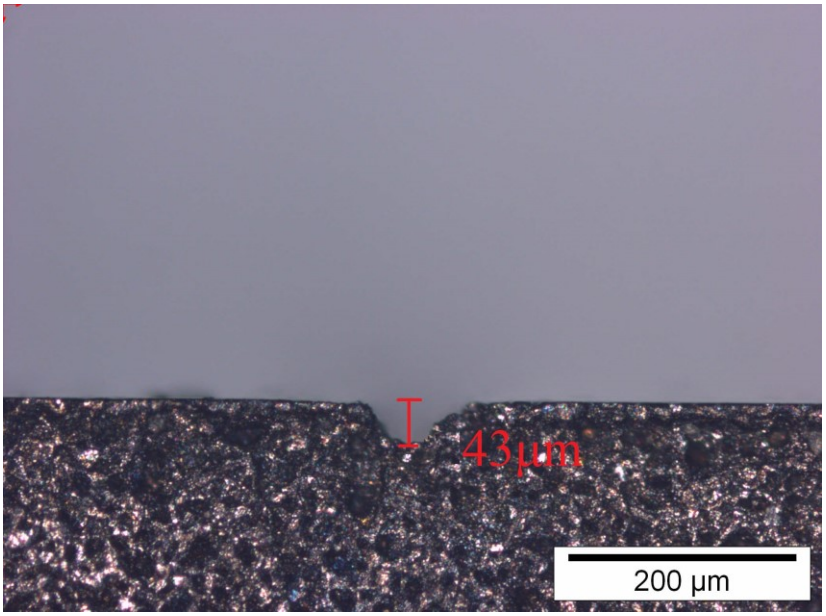

Figure 50: Day 1, Feather razor blade after 6 hours and a weight of 300 g

After 6 additional hours of scratching, with an increased weight of 400 g and diamond paste with a grain size of 6 µm, it was possible to get to a depth of 101 µm (+58 µm). The razor blades were changed every 60 min.

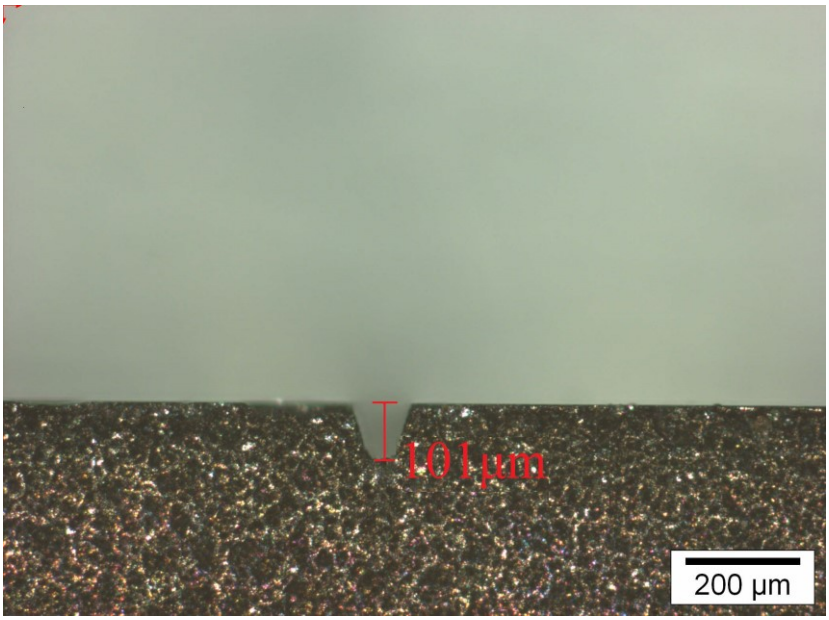

Figure 51: Day 2, Feather razor blade after 6 hours and a weight of 400 g

Finally, after 7 hours of scratching, with a weight of 200 g and diamond paste with a grain size of 6 µm, it was possible to get to a depth of 173 µm (+72 µm). The razor blades were changed every 30 min.

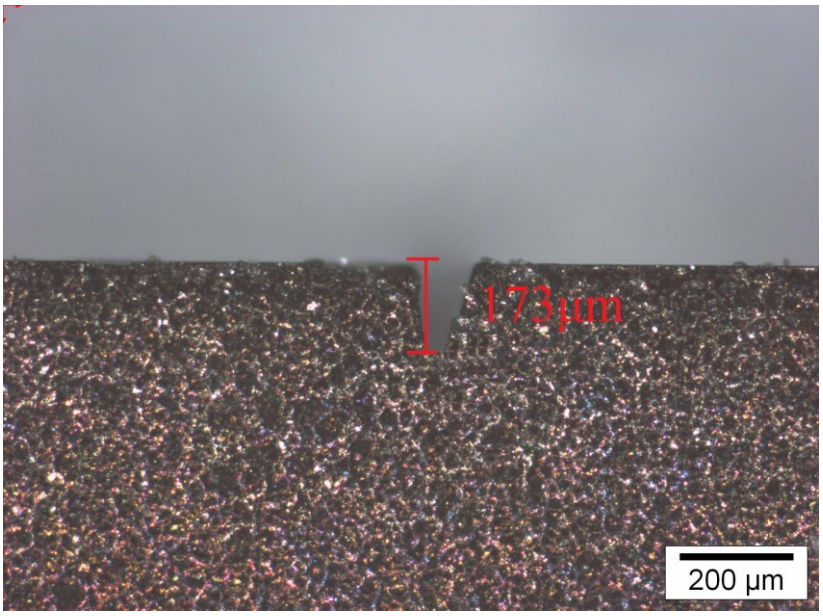

Figure 52: Day 3, Feather razor blade after 7 hours and a weight of 200 g

The test shows that it is possible to achieve 10 µm per hour. Therefore the test was discontinued after 19 hours.

6 Summary and Future Work

6.1 Summary of the Results

In this thesis, the mechanical properties of different grades of thermally stable and thermally unstable diamond composites and different grades of polycrystalline cubic boron nitride composites with and without heat treatment were investigated. The focus of the investigation was on the edge toughness test and the biaxial Ball-on-Three-Balls Test for determining the strength. Additional SEM pictures and investigations with a differential scanning calorimetry were done on selected materials and specimens.

The first test was to prove catalytic graphitisation at high temperatures using DSC. After testing a Co-bonded solid PCD and a TSDC it was possible to see a significant peak at about 900 °C which could be catalytic graphitisation, and no corresponding peak on the thermally stable material. A repeat run with the Co-bonded PCD showed no significant peak at 900 °C which fits to the assumption the peak corresponds to graphitisation, as further graphitisation would not be expected to occur on the second run. The final proof for catalytic graphitisation in solid PCD was done with x-ray phase analysis. A significant peak was found on the specimen tested in the DSC, at approximately 12° on the 2-theta scale which is graphite. This peak was not found on the sample without a DSC run and therefore it is obvious that catalytic graphitisation happens as a result of the Co-diamond reaction at approximately 900 °C.

The strength tests were performed with the biaxial Ball-on-Three-Balls Test at the ISFK in Leoben. Three different grades of thermally unstable Co-bonded diamond composites and one thermally stable SiC-bonded diamond composite were investigated. This was a consequence of the sophisticated sample preparation and the complex material behaviour during cutting operations. Nevertheless, the not heat treated solid PCD, S-A, showed the highest strength but lost 75 % of its strength after the thermal treatment. Whereas, the multimodal solid PCD was almost as strong without heat treatment and it only lost approximately 25 % after the heat treatment. The thermally stable T-A showed an expected behaviour and did not lose any strength at all but it had only half the strength of S-A without thermal treatment. S-A and S-C showed visible thermal damages on the surfaces, this behaviour had a big influence on the strength test results.

The edge toughness was investigated with a fine grain tungsten carbide indenter with a cobalt content of 10 %. The solid PCDs showed particular a surprising behaviour and the edge toughness after heat treatment did not always decrease. A significant drop in S-A occurred, but not in S-C and S-D. However, the scatter of the results increased after heat treatment on all solid PCDs. It was not possible to test S-B because the material was completely damaged during the heat treatment. The multimodal diamond composite, S-D, is perhaps the most suitable solid PCD in this class and the edge toughness after heat treatment is higher compared to edge toughness of the other samples without any heat treatment. The scatter of the carbide-backed H-A dramatically increased after it was exposed to high temperatures and there is no obvious reason why the edge toughness should

increase after heat treatment. This higher edge toughness could come from one or two inaccurate higher results or as a result of the release of internal stresses. Nevertheless, there were only 5 indentations possible on each sample and therefore one inaccurate result could increase the edge toughness significantly. Overall, all grades of the carbide backed cobalt bonded PCDs showed the same edge toughness. All TSDCs, which are thermally stable, showed an expected behaviour and had the same edge toughness values with and without heat treatment. Only T-D showed a significant decrease in the edge toughness which could be a result of a very different structure or elemental composition, but this could not be investigated in detail due to time reasons and the need of special sample preparation capabilities. T-A, although it is from a high pressure and high temperature manufacturing process, had a higher edge toughness than some but not all of the low pressure TSDCs.. The last investigated material for its edge toughness was PcBN. P-A showed a surprising behaviour and there was also no obvious reason why the edge toughness increases after a thermal treatment. P-C did not look to be thermally stable but the increasing scatter and therefore the overlap of the confidential intervals gave the same edge toughness with and without heat treatment. The influence of the different indenter material was investigated on the T-B material. The results from indenter 1 were slightly higher than the results from indenter 2. There was no overlap of the standard deviations and therefore a different indenter material provides different results. It is very important to test the edge toughness of a material with the same indenter material in the future.

A study on the possibility of notching PCD bars to test the fracture toughness was performed and different razor blades and different weights were used to create an accurate notch. The main problem was the limited time when the notch preparation could be done. By increasing the weight, the wear of the razor blades was much bigger without a significant material removal. However, a weight of 200 g at maximum speed, a 6 µm diamond paste and a changing rate of the razor blades every 30 minutes shows the best results and it was possible to notch 10 µm per hour. There is also a difference between the cheaper razor blade and the more expensive one which had an effect on the cutting width. Generally it is possible to say that the more expensive razor blades showed a more accurate notching behaviour. However, even with this best notching process, it was not possible to create fracture toughness samples for testing for this thesis.

6.2 Future Work

Given the evident difficulties in producing diamond composite samples for fracture toughness testing, a proven relationship between fracture toughness results and biaxial B3B results would be highly valuable. A recommendation for future work is therefore to find an optimal way of creating a V-Notch on a small number of diamond composite samples in order to test their fracture toughness. It would also be useful to get a better confidence in the strength results from the B3B test. This could be obtained by increasing the number of tested specimens to a minimum of 30.

It was not possible to perform a detailed microscopic work of T-D (the thermally stable diamond composite that did not show thermally stable behaviour in the edge toughness test). The reason was that very special grinding and polishing capabilities are needed to prepare diamond composite specimens for further microscopic investigations. It would be useful to perform this in order to get a deeper understanding of the different inclusion contents and microstructures of different grades from TSDCs. The repeatability of the edge toughness test could be increased by finding a way to have a controlled and automatic placement of the indenter. This would either enable multiple indentations to be performed at exactly the same distance from the sample edge, or a range of different indenter distances to be accurately used.

Two forms of diamond materials are used for abrasive applications: particulate (“grit”) diamond and the diamond composites (such as PCD) reported here. Within the field of diamond grit, the key laboratory characteristics that influence application behaviour are well known [52]. However, for diamond composites such as PCD, the most influential laboratory characteristics are less well understood, and consequently there is a much greater emphasis on using applications tests to rank and compare materials. [52]. It would therefore be very interesting to compare the composite materials reported in this thesis in abrasive applications. This could identify how well the Ball-on-Three-Balls test and the edge toughness test can help predict application behaviour.

7 BIBLIOGRAPHY

[1] U. Schwarz, Diamant: naturgewachsener Edelstein und massgeschneidertes Material, Chemie in unserer Zeit, vol. 2000, 212–222

[2] W. Schmidt and H. Malzahn, Industriemineral Diamant, VE B deutscher Verlag für Grundstoffindustrie, vol. 1980, 1980

[3] G. E. Harlow, The Nature of Diamonds, Canbridge University Press, vol. 1998.

[4] M. Arima, M. Nkakayama, M. Akaishi, S. Yamaoka, and H. Kanda, Geology, vol. 21, 1993

[5] J. E. Field, The properties of diamond, Academic Press, London, 1979

[6] F. P. Bundy, H. T. Hall, H. M. Strong, and R. H. Wentdorf, Man-Made Diamonds, Nature, vol. 176, no. 4471, 1955, 51–55

[7] S. Nailer, W. Gallagher, and W. Leahy, Die Eigenschaften natürlicher und synthetischer Diamantschleifkörnungen, vol. 2007, 54–63

[8] A. Krüger, Neue kohlenstoffmaterialen - Eine Einführung, Teubener Verlag, Wiesbaden, 2007

[9] H. T. Hall, Sintered diamond: a synthetic carbonado (eng), Science (New York, N.Y.), vol. 169, no. 3948, 1970, 868–869

[10] X. S. Li and J. Boland, The wear characteristics of superhard composite materials in abrasive cutting operations, no. 259, 2005, 1128–1136

[11] D'Evelyn M. P, .Industrial diamond. Handbook of Ceramics, Glasses and Diamonds, 2001

[12] P. J. Heath, European Journal of Engineering Education, vol. 1987, no. 12.

[13] S. N. Monteiro, Skury, A, L, D, M. Giardinieri de Azevedo, and Bobrovnitchii, G, S, Cubic boron nitride competing with diamond as a superhard engineering material - an overview, Journal of Materials Research and Technology, no. 2(1), 2013, 68–74

[14] F. Bellin, A. Dourfaye, W. King, and M. Thigpen, The current state of PCD bit technology, 2010, 67–71

[15] D. McNamara, The Mechanical and Fracture Properties of Polycrystalline Diamond as a Function of Microstructure, Dissertation, School of Mechanical & Materials Engineering, University College Dublin, 2015

[16] A. Minoru, O. Toshikazu, and Y. Shinobu, Synthesis of Fine-Grained Polycrystalline Diamond Compact and Its Microstructure, no. 74, 1991, 5–10

[17] M. Herrmann, B. Matthey, S. Höhn, I. Kinski, D. Rafaja, and A. Michaelis, Diamond-ceramics composites—New materials for a wide range of challenging applications, Journal of the European Ceramic Society, vol. 32, no. 9, 2012, 1915–1923

[18] A. S. Osipov, N. A. Bondarenko, I. A. Petrusha, and V. A. Mechnik, Drill bits with thermostable PCD inserts, Diamond Tooling Journal, no. 3, 2010, 31–34

[19] K. Mlungwane, M. Herrmann, and I. Sigalas, The low-pressure infiltration of diamond by silicon to form diamond–silicon carbide composites, Journal of the European Ceramic Society, vol. 28, no. 1, 2008, 321–326

[20] J. Qian, G. Voronin, T. W. Zerda, D. He, and Y. Zhao, High-pressure, high-temperature sintering of diamond–SiC composites by ball-milled diamond–Si mixtures, J. Mater. Res, vol. 17, no. 08, 2002, 2153–2160

[21] P. J. Heath, Properties and uses of amborite, Carbide and Tool Journal, no. 19, 1987, 12–22

[22] P. Alveen, An Experimental-Numerical Investigation into the Properties of Polycrystalline Cubic Boron Nitride towards Materials Optimisation, Dissertation, School of Mechanical & Materials Engineering, University collage Dublin, Dublin, 2015

[23] R. H. Wentorf, JR, Cubic Boron Nitride, Journal of Chemical Physics, no. 26, 1957, p. 956

[24] C. J. Pretorius, N. Can, and P. M. Michael, "Methods of making CBN compacts", US Patent.

[25] E. Benko, J. Morgiel, and T. Czeppe, BN sintered with AlMicrostructure and hardness, Ceramics International, vol. 23, no. 1, 1997, 89–91

[26] P. Klimczyk, E. Benko, K. Lawniczak-Jablonska, E. Piskorska, M. Heinonen, A. Ormaniec, W. Gorczynska–Zawislan, and V. S. Urbanovich, Cubic boron nitride—Ti/TiN compositesHardness and phase equilibrium as function of temperature, Journal of Alloys and Compounds, vol. 382, no. 1-2, 2004, 195–205

[27] Werkstoffkunde und Prüfung der Kunststoffe, Ed, Werkstoffprüfung der Kunststoffe, Leoben, 2012

[28] R. Danzer, P. Supancic, and W. Harrer, Technische keramische Werkstoffe, Der 4-Kugelversuch zur Ermittlung der biaxialen Biegefestigkeit spröder Werkstoffe, Jochen Kriegesmann, Ellerau, 2009

[29] W. A. Bassali, The transverse flexure of thin elastic plates supported at several points, Proceedings of the Cambridge Philosophic Society, vol. 1957, no. 53, 1957, 728–743

[30] A. F. Kirstein and R. M. Wooley, Symmetrical bedning of thin circular elastic plates on equally spaced point supports, J. Res. Natl. Bur. Stand. Sect. C, vol. 1967, no. 71, 1967, 1–10

[31] Institut für Struktur und Funktionskeramik, http://www.isfk.at/de/960. 2016,

[32] A. Börger, P. Supancic, and R. Danzer, The ball on three balls test for strength testing of brittle discs - Stress Distribution in the Disc, J. Eur. Ceram.Soc 22, no. 8, 2002, 1425–1436

[33] The ball on three balls test for strength testing of brittle discs - Part IIStress distribution in the disc, Journal of the European Ceramic Society, no. 9-10, 1425–1436, 2002

[34] R. Danzer, G. Reisner, and H. Schubert, Der Einfluss von Gradienten in der Defektdichte und Festigkeit auf die Bruchstatistik von spröden Werkstoffen, Zeitschrift für Metallkunde, no. 83, 1992, 508–517

[35] R. Danzer, A General Strength Distribiution Function for Brittle Materials, Journal of the European Ceramic Society, no. 10, 1992, 461–472

[36] W. Weibull, A statistical distribution function of wide applicability, Journal of Applied Mechanics, no. 18, 1951, 293–297

[37] A statistical theory of strength of materials, Royal Swedish Institude for Engineering Research, Stockholm, vol. 1939, 1–45, 1939

[38] CEN/TS 843-9: Hochleistungskeramik - Mechanische Eigenschaften monolithischer Keramik bei Raumtemperatur - Teil 9: Prüfverfahren zur Bestimmung der Kantenbeständigkeit gegen Abplatzung, 2010

[39] R. Morrell, R. Danzer, P. Supancic, W. Harrer, S. Puchegger, and H. Peterlik, Meso-scale mechanical testing methods for diamond composite materials, International Journal of Refractory Metals and Hard Materials, vol. 28, no. 4, 2010, 508–515

[40] E. A. Almond and N. McCormick, Constant-geometry edge-flaking of brittle materials, vol. Nature, no. 321, 1986, 53–55

[41] R. Danzer, M. Hangl, and Paar R, Edge Chipping of Brittle MaterialsFractography of Glasses and Ceramics IV, Ceramic Transactions, 2001, 43–55

[42] R. Paar, Kantenfestigkeit von Hochleistungskeramiken, Diploma Thesis, ISFK, Montanuniversität, Leoben, 1994

[43] R. Damani, C. Schuster, and R. Danzer, Polished Notch Modification of SENB-S Fracture Toughness Testing, J. Eur. Ceram.Soc 17, no. 14, 1997, 1685–1689

[44] R. Damani, R. Gstrein, and R. Danzer, Critical notch-root radius effect in SENB-S fracture toughness testing, Journal of the European Ceramic Society, vol. 16, no. 7, 1996, 695–702

[45] ISO/FDIS 23146: Fine Ceramics (advanced ceramics, advanced technical ceramics)- Test metods for fracture toughness of monolithic ceramics-Single-edge V-notch beam (SEVNB) method, 2008

[46] A. A. Griffith, The phenomena of rapture and flow in solids, Philos. Trans. Roy. Soc. London, vol. 1921, no. 221, 1921, 163–198

[47] G. R. Irwin, Analysis of stresses and strains near the end of crack traversing a plate, Journal of Applied Mechanics, vol. 1957, no. 24, 1957, 361–364

[48] EN 843-5: Advanced technical ceramics, monolithic ceramics - Mechanical tests at room temperature, Part 5: Statistical analysis, 1996

[49] R. Danzer, Mechanical Failure of Advanced Ceramics: The Value of Fractography, Key Eng. Mat, no. 223, 2002, 1–18

[50] J. Dusza and M. Steen, Fractography and Fracture Mechanics Property Assessment of Advanced Structural Ceramics, Int. Materials Reviews, no. 44, 1999, p. 165

[51] R. Danzer, P. Supancic, J. Pascual, and T. Lube, Fracture statistics of ceramics – Weibull statistics and deviations from Weibull statistics, Engineering Fracture Mechanics, vol. 74, no. 18, 2007, 2919–2932

[52] J. Gallagher, P. Scanlon, and S. G. Nailer, Characterisation techniques for the study of high-strength, coarse diamond, Industrial Diamond Review, vol. 2006, no. 3, 2006, 58–65.

List of Tables

List of Figures

ANNEXES

A Test Reports

A1: Edge Toughness Tests

Kantenfestigkeit	T-A RT			Abstand	Kraft	F/d
				d [mm]	[N]	[N/mm]
				0	0	
Auftraggeber:				0.804	2239	2785
Material:	T-A RT			0.593	1573	2653
Operator:	Fabbro			0.529	1248	2359
Datum:	05.07.2017			0.974	2458	2524
Belastungsgeschwindigkeit:	0,50 mm			0.486	1126	2317
Oberfläche:	as sintered					
Geometrie:	90°					
Kantenfestigkeit [N/mm]*):						
Kantenfestigkeit [N/mm]:	**2527.42**					
(in Anlehnung an prTS 843-9)						
***) durch lineare Regression ermittelt**						

Kantenfestigkeit	T-A HT			Abstand	Kraft	F/d
				d [mm]	[N]	[N/mm]
				0	0	
Auftraggeber:				0.558	1457	2611
Material:	T-A HT			0.344	766	2227
Operator:	Fabbro			0.126	572	4540
Datum:	05.07.2017			0.089	97	1090
Belastungsgeschwindigkeit:	0,50 mm			0.072	111	1542
Oberfläche:	as sintered					
Geometrie:	90°					
Kantenfestigkeit [N/mm]*):						
Kantenfestigkeit [N/mm]:	**2401.82**					
(in Anlehnung an prTS 843-9)						
***) durch lineare Regression ermittelt**						

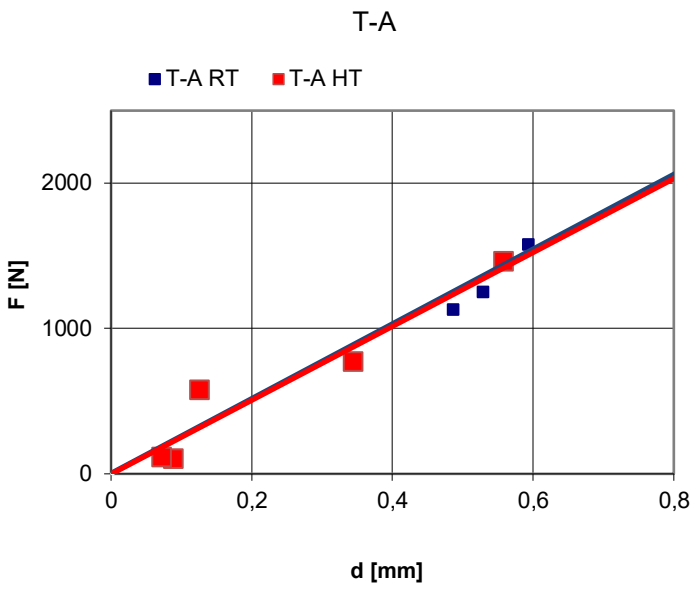

Kantenfestigkeit	T-B RT			Abstand	Kraft	F/d
				d [mm]	[N]	[N/mm]
				0	0	
Auftraggeber:				0.142	173	1218
Material:	T-B RT			0.323	738	2285
Operator:	Fabbro			0.438	1259	2874
Datum:	05.07.2017			0.447	903	2020
Belastungsgeschwindigkeit:	0,50 mm			0.536	1560	2910
Oberfläche:	as sintered			0.521	1012	1942
Geometrie:	90°			0.318	420	1321
Kantenfestigkeit [N/mm]*):				0.335	513	1531
Kantenfestigkeit [N/mm]:	**1872.69**			0.532	773	1453
(in Anlehnung an prTS 843-9)				0.257	301	1171
***) durch lineare Regression ermittelt**						

Kantenfestigkeit	T-B HT			Abstand	Kraft	F/d
				d [mm]	[N]	[N/mm]
				0	0	
Auftraggeber:				0.336	700	2083
Material:	T-B HT			0.137	339	2474
Operator:	Fabbro			0.438	713	1628
Datum:	05.07.2017			0.257	374	1455
Belastungsgeschwindigkeit:	0,50 mm			0.165	217	1315
Oberfläche:	as sintered					
Geometrie:	90°					
Kantenfestigkeit [N/mm]*):						
Kantenfestigkeit [N/mm]:	**1791.21**					
(in Anlehnung an prTS 843-9)						
***) durch lineare Regression ermittelt**						

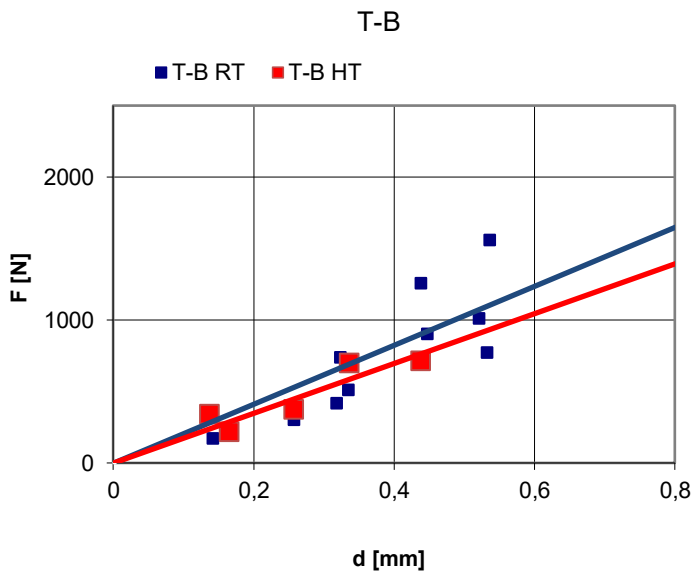

Kantenfestigkeit	T-C RT			Abstand	Kraft	F/d
				d [mm]	[N]	[N/mm]
				0	0	
Auftraggeber:				0.269	529	1967
Material:	T-C RT			0.185	134	724
Operator:	Fabbro			0.373	440	1180
Datum:	07.07.2017			0.159	259	1629
Belastungsgeschwindigkeit:	0,50 mm			0.298	423	1419
Oberfläche:	as sintered					
Geometrie:	90°					
Kantenfestigkeit [N/mm]*):						
Kantenfestigkeit [N/mm]:	**1383.78**					
(in Anlehnung an prTS 843-9)						
***) durch lineare Regression ermittelt**						

Kantenfestigkeit	T-C HT			Abstand	Kraft	F/d
				d [mm]	[N]	[N/mm]
				0	0	
Auftraggeber:				0.649	1552	2391
Material:	T-C HT			0.392	659	1681
Operator:	Fabbro			0.366	433	1183
Datum:	07.07.2017			0.790	1706	2159
Belastungsgeschwindigkeit:	0,50 mm			0.441	530	1202
Oberfläche:	as sintered					
Geometrie:	90°					
Kantenfestigkeit [N/mm]*):						
Kantenfestigkeit [N/mm]:	**1723.37**					
(in Anlehnung an prTS 843-9)						
***) durch lineare Regression ermittelt**						

T-C

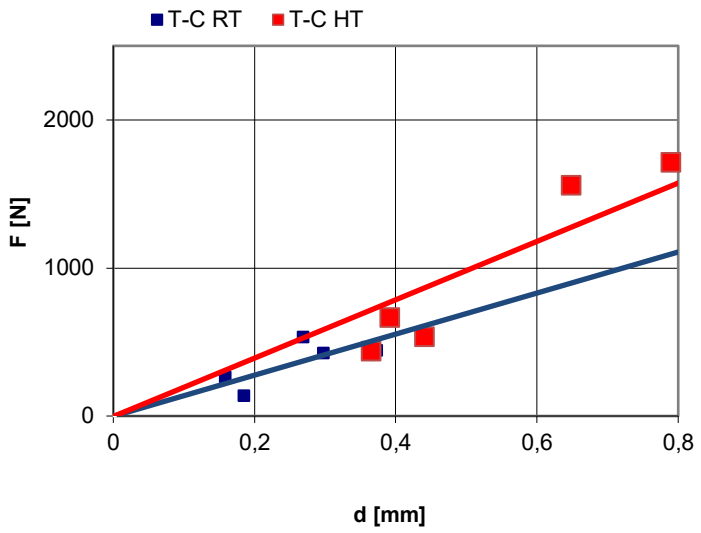

Kantenfestigkeit	T-D RT			Abstand	Kraft	F/d
				d [mm]	[N]	[N/mm]
				0	0	
Auftraggeber:				0.275	885	3218
Material:	T-D RT			0.632	2028	3209
Operator:	Fabbro			0.602	1847	3068
Datum:	06.07.2017			0.268	580	2164
Belastungsgeschwindigkeit:	0,50 mm			0.176	540	3068
Oberfläche:	as sintered					
Geometrie:	90°					
Kantenfestigkeit [N/mm]*):						
Kantenfestigkeit [N/mm]:	**2945.50**					
(in Anlehnung an prTS 843-9)						
***) durch lineare Regression ermittelt**						

Kantenfestigkeit	T-D HT			Abstand	Kraft	F/d
				d [mm]	[N]	[N/mm]
				0	0	
Auftraggeber:				0.484	996	2058
Material:	T-D HAT			0.399	592	1484
Operator:	Fabbro			0.547	1010	1846
Datum:	06.07.2017			0.525	843	1606
Belastungsgeschwindigkeit:	0,50 mm			0.388	653	1683
Oberfläche:	as sintered					
Geometrie:	90°					
Kantenfestigkeit [N/mm]*):						
Kantenfestigkeit [N/mm]:	**1735.34**					
(in Anlehnung an prTS 843-9)						
***) durch lineare Regression ermittelt**						

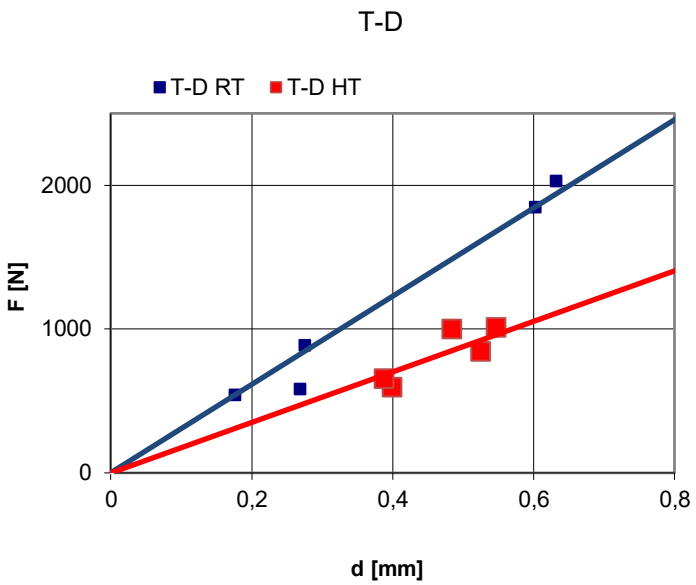

Kantenfestigkeit	T-E RT			Abstand	Kraft	F/d
				d [mm]	[N]	[N/mm]
				0	0	
Auftraggeber:				0.353	470	1331
Material:	T-E RT			0.662	927	1400
Operator:	Fabbro			0.396	436	1101
Datum:	08.07.2017			0.412	423	1027
Belastungsgeschwindigkeit:	0,50 mm			0.199	267	1342
Oberfläche:	as sintered					
Geometrie:	90°					
Kantenfestigkeit [N/mm]*):						
Kantenfestigkeit [N/mm]:	**1240.23**					
(in Anlehnung an prTS 843-9)						
***) durch lineare Regression ermittelt**						

Kantenfestigkeit	T-E HT			Abstand	Kraft	F/d
				d [mm]	[N]	[N/mm]
				0	0	
Auftraggeber:				0.373	601	1611
Material:	T-E HAT			0.418	561	1342
Operator:	Fabbro			0.176	336	1909
Datum:	08.07.2017			0.710	1402	1975
Belastungsgeschwindigkeit:	0,50 mm			0.262	268	1023
Oberfläche:	as sintered					
Geometrie:	90°					
Kantenfestigkeit [N/mm]*):						
Kantenfestigkeit [N/mm]:	**1572.00**					
(in Anlehnung an prTS 843-9)						
***) durch lineare Regression ermittelt**						

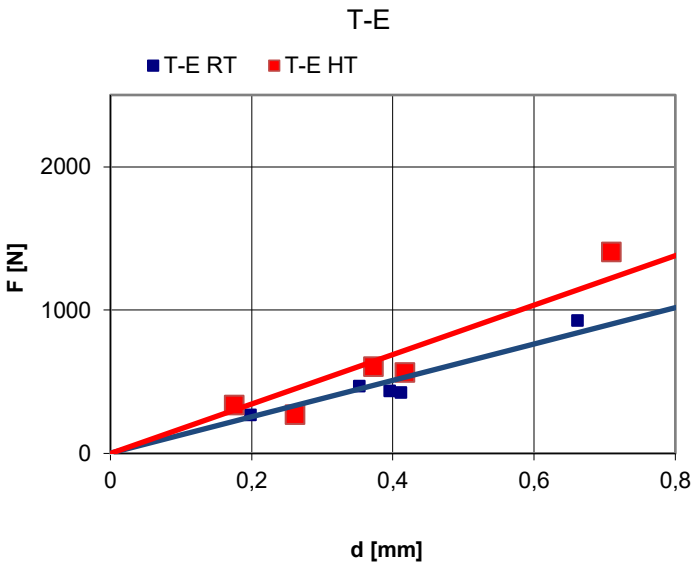

Kantenfestigkeit	T-F RT			Abstand	Kraft	F/d
				d [mm]	[N]	[N/mm]
				0	0	
Auftraggeber:				0.516	1636	3171
Material:	T-F RT			0.523	1361	2602
Operator:	Fabbro			0.370	972	2627
Datum:	07.07.2016			0.390	965	2474
Belastungsgeschwindigkeit:	0,50 mm			0.312	894	2865
Oberfläche:	as sintered					
Geometrie:	90°					
Kantenfestigkeit [N/mm]*):						
Kantenfestigkeit [N/mm]:	**2747.92**					
(in Anlehnung an prTS 843-9)						
***) durch lineare Regression ermittelt**						

Kantenfestigkeit	T-F HT			Abstand	Kraft	F/d
				d [mm]	[N]	[N/mm]
				0	0	
Auftraggeber:				0.270	976	3615
Material:	T-F HT			0.416	1033	2483
Operator:	Fabbro			0.172	523	3041
Datum:	07.07.2016			0.473	1088	2300
Belastungsgeschwindigkeit:	0,50 mm			0.314	816	2599
Oberfläche:	as sintered					
Geometrie:	90°					
Kantenfestigkeit [N/mm]*):						
Kantenfestigkeit [N/mm]:	**2807.52**					
(in Anlehnung an prTS 843-9)						
***) durch lineare Regression ermittelt**						

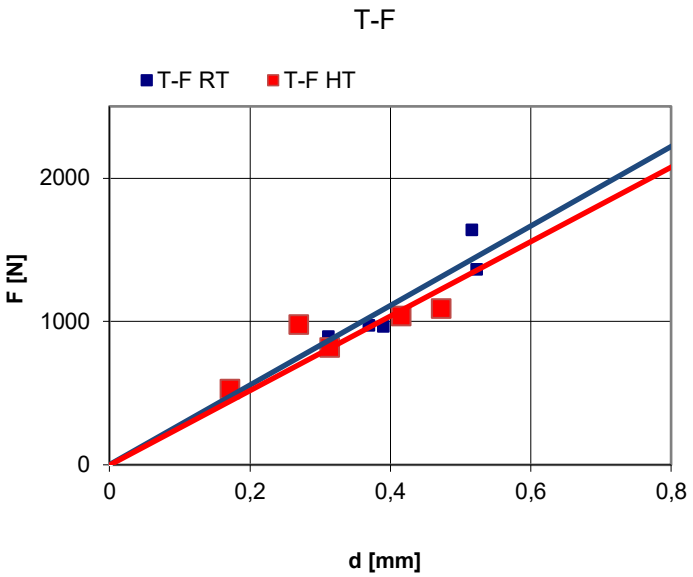

Kantenfestigkeit	T-G RT			Abstand	Kraft	F/d
				d [mm]	[N]	[N/mm]
				0	0	
Auftraggeber:				0.726	1819	2506
Material:	T-G RT			0.298	609	2044
Operator:	Fabbro			0.314	630	2006
Datum:	12.07.2016			0.414	945	2283
Belastungsgeschwindigkeit:	0,50 mm			0.902	2182	2419
Oberfläche:	as sintered					
Geometrie:	90°					
Kantenfestigkeit [N/mm]*):						
Kantenfestigkeit [N/mm]:	**2251.44**					
(in Anlehnung an prTS 843-9)						
***) durch lineare Regression ermittelt**						

Kantenfestigkeit	T-G HT			Abstand	Kraft	F/d
				d [mm]	[N]	[N/mm]
				0	0	
Auftraggeber:				0.488	1017	2084
Material:	T-G HT			0.512	1175	2295
Operator:	Fabbro			0.250	609	2436
Datum:	12.07.2016			0.606	1464	2416
Belastungsgeschwindigkeit:	0,50 mm			0.279	609	2183
Oberfläche:	as sintered					
Geometrie:	90°					
Kantenfestigkeit [N/mm]*):						
Kantenfestigkeit [N/mm]:	**2282.72**					
(in Anlehnung an prTS 843-9)						
***) durch lineare Regression ermittelt**						

T-G

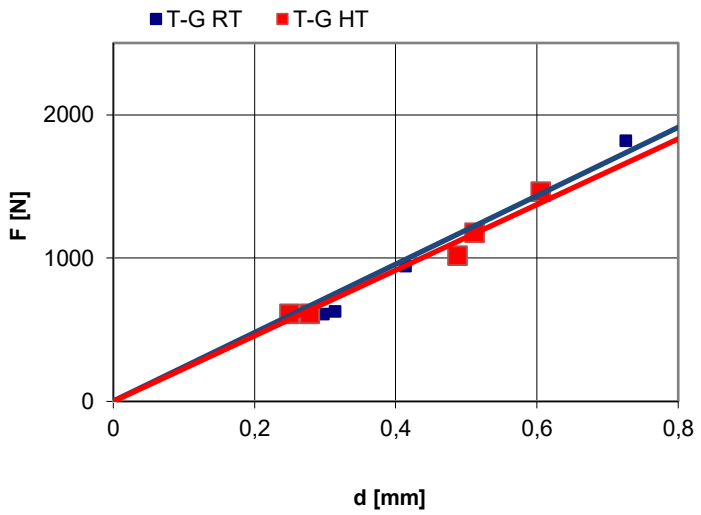

Kantenfestigkeit	H-A RT			Abstand	Kraft	F/d
				d [mm]	[N]	[N/mm]
				0	0	
Auftraggeber:				0.122	353	2893
Material:	H-A RT			0.704	2248	3193
Operator:	Fabbro			0.179	468	2615
Datum:	08.08.2016			0.370	1326	3584
Belastungsgeschwindigkeit:	0,50 mm			0.172	315	1831
Oberfläche:	as sintered					
Geometrie:	90°					
Kantenfestigkeit [N/mm]*):						
Kantenfestigkeit [N/mm]:	**2823.27**					
(in Anlehnung an prTS 843-9)						
***) durch lineare Regression ermittelt**						

Kantenfestigkeit	H-A HT			Abstand	Kraft	F/d
				d [mm]	[N]	[N/mm]
				0	0	
Auftraggeber:				0.266	427	1605
Material:	H-A HT			0.177	519	2932
Operator:	Fabbro			0.697	908	1303
Datum:	08.08.2016			0.235	1651	7026
Belastungsgeschwindigkeit:	0,50 mm			0.205	1027	5010
Oberfläche:	as sintered					
Geometrie:	90°					
Kantenfestigkeit [N/mm]*):						
Kantenfestigkeit [N/mm]:	**3575.10**					
(in Anlehnung an prTS 843-9)						
***) durch lineare Regression ermittelt**						

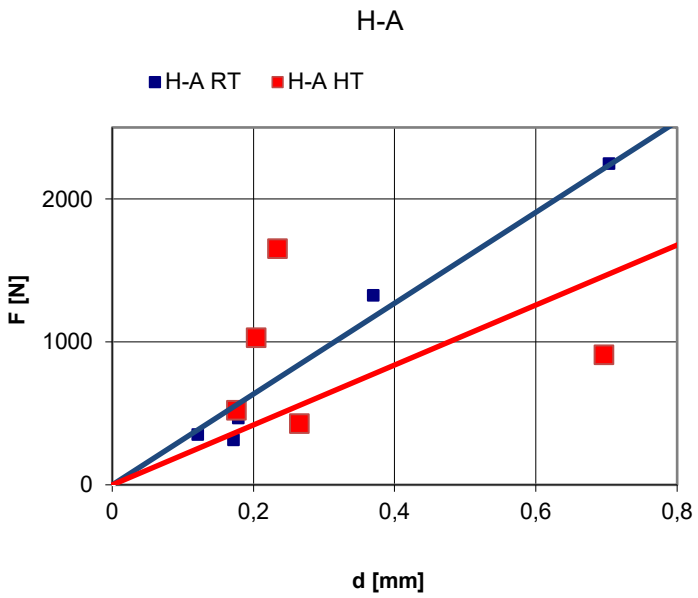

Kantenfestigkeit	H-B RT			Abstand	Kraft	F/d
				d [mm]	[N]	[N/mm]
				0	0	
Auftraggeber:				0.614	2566	4179
Material:	H-B RT			0.510	1609	3155
Operator:	Fabbro			0.416	1402	3370
Datum:	10.08.2016			0.331	1178	3559
Belastungsgeschwindigkeit:	0,50 mm			0.272	689	2533
Oberfläche:	as sintered					
Geometrie:	90°					
Kantenfestigkeit [N/mm]*):						
Kantenfestigkeit [N/mm]:	**3359.2**					
(in Anlehnung an prTS 843-9)						
***) durch lineare Regression ermittelt**						

Kantenfestigkeit	H-B HT			Abstand	Kraft	F/d
				d [mm]	[N]	[N/mm]
				0	0	
Auftraggeber:				0.201	587	2920
Material:	H-B HT			0.494	1501	3038
Operator:	Fabbro			0.314	989	3150
Datum:	10.08.2016			0.405	1325	3272
Belastungsgeschwindigkeit:	0,50 mm			0.477	1783	3738
Oberfläche:	as sintered					
Geometrie:	90°					
Kantenfestigkeit [N/mm]*):						
Kantenfestigkeit [N/mm]:	**3223.6183**					
(in Anlehnung an prTS 843-9)						
***) durch lineare Regression ermittelt**						

H-B

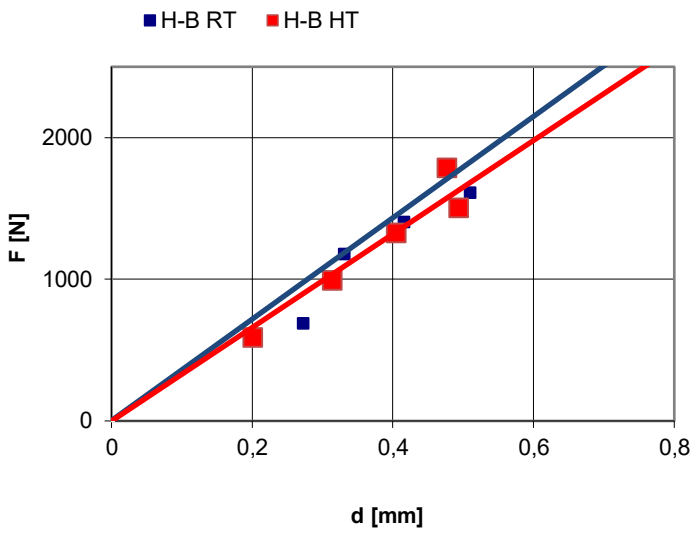

Kantenfestigkeit	H-C RT			Abstand	Kraft	F/d
				d [mm]	[N]	[N/mm]
				0	0	
Auftraggeber:				0.283	1110	3922
Material:	H-C RT			0.085	145	1706
Operator:	Fabbro			0.237	696	2937
Datum:	10.08.2016			0.542	1607	2965
Belastungsgeschwindigkeit:	0,50 mm			0.220	749	3405
Oberfläche:	as sintered					
Geometrie:	90°					
Kantenfestigkeit [N/mm]*):						
Kantenfestigkeit [N/mm]:	**2986.87**					
(in Anlehnung an prTS 843-9)						
***) durch lineare Regression ermittelt**						

Kantenfestigkeit	H-C HT			Abstand	Kraft	F/d
				d [mm]	[N]	[N/mm]
				0	0	
Auftraggeber:				0.237	539	2274
Material:	H-C HT			0.370	1033	2792
Operator:	Fabbro			0.211	320	1517
Datum:	10.08.2016			0.241	413	1714
Belastungsgeschwindigkeit:	0,50 mm			0.166	630	3795
Oberfläche:	as sintered					
Geometrie:	90°					
Kantenfestigkeit [N/mm]*):						
Kantenfestigkeit [N/mm]:	**2418.32**					
(in Anlehnung an prTS 843-9)						
***) durch lineare Regression ermittelt**						

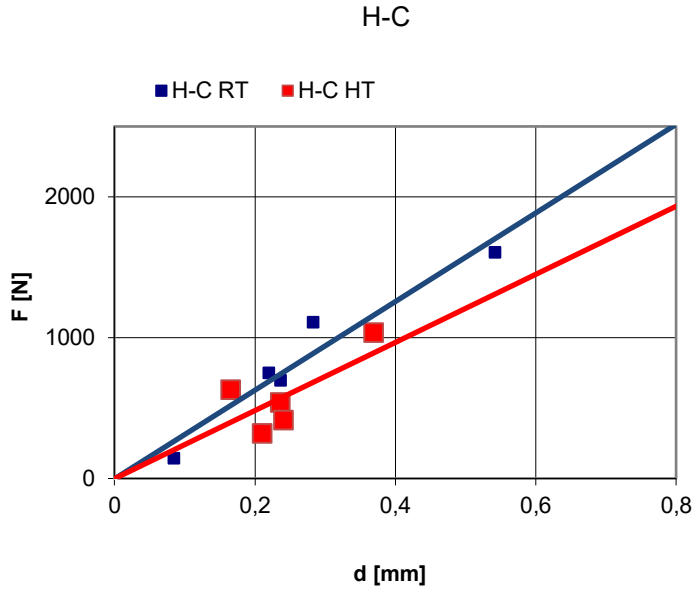

Kantenfestigkeit	S-A RT			Abstand	Kraft	F/d
				d [mm]	[N]	[N/mm]
				0	0	
Auftraggeber:				0.451	1023	2268
Material:	S-A RT			0.641	2135	3331
Operator:	Fabbro			0.416	1313	3156
Datum:	09.08.2017			0.497	1345	2706
Belastungsgeschwindigkeit:	0,50 mm			0.477	1287	2698
Oberfläche:	as sintered					
Geometrie:	90°					
Kantenfestigkeit [N/mm]*):						
Kantenfestigkeit [N/mm]:	**2831.93**					
(in Anlehnung an prTS 843-9)						
***) durch lineare Regression ermittelt**						

Kantenfestigkeit	S-A HT			Abstand	Kraft	F/d
				d [mm]	[N]	[N/mm]
				0	0	
Auftraggeber:				0.625	1268	2029
Material:	S-A HT			0.421	369	876
Operator:	Fabbro			0.567	268	473
Datum:	09.08.2017			0.305	112	367
Belastungsgeschwindigkeit:	0,50 mm			0.516	282	547
Oberfläche:	as sintered					
Geometrie:	90°					
Kantenfestigkeit [N/mm]*):						
Kantenfestigkeit [N/mm]:	**858.33**					
(in Anlehnung an prTS 843-9)						
***) durch lineare Regression ermittelt**						

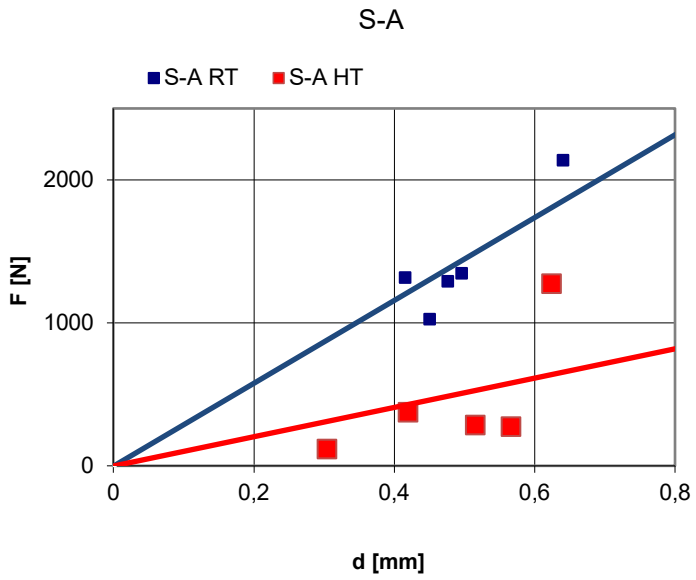

Kantenfestigkeit	S-C RT			Abstand	Kraft	F/d
				d [mm]	[N]	[N/mm]
				0	0	
Auftraggeber:				0.142	557	3923
Material:	S-C RT			0.477	1343	2816
Operator:	Fabbro			0.246	566	2301
Datum:	10.08.2017			0.370	1149	3105
Belastungsgeschwindigkeit:	0,50 mm			0.852	2556	3000
Oberfläche:	as sintered					
Geometrie:	90°					
Kantenfestigkeit [N/mm]*):						
Kantenfestigkeit [N/mm]:	**3028.85**					
(in Anlehnung an prTS 843-9)						
***) durch lineare Regression ermittelt**						

Kantenfestigkeit	S-C HT			Abstand	Kraft	F/d
				d [mm]	[N]	[N/mm]
				0	0	
Auftraggeber:				0.366	2188	5978
Material:	S-C HT			0.261	436	1670
Operator:	Fabbro			0.312	771	2471
Datum:	10.08.2017			0.331	873	2637
Belastungsgeschwindigkeit:	0,50 mm			0.253	603	2383
Oberfläche:	as sintered					
Geometrie:	90°					
Kantenfestigkeit [N/mm]*):						
Kantenfestigkeit [N/mm]:	**3028.13**					
(in Anlehnung an prTS 843-9)						
***) durch lineare Regression ermittelt**						

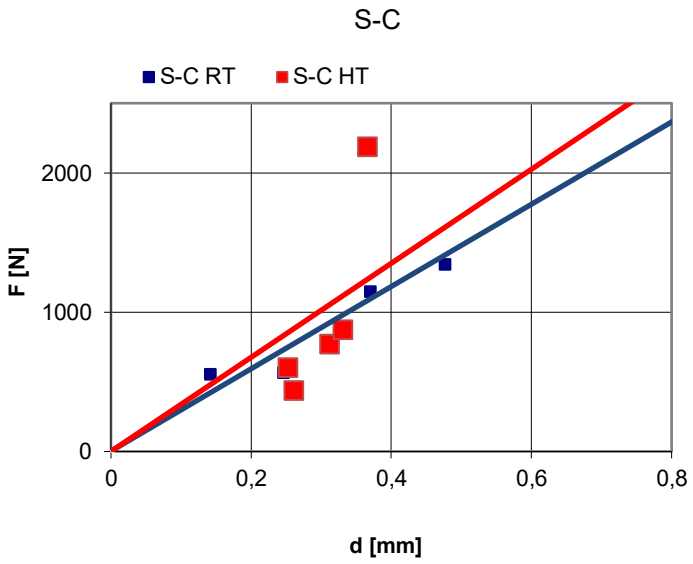

Kantenfestigkeit	S-D RT			Abstand	Kraft	F/d
				d [mm]	[N]	[N/mm]
				0	0	
Auftraggeber:				0.518	1947	3759
Material:	S-D RT			0.688	2414	3509
Operator:	Fabbro			0.594	2166	3646
Datum:	09.08.2016			0.852	3211	3769
Belastungsgeschwindigkeit:	0,50 mm			0.444	1268	2856
Oberfläche:	as sintered					
Geometrie:	90°					
Kantenfestigkeit [N/mm]*):						
Kantenfestigkeit [N/mm]:	**3507.70**					
(in Anlehnung an prTS 843-9)						
***) durch lineare Regression ermittelt**						

Kantenfestigkeit	S-D HT			Abstand	Kraft	F/d
				d [mm]	[N]	[N/mm]
				0	0	
Auftraggeber:				0.168	473	2815
Material:	S-D HT			0.165	429	2600
Operator:	Fabbro			0.285	1446	5074
Datum:	09.08.2016			0.309	1218	3942
Belastungsgeschwindigkeit:	0,50 mm			0.089	127	1427
Oberfläche:	as sintered					
Geometrie:	90°					
Kantenfestigkeit [N/mm]*):						
Kantenfestigkeit [N/mm]:	**3171.57**					
(in Anlehnung an prTS 843-9)						
***) durch lineare Regression ermittelt**						

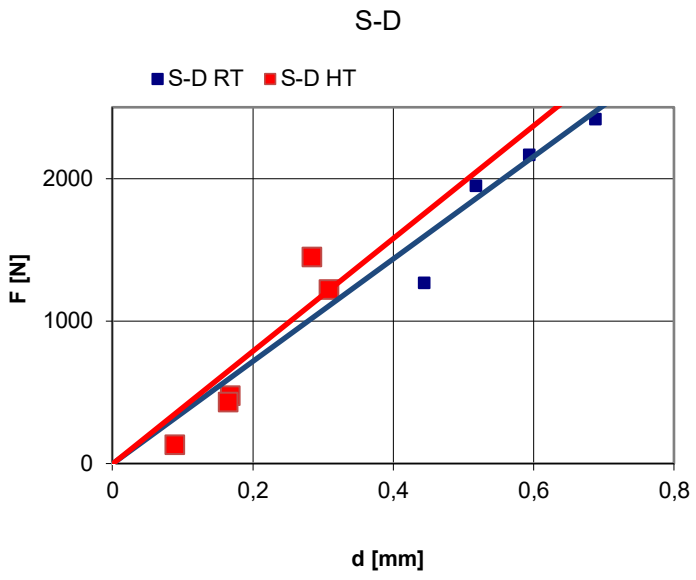

Kantenfestigkeit	P-A RT			Abstand	Kraft	F/d
				d [mm]	[N]	[N/mm]
				0	0	
Auftraggeber:				0.447	962	2152
Material:	P-A RT			0.495	1095	2212
Operator:	Fabbro			0.094	424	4511
Datum:	08.08.2016			0.451	776	1721
Belastungsgeschwindigkeit:	0,50 mm			0.224	491	2192
Oberfläche:	as sintered					
Geometrie:	90°					
Kantenfestigkeit [N/mm]*):						
Kantenfestigkeit [N/mm]:	**2557.49**					
(in Anlehnung an prTS 843-9)						
***) durch lineare Regression ermittelt**						

Kantenfestigkeit	P-A HT			Abstand	Kraft	F/d
				d [mm]	[N]	[N/mm]
				0	0	
Auftraggeber:				0.614	1644	2678
Material:	P-A RT			0.322	1438	4466
Operator:	Fabbro			0.185	188	1016
Datum:	08.08.2016			0.506	1702	3364
Belastungsgeschwindigkeit:	0,50 mm			0.405	3194	7886
Oberfläche:	as sintered					
Geometrie:	90°					
Kantenfestigkeit [N/mm]*):						
Kantenfestigkeit [N/mm]:	**3881.93**					
(in Anlehnung an prTS 843-9)						
***) durch lineare Regression ermittelt**						

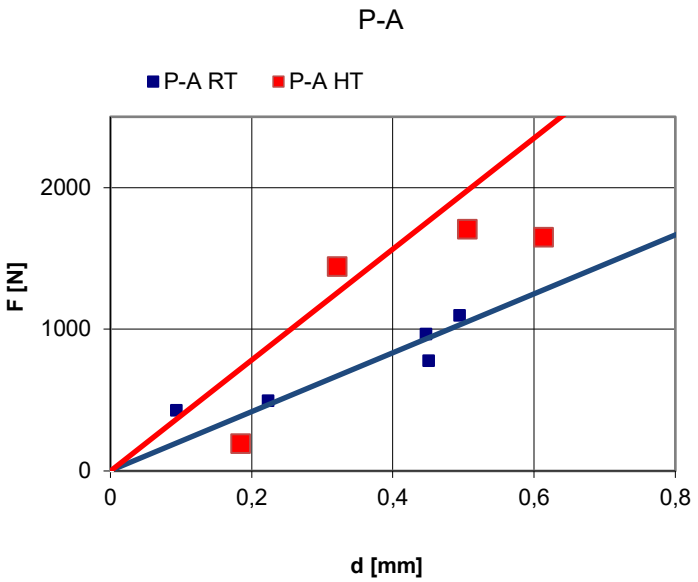

Kantenfestigkeit	P-B RT			Abstand	Kraft	F/d
				d [mm]	[N]	[N/mm]
				0	0	
Auftraggeber:				0.619	1368	2210
Material:	P-B RT			0.344	589	1712
Operator:	Fabbro			0.542	1521	2806
Datum:	08.08.2016			0.503	1293	2571
Belastungsgeschwindigkeit:	0,50 mm			0.451	904	2004
Oberfläche:	as sintered					
Geometrie:	90°					
Kantenfestigkeit [N/mm]*):						
Kantenfestigkeit [N/mm]:	**2260.70**					
(in Anlehnung an prTS 843-9)						
***) durch lineare Regression ermittelt**						

Kantenfestigkeit	P-B HT			Abstand	Kraft	F/d
				d [mm]	[N]	[N/mm]
				0	0	
Auftraggeber:				0.691	1563	2262
Material:	P-B HT			0.229	453	1978
Operator:	Fabbro			0.649	2346	3615
Datum:	08.08.2016			0.115	217	1887
Belastungsgeschwindigkeit:	0,50 mm			0.765	1968	2573
Oberfläche:	as sintered					
Geometrie:	90°					
Kantenfestigkeit [N/mm]*):						
Kantenfestigkeit [N/mm]:	**2462.88**					
(in Anlehnung an prTS 843-9)						
***) durch lineare Regression ermittelt**						

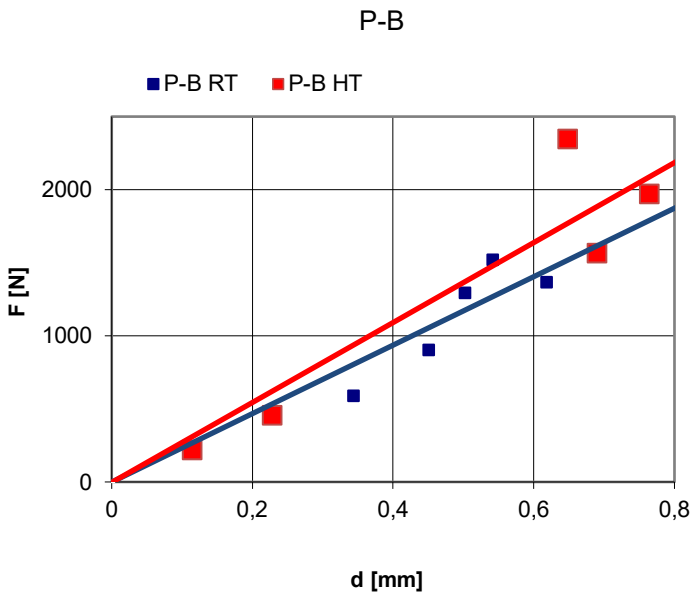

Kantenfestigkeit	P-C RT			Abstand	Kraft	F/d
				d [mm]	[N]	[N/mm]
				0	0	
Auftraggeber:				0.721	3201	4440
Material:	P-C RT			0.399	1571	3937
Operator:	Fabbro			0.227	615	2709
Datum:	08.08.2016			0.331	1369	4136
Belastungsgeschwindigkeit:	0,50 mm			0.604	2641	4373
Oberfläche:	as sintered					
Geometrie:	90°					
Kantenfestigkeit [N/mm]*):						
Kantenfestigkeit [N/mm]:	**3918.95**					
(in Anlehnung an prTS 843-9)						
***) durch lineare Regression ermittelt**						

Kantenfestigkeit	P-C HT			Abstand	Kraft	F/d
				d [mm]	[N]	[N/mm]
				0	0	
Auftraggeber:				0.253	697	2755
Material:	P-C RT			0.285	499	1751
Operator:	Fabbro			0.322	1185	3680
Datum:	08.08.2016			0.318	641	2016
Belastungsgeschwindigkeit:	0,50 mm			0.314	806	2567
Oberfläche:	as sintered					
Geometrie:	90°					
Kantenfestigkeit [N/mm]*):						
Kantenfestigkeit [N/mm]:	**2553.71**					
(in Anlehnung an prTS 843-9)						
***) durch lineare Regression ermittelt**						

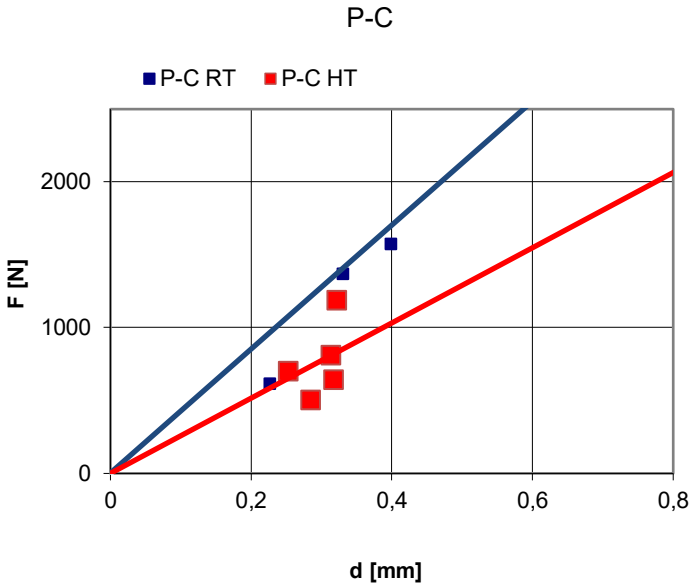

Kantenfestigkeit	P-D RT			Abstand	Kraft	F/d
				d [mm]	[N]	[N/mm]
				0	0	
Auftraggeber:				0.233	442	1897
Material:	P-D RT			0.305	642	2105
Operator:	Fabbro			0.325	755	2323
Datum:	09.08.2016			0.275	640	2327
Belastungsgeschwindigkeit:	0,50 mm			0.586	1402	2392
Oberfläche:	as sintered					
Geometrie:	90°					
Kantenfestigkeit [N/mm]*):						
Kantenfestigkeit [N/mm]:	**2208.95**					
(in Anlehnung an prTS 843-9)						
***) durch lineare Regression ermittelt**						

Kantenfestigkeit	P-D HT			Abstand	Kraft	F/d
				d [mm]	[N]	[N/mm]
				0	0	
Auftraggeber:				0.327	684	2092
Material:	P-D HT			0.129	108	837
Operator:	Fabbro			0.591	1597	2702
Datum:	09.08.2016			0.555	1306	2353
Belastungsgeschwindigkeit:	0,50 mm			0.451	913	2024
Oberfläche:	as sintered					
Geometrie:	90°					
Kantenfestigkeit [N/mm]*):						
Kantenfestigkeit [N/mm]:	**2001.74**					
(in Anlehnung an prTS 843-9)						
***) durch lineare Regression ermittelt**						

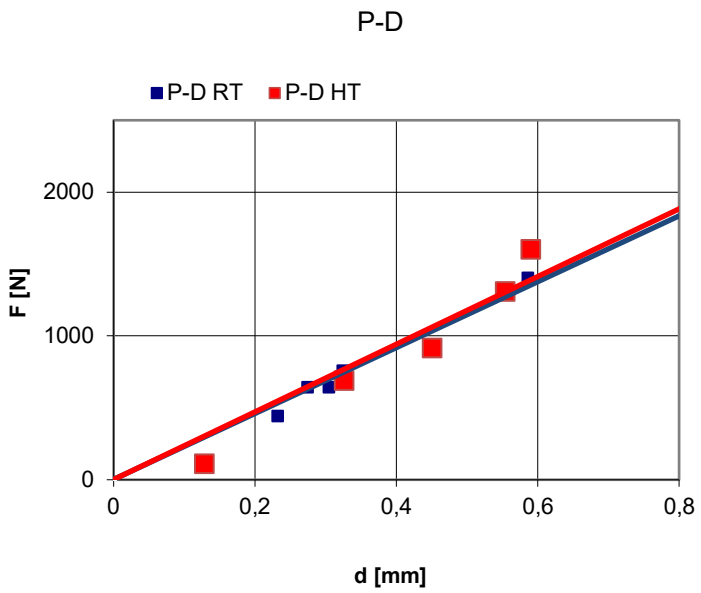

Kantenfestigkeit	P-E RT			Abstand	Kraft	F/d
				d [mm]	[N]	[N/mm]
				0	0	
Auftraggeber:				0.577	1565	2712
Material:	P-E RT			0.610	1848	3030
Operator:	Fabbro			0.233	475	2039
Datum:	09.08.2016			0.494	997	2018
Belastungsgeschwindigkeit:	0,50 mm			0.567	1542	2720
Oberfläche:	as sintered					
Geometrie:	90°					
Kantenfestigkeit [N/mm]*):						
Kantenfestigkeit [N/mm]:	**2503.65**					
(in Anlehnung an prTS 843-9)						
***) durch lineare Regression ermittelt**						

Kantenfestigkeit	P-E HT			Abstand	Kraft	F/d
				d [mm]	[N]	[N/mm]
				0	0	
Auftraggeber:				0.288	762	2646
Material:	P-E HT			0.373	802	2150
Operator:	Fabbro			0.340	639	1879
Datum:	09.08.2016			0.701	1405	2004
Belastungsgeschwindigkeit:	0,50 mm			0.379	915	2414
Oberfläche:	as sintered					
Geometrie:	90°					
Kantenfestigkeit [N/mm]*):						
Kantenfestigkeit [N/mm]:	**2218.78**					
(in Anlehnung an prTS 843-9)						
***) durch lineare Regression ermittelt**						

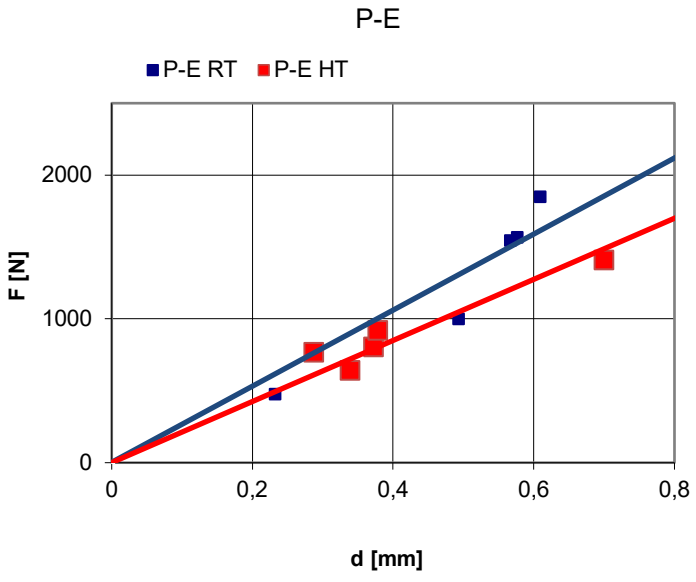

A2: B3B Tests

Auswertung 4-Kugelversuch & Weibullauswertung

Statistische Auswertung nach EN 843-5

Kugeldurchmesser D_k [mm]:	9.525	Datum:	05.07.2016
Auflagerdurchmesser D_a [mm]:	10.999	Prüfer:	Fabbro
Auflagervariante:		Prüfmaschine:	Zwick 010/10kN
		nominelle Vorkraft:	10.0 N
Probenmaterial:	T-A	Belastungsgeschw.:	0.50 mm/min
Charge:		Temperatur:	24.6 °C
Oberflächenbearbeitung:	as sintered	Luftfeuchtigkeit:	41.0 %
geprüfte Proben:	20		
Probenanzahl n:	20	Querdehnungszahl ν:	0,2

i	ID	F [N]	h_1 [mm]	h_2 [mm]	h_3 [mm]	D [mm]	Bruch-zeit [s]	h_{mittel} [mm]	$h_{St.abweich.}$ [mm]	σ_i [MPa]	Bruch-stücke
1		441.354	0.999	0.999	0.999	14.068		0.999	0.000	831.367	
2		440.576	0.994	0.994	0.994	14.039		0.994	0.000	836.684	
3		455.334	1.002	1.002	1.002	14.003		1.002	0.000	852.411	
4		457.704	1.001	1.001	1.001	14.082		1.001	0.000	858.126	
5		451.493	0.994	0.994	0.994	14.055		0.994	0.000	860.354	
6		456.735	0.998	0.998	0.998	14.061		0.998	0.000	862.365	
7		457.375	0.996	0.996	0.996	14.037		0.996	0.000	867.735	
8		464.624	1.002	1.002	1.002	14.017		1.002	0.000	869.681	
9		455.974	0.992	0.992	0.992	14.007		0.992	0.000	873.305	
10		463.327	0.997	0.997	0.997	14.077		0.997	0.000	876.673	
11		465.23	0.996	0.996	0.996	14.051		0.996	0.000	882.516	
12		473.223	1.001	1.001	1.001	14.017		1.001	0.000	887.794	
13		472.756	0.998	0.998	0.998	14.033		0.998	0.000	892.862	
14		466.337	0.991	0.991	0.991	14.051		0.991	0.000	894.816	
15		477.843	0.999	0.999	0.999	14.074		0.999	0.000	900.047	
16		476.147	0.996	0.996	0.996	14.046		0.996	0.000	903.269	
17		485.438	1.003	1.003	1.003	14.015		1.003	0.000	906.595	
18		483.414	0.998	0.998	0.998	14.097		0.998	0.000	912.414	
19		446.977	0.959	0.959	0.959	14.04		0.959	0.000	924.32	
20		502.358	0.996	0.996	0.996	14.028		0.996	0.000	953.163	

Ergebnisse

Mittelwerte & Standardabweichungen

Probendicke h:	0.996	±	0.009	mm
Proben∅ D:	14.045	±	0.026	mm
Bruchspannung σ_b:	**882.32**	±	**29.78**	**MPa**
Zeit bis zum Bruch t_f:	n. a.			

Weibullstatistik 20 Proben, Konfidenzniveau 1 - α = 90%

		Konf. Int.
m =	29.13	20.09
		36.89
m_{korr} =	27.12	

			Konf. Int.	
σ_0 =	896.82	MPa	883.89	MPa
			910.17	MPa

Auswertung 4-Kugelversuch & Weibullauswertung

Statistische Auswertung nach EN 843-5

Kugeldurchmesser D_k [mm]:	**6.350**	Datum:	**06.07.2016**
Auflagerdurchmesser D_a [mm]:	**7.332**	Prüfer:	**Fabbro**
Auflagervariante:		Prüfmaschine:	**Zwick 010/10kN**
		nominelle Vorkraft:	**10.0 N**
Probenmaterial:	**S-A**	Belastungsgeschw.:	**0.50 mm/min**
Charge:		Temperatur:	**22.6 °C**
Oberflächenbearbeitung:	**as sintered**	Luftfeuchtigkeit:	**43.0 %**
geprüfte Proben:	**20**		
Probenanzahl n:	**20**	Querdehnungszahl ν:	**0,2**

i	ID	F [N]	h_1 [mm]	h_2 [mm]	h_3 [mm]	D [mm]	Bruch-zeit [s]	h_{mittel} [mm]	$h_{St.abweich.}$ [mm]	σ_i [MPa]	Bruch-stücke
1	T-B	220.037	0.65	0.65	0.65	10.076		0.650	0.000	976.489	
2	T-B	205.071	0.565	0.565	0.565	10.024		0.565	0.000	1252.73	
3	T-B	216.992	0.571	0.571	0.571	10.016		0.571	0.000	1294.25	
4	T-B	207.995	0.553	0.553	0.553	10.015		0.553	0.000	1334.19	
5	T-B	302.771	0.65	0.65	0.65	10.044		0.650	0.000	1344.17	
6	T-B	213.393	0.557	0.557	0.557	10.013		0.557	0.000	1346.64	
7	T-B	219.916	0.562	0.562	0.562	10.011		0.562	0.000	1359.96	
8	T-B	299.346	0.639	0.639	0.639	10.024		0.639	0.000	1382.03	
9	T-B	247.805	0.574	0.574	0.574	10.014		0.574	0.000	1460.57	
10	T-B	261.196	0.581	0.581	0.581	10.032		0.581	0.000	1497.36	
11	T-B	248.791	0.568	0.568	0.568	10.067		0.568	0.000	1500.89	
12	T-B	226.421	0.543	0.543	0.543	10.016		0.543	0.000	1513.77	
13	T-B	343.031	0.641	0.641	0.641	10.032		0.641	0.000	1572.32	
14	T-B	251.906	0.557	0.557	0.557	10.02		0.557	0.000	1589.55	
15	T-B	346.405	0.635	0.635	0.635	10.019		0.635	0.000	1622.44	
16	T-B	271.459	0.562	0.562	0.562	10.02		0.562	0.000	1678.53	
17	T-B	346.543	0.615	0.615	0.615	10.027		0.615	0.000	1745.64	
18	T-B	382.132	0.619	0.619	0.619	10.097		0.619	0.000	1895.13	
19	T-B	304.571	0.56	0.56	0.56	10.017		0.560	0.000	1898.64	
20	T-B	297.131	0.541	0.541	0.541	10.012		0.541	0.000	2003.29	

Ergebnisse

Mittelwerte & Standardabweichungen

Probendicke h:	0.587	±	0.038	mm
Proben∅ D:	10.030	±	0.024	mm
Bruchspannung σ_b:	**1513.43**	±	**248.50**	**MPa**
Zeit bis zum Bruch t_f:	n. a.			

Weibullstatistik 20 Proben, Konfidenzniveau 1 - α = 90%

		Konf. Int.
m =	**6.70**	**4.62**
		8.48
m_{korr} =	6.24	

		Konf. Int.	
σ_0 =	**1617.48 MPa**	**1518.49**	**MPa**
		1724.89	**MPa**

Auswertung 4-Kugelversuch & Weibullauswertung

Statistische Auswertung nach EN 843-5

Kugeldurchmesser D_k [mm]:	6.350		Datum:	07.07.2017	
Auflagerdurchmesser D_a [mm]:	7.332		Prüfer:	Fabbro	
Auflagervariante:			Prüfmaschine:	Zwick 010/10kN	
			nominelle Vorkraft:	10.00	N
Probenmaterial:	S-C		Belastungsgeschw.:	0.50	mm/min
Charge:			Temperatur:	22.8	°C
Oberflächenbearbeitung:	as sintered		Luftfeuchtigkeit:	50.0	%
geprüfte Proben:	20				
Probenanzahl n:	20		Querdehnungszahl ν:	0,2	

i	ID	F [N]	h_1 [mm]	h_2 [mm]	h_3 [mm]	D [mm]	Bruch-zeit [s]	h_{mittel} [mm]	$h_{St.abweich.}$ [mm]	σ_i [MPa]	Bruch-stücke
1	S-C	199.325	0.578	0.578	0.578	10.189		0.578	0.000	1154.11	
2	S-C	196.489	0.574	0.574	0.574	10.018		0.574	0.000	1158.06	
3	S-C	211.795	0.58	0.58	0.58	10.029		0.580	0.000	1218.96	
4	S-C	210.117	0.571	0.571	0.571	10.017		0.571	0.000	1253.23	
5	S-C	232.053	0.583	0.583	0.583	10.023		0.583	0.000	1320.08	
6	S-C	235.576	0.583	0.583	0.583	10.046		0.583	0.000	1339.76	
7	S-C	234.088	0.581	0.581	0.581	10.034		0.581	0.000	1341.92	
8	S-C	227.36	0.573	0.573	0.573	10.192		0.573	0.000	1342.65	
9	S-C	223.953	0.569	0.569	0.569	10.166		0.569	0.000	1344.14	
10	S-C	214.112	0.554	0.554	0.554	10.02		0.554	0.000	1367.73	
11	S-C	233.241	0.569	0.569	0.569	10.019		0.569	0.000	1402.25	
12	S-C	256.226	0.592	0.592	0.592	10.027		0.592	0.000	1407.63	
13	S-C	259.391	0.594	0.594	0.594	10.16		0.594	0.000	1411.94	
14	S-C	236.406	0.569	0.569	0.569	10.033		0.569	0.000	1421.04	
15	S-C	263.542	0.596	0.596	0.596	10.039		0.596	0.000	1425.61	
16	S-C	235.316	0.566	0.566	0.566	10.056		0.566	0.000	1431.2	
17	S-C	291.836	0.611	0.611	0.611	10.019		0.611	0.000	1492.21	
18	S-C	265.548	0.584	0.584	0.584	10.005		0.584	0.000	1505.07	
19	S-C	258.529	0.566	0.566	0.566	10.018		0.566	0.000	1573.07	
20	S-C	275.493	0.569	0.569	0.569	10.034		0.569	0.000	1655.98	

Ergebnisse

Mittelwerte & Standardabweichungen

Probendicke h:	0.578	±	0.013 mm
Proben∅ D:	10.057	±	0.063 mm
Bruchspannung σ_b:	**1378.33**	±	**126.09 MPa**
Zeit bis zum Bruch t_f:	n. a.		

Weibullstatistik 20 Proben, Konfidenzniveau 1 - α = 90%

		Konf. Int.
m =	11.62	8.01
		14.71
m_{korr} =	10.82	

		Konf. Int.	
σ_0 =	1434.98 MPa	1383.67	MPa
		1489.16	MPa

Auswertung 4-Kugelversuch & Weibullauswertung

Statistische Auswertung nach EN 843-5

Kugeldurchmesser D_k [mm]:	**6.350**		Datum:	**05.08.2017**	
Auflagerdurchmesser D_a [mm]:	**7.332**		Prüfer:	**Fabbro**	
Auflagervariante:			Prüfmaschine:	**Zwick 010/10kN**	
			nominelle Vorkraft:	**10.0**	**N**
Probenmaterial:	**S-D**		Belastungsgeschw.:	**0.80**	**mm/min**
Charge:			Temperatur:	**23.0**	**°C**
Oberflächenbearbeitung:	**as sintered**		Luftfeuchtigkeit:	**49.0**	**%**
geprüfte Proben:	**22**				
Probenanzahl n:	**22**		Querdehnungszahl ν:	**0,2**	

i	ID	F [N]	h_1 [mm]	h_2 [mm]	h_3 [mm]	D [mm]	Bruch-zeit [s]	h_{mittel} [mm]	$h_{St.abweich.}$ [mm]	σ_i [MPa]	Bruch-stücke
1	D18	518,889	0.875	0.875	0.875	10.050		0.875	0.000	1243.526	
2	D17	534,164	0.876	0.876	0.876	10.040		0.876	0.000	1276.880	
3	D16	567,362	0.884	0.884	0.884	10.020		0.884	0.000	1328.309	
4	D12	577,101	0.881	0.881	0.881	10.040		0.881	0.000	1361.504	
5	D7	331,624	0.691	0.691	0.691	10.040		0.691	0.000	1367.586	
6	D5	910,545	1.068	1.068	1.068	10.040		1.068	0.000	1374.837	
7	D11	590,664	0.880	0.880	0.880	10.020		0.880	0.000	1397.425	
8	D8	595,162	0.882	0.882	0.882	10.020		0.882	0.000	1400.703	
9	D19	598,466	0.880	0.880	0.880	10.040		0.880	0.000	1415.617	
10	D14	639,846	0.901	0.901	0.901	10.030		0.901	0.000	1433.367	
11	D3	366,534	0.706	0.706	0.706	10.030		0.706	0.000	1439.156	
12	D21	591,46	0.864	0.864	0.864	10.020		0.864	0.000	1459.859	
13	D1	368,623	0.698	0.698	0.698	10.080		0.698	0.000	1484.979	
14	D22	627,39	0.879	0.879	0.879	10.050		0.879	0.000	1487.798	
15	D6	1060,201	1.066	1.066	1.066	10.030		1.066	0.000	1607.963	
16	D13	711,794	0.891	0.891	0.891	10.170		0.891	0.000	1634.123	
17	D15	689,996	0.878	0.878	0.878	10.060		0.878	0.000	1640.417	
18	D9	700,532	0.876	0.876	0.876	10.020		0.876	0.000	1674.885	
19	D10	434.64	0.711	0.711	0.711	10.030		0.711	0.000	1679.208	
20	D4	1101,581	1.059	1.059	1.059	10.030		1.059	0.000	1696.536	
21	D2	1165,831	1.066	1.066	1.066	10.030		1.066	0.000	1768.168	
22	D20	762,948	0.881	0.881	0.881	10.030		0.881	0.000	1800.126	

Ergebnisse

Mittelwerte & Standardabweichungen

Probendicke h:	0.882	±	0.111	mm
Proben∅ D:	10.042	±	0.032	mm
Bruchspannung σ_b:	**1498.77**	±	**161.50**	**MPa**
Zeit bis zum Bruch t_f:	n. a.			

Weibullstatistik 22 Proben, Konfidenzniveau 1 - α = 90%

		Konf. Int.
m =	**10.06**	**7.09**
		12.63
m_{korr} =	9.43	

		Konf. Int.	
σ_0 =	**1571.72 MPa**	**1510.42**	**MPa**
		1636.56	**MPa**

Auswertung 4-Kugelversuch & Weibullauswertung

Statistische Auswertung nach EN 843-5

Kugeldurchmesser D_k [mm]:	9.525	Datum:	08.08.2016
Auflagerdurchmesser D_a [mm]:	10.999	Prüfer:	Fabbro
Auflagervariante:		Prüfmaschine:	Zwick 010/10kN
		nominelle Vorkraft:	10.0 N
Probenmaterial:	T-A heat treated	Belastungsgeschw.:	0.50 mm/min
Charge:		Temperatur:	21.7 °C
Oberflächenbearbeitung:	as sintered	Luftfeuchtigkeit:	44.0 %
geprüfte Proben:	15		
Probenanzahl n:	15	Querdehnungszahl ν:	0,2

i	ID	F [N]	h_1 [mm]	h_2 [mm]	h_3 [mm]	D [mm]	Bruch-zeit [s]	h_{mittel} [mm]	$h_{St.abweich.}$ [mm]	σ_i [MPa]	Bruch-stücke
1	5	471.345	1.019	1.019	1.019	14.04		1.019	0.000	904.564	
2	3	466.432	1.003	1.003	1.003	14.01		1.003	0.000	928.322	
3	6	470.878	1.002	1.002	1.002	14.06		1.002	0.000	938.931	
4	4	561.312	1.079	1.079	1.079	14.01		1.079	0.000	945.290	
5	7	475.531	1.003	1.003	1.003	14.05		1.003	0.000	946.127	
6	10	476.508	0.998	0.998	0.998	14.03		0.998	0.000	959.108	
7	14	477.009	0.997	0.997	0.997	14.08		0.997	0.000	961.933	
8	9	478.099	0.996	0.996	0.996	14.05		0.996	0.000	966.574	
9	15	475.833	0.993	0.993	0.993	14.04		0.993	0.000	968.720	
10	11	483.427	0.999	0.999	0.999	14.04		0.999	0.000	970.734	
11	1	486.394	0.992	0.992	0.992	14.06		0.992	0.000	992.343	
12	12	487.682	0.988	0.988	0.988	14.06		0.988	0.000	1004.192	
13	2	504.903	0.999	0.999	0.999	14.06		0.999	0.000	1013.696	
14	13	498.632	0.993	0.993	0.993	14.06		0.993	0.000	1014.973	
15	8	529.111	0.995	0.995	0.995	14.03		0.995	0.000	1072.334	

Ergebnisse

Mittelwerte & Standardabweichungen

Probendicke h:	1.004	±	0.021 mm
Proben∅ D:	14.045	±	0.020 mm
Bruchspannung σ_b:	**972.52**	**±**	**41.70 MPa**
Zeit bis zum Bruch t_f:	n. a.		

Weibullstatistik 15 Proben, Konfidenzniveau 1 - α = 90%

		Konf. Int.
m =	22.12	14.15
		28.79
m_{korr} =	20.05	

			Konf. Int.	
σ_0 =	992.88	MPa	970.67	MPa
			1016.13	MPa

Auswertung 4-Kugelversuch & Weibullauswertung

Statistische Auswertung nach EN 843-5

Kugeldurchmesser D_k [mm]:	6.350	Datum:	08.08.2016
Auflagerdurchmesser D_a [mm]:	7.332	Prüfer:	Fabbro
Auflagervariante:		Prüfmaschine:	Zwick 010 / 10kN
		nominelle Vorkraft:	10.0 N
Probenmaterial:	S-A heat treated	Belastungsgeschw.:	0.50 mm/min
Charge:		Temperatur:	22.6 °C
Oberflächenbearbeitung:	as sintered	Luftfeuchtigkeit:	44.0 %
geprüfte Proben:	9		
Probenanzahl n:	9	Querdehnungszahl ν:	0,2

i	ID	F [N]	h_1 [mm]	h_2 [mm]	h_3 [mm]	D [mm]	Bruchzeit [s]	h_{mittel} [mm]	$h_{St.abweich.}$ [mm]	σ_i [MPa]	Bruchstücke
1	23	16.507	0.614	0.614	0.614	10.41		0.614	0.000	88.897	
2	24	41.248	0.68	0.68	0.68	10.24		0.680	0.000	176.171	
3	26	54.552	0.604	0.604	0.604	10.31		0.604	0.000	305.207	
4	27	55.054	0.582	0.582	0.582	10.55		0.582	0.000	334.590	
5	21	58.705	0.59	0.59	0.59	10.41		0.590	0.000	346.200	
6	22	60.85	0.598	0.598	0.598	10.48		0.598	0.000	347.847	
7	25	61.455	0.592	0.592	0.592	10.44		0.592	0.000	359.562	
8	28	82.01	0.588	0.588	0.588	10.48		0.588	0.000	487.150	
9	29	138.637	0.595	0.595	0.595	10.2		0.595	0.000	803.293	

Ergebnisse

Mittelwerte & Standardabweichungen

Probendicke h:	0.605	±	0.029 mm
Proben∅ D:	10.391	±	0.117 mm
Bruchspannung σ_b:	**360.99**	**±**	**201.23 MPa**
Zeit bis zum Bruch t_f:	n. a.		

Weibullstatistik — 9 Proben, Konfidenzniveau 1 - α = 90%

		Konf. Int.
m =	2.01	1.06
		2.74
m_{korr} =	1.69	

		Konf. Int.	
σ_0 =	408.15 MPa	289.72	MPa
		582.34	MPa

Auswertung 4-Kugelversuch & Weibullauswertung

Statistische Auswertung nach EN 843-5

Kugeldurchmesser D_k [mm]:	6.350		Datum:	08.08.2016	
Auflagerdurchmesser D_a [mm]:	7.332		Prüfer:	Fabbro	
Auflagervariante:			Prüfmaschine:	Zwick 010 / 10kN	
			nominelle Vorkraft:	10.0	N
Probenmaterial:	S-C heat treated		Belastungsgeschw.:	0.50	mm/min
Charge:			Temperatur:	22.7	°C
Oberflächenbearbeitung:	as sintered		Luftfeuchtigkeit:	44.0	%
geprüfte Proben:	14				
Probenanzahl n:	14		Querdehnungszahl ν:	0,2	

i	ID	F [N]	h_1 [mm]	h_2 [mm]	h_3 [mm]	D [mm]	Bruch-zeit [s]	h_{mittel} [mm]	$h_{St.abweich.}$ [mm]	σ_i [MPa]	Bruch-stücke
1	1	23.375	0.586	0.586	0.586	10.36		0.586	0.000	140.049	
2	8	56.023	0.598	0.598	0.598	10.41		0.598	0.000	320.410	
3	11	59.829	0.603	0.603	0.603	10.39		0.603	0.000	335.799	
4	14	77.909	0.607	0.607	0.607	10.38		0.607	0.000	430.772	
5	10	91.646	0.59	0.59	0.59	10.43		0.590	0.000	540.387	
6	7	168.257	0.587	0.587	0.587	10.03		0.587	0.000	1006.820	
7	13	193.846	0.622	0.622	0.622	10.12		0.622	0.000	1015.849	
8	9	219.106	0.636	0.636	0.636	10.17		0.636	0.000	1090.943	
9	3	224.469	0.627	0.627	0.627	10.08		0.627	0.000	1155.435	
10	4	244.227	0.63	0.63	0.63	10.1		0.630	0.000	1243.318	
11	12	238.085	0.622	0.622	0.622	10.11		0.622	0.000	1247.786	
12	5	300.266	0.648	0.648	0.648	10.09		0.648	0.000	1433.547	
13	2	309.972	0.648	0.648	0.648	10.1		0.648	0.000	1479.761	
14	6	316.149	0.648	0.648	0.648	10.09		0.648	0.000	1509.376	

Ergebnisse

Mittelwerte & Standardabweichungen

Probendicke h:	0.618	±	0.022 mm
Proben∅ D:	10.204	±	0.150 mm
Bruchspannung σ_b:	**925.02**	±	**474.75 MPa**
Zeit bis zum Bruch t_f:	n. a.		

Weibullstatistik 14 Proben, Konfidenzniveau 1 - α = 90%

		Konf. Int.
m =	2.10	1.32
		2.76
m_{korr} =	1.89	

		Konf. Int.	
σ_0 =	1040.64 MPa	812.39	MPa
		1341.37	MPa

Auswertung 4-Kugelversuch & Weibullauswertung

Statistische Auswertung nach EN 843-5

Kugeldurchmesser D_k [mm]:	**6.350**		Datum:	**09.08.2016**	
Auflagerdurchmesser D_a [mm]:	**7.332**		Prüfer:	**Fabbro**	
Auflagervariante:			Prüfmaschine:	**Zwick 010 / 10kN**	
			nominelle Vorkraft:	**10.0**	**N**
Probenmaterial:	**S-D heat treated**		Belastungsgeschw.:	**0.50**	**mm/min**
Charge:			Temperatur:	**22.8**	**°C**
Oberflächenbearbeitung:	**as sintered**		Luftfeuchtigkeit:	**44.0**	**%**
geprüfte Proben:	**22**				
Probenanzahl n:	**22**		Querdehnungszahl ν:	**0,2**	

i	ID	*F* [N]	h_1 [mm]	h_2 [mm]	h_3 [mm]	*D* [mm]	*Bruch-zeit* [s]	h_{mittel} [mm]	$h_{St.abweich.}$ [mm]	σ_i [MPa]	*Bruch-stücke*
1	D9	215,334	0.912	0.912	0.912	10,29		0.912	0.000	467.955	
2	D7	284,187	0.883	0.883	0.883	10,11		0.883	0.000	666.526	
3	D8	245,954	0.753	0.753	0.753	10,05		0.753	0.000	832.884	
4	D13	356,275	0.882	0.882	0.882	10,03		0.882	0.000	838.408	
5	D2	367,274	0.88	0.88	0.88	10,04		0.880	0.000	868.753	
6	D15	385,318	0.881	0.881	0.881	10,08		0.881	0.000	908.710	
7	D10	417,199	0.872	0.872	0.872	10,03		0.872	0.000	1007.972	
8	D18	425,594	0.878	0.878	0.878	10,04		0.878	0.000	1012.008	
9	D11	437,744	0.884	0.884	0.884	10,05		0.884	0.000	1024.558	
10	D19	431,946	0.873	0.873	0.873	10,07		0.873	0.000	1040.457	
11	D16	454,048	0.878	0.878	0.878	10,11		0.878	0.000	1078.974	
12	D6	465,852	0.884	0.884	0.884	10,09		0.884	0.000	1089.944	
13	D3	504,024	0.9	0.9	0.9	10,07		0.900	0.000	1131.580	
14	D5	492,105	0.889	0.889	0.889	10,04		0.889	0.000	1136.988	
15	D20	487,781	0.855	0.855	0.855	10,09		0.855	0.000	1232.605	
16	D4	753,783	1.027	1.027	1.027	10,07		1.027	0.000	1246.260	
17	D14	517,136	0.867	0.867	0.867	10,04		0.867	0.000	1266.003	
18	D21	549,259	0.872	0.872	0.872	10,04		0.872	0.000	1326.911	
19	D17	549,606	0.871	0.871	0.871	10,15		0.871	0.000	1329.945	
20	D1	567,57	0.883	0.883	0.883	10,06		0.883	0.000	1331.776	
21	D12	565,442	0.874	0.874	0.874	10,07		0.874	0.000	1358.423	
22	D22	612,762	0.876	0.876	0.876	10,03		0.876	0.000	1464.900	

Ergebnisse

Mittelwerte & Standardabweichungen

Probendicke h:	0.881	±	0.043	mm
Proben∅ D:	#DIV/0!	±	#DIV/0!	mm
Bruchspannung σ_b:	**1075.57**	±	**244.66**	**MPa**
Zeit bis zum Bruch t_f:	n. a.			

Weibullstatistik 22 Proben, Konfidenzniveau 1 - α = 90%

		Konf. Int.
m =	**5.48**	**3.86**
		6.87
m_{korr} =	5.13	

		Konf. Int.	
σ_0 =	**1167.49 MPa**	**1085.21**	**MPa**
		1257.50	**MPa**